Rheological Properties of Protein Hydrogels

Shane Scott

Thesis submitted to the
Faculty of Graduate and Postdoctoral Studies
In partial fulfillment of the requirements
For the MSc degree in Physics

Department of Physics
Faculty of Science
University of Ottawa

© Shane Scott, Ottawa, Canada, 2012

Abstract

Certain hydrogel forming *de novo* proteins that utilize different crosslinking methods are studied experimentally on a rheometer. The stress reaxation modulus of CRC, a telechelic, triblock protein, is shown to be that of a stretched exponential function with a value of $\beta \cong 0.5$. The insertion of an integrin binding domain and changes in pH within the range 6.5–8.5 are shown not to significantly affect the resulting rheological behavior. A selective chemical crosslinker is used on CRC hydrogel systems and is shown to change the rheological behavior of the system to that of a combination of a chemically and physically crosslinked system. Chemically crosslinked hydrogels composed of W6, a wheat gluten-based protein, demonstrate a storage modulus weakly dependent on the angular frequency that is much greater than the loss modulus, with a modulus concentration dependence of $c^{9/4}$.

Statement of Originality

Except stated otherwise, the results presented in this thesis were obtained by the author during the period of his M. Sc. research project under the supervision of Dr. James Harden. They are to the best of his knowledge original.

Acknowledgements

I would like to thank Dr. James Harden for all the help and support he has given me while working on this project. I also want to thank Dr. Scott Dick for his guidance and advice, Dr. Stephen Fischer for the many hours he spent training me and the aid he gave, and Fan Wan for her insight. In addition, I would like to acknowledge Hilary Paulin and in particular Meredith Nichols for their contributions and help with the protein purification. I want to extend my thanks to Dr. Chris Boddy and his lab group for their permission and instruction in the use of their lab equipment. I am grateful for the frequent and fervent support of my family and friends throughout the years. Finally, I would like to thank my girlfriend for her encouragement and constant companionship during the long hours I spent working on this project.

Contents

List of Figures

List of Tables

List of Symbols

b: Kuhn length (m)
c: Concentration $(\frac{kg}{mol})$
C: Fresnel cosine integral
E: Internal energy of a system (J)
f_{EL}: Free energy of helix elongation per residue
f_H: Free energy of formation of a hydrogen bond
f_{INIT}: Free energy of helix initiation
F: Helmholtz free energy (J)
$\mathcal{F}$: Fourier transform
g: Number of polymers in a blob
G: Stress relaxation modulus or shear modulus (Pa)
G_∞: Shear modulus at an infinite time (Pa)
G_M: Maxwell modulus (Pa)
G^*: Complex modulus (Pa)
G': Storage modulus (Pa)
G'': Loss modulus (Pa)
k_b: Boltzmann constant$(\frac{J}{K})$
n: Number of polymer chains in a system
N: Number of monomers in a polymer chain
P: Pressure (Pa)
P_α: Probability of a system being in a certain state, α
$\Re$: Ideal gas constant $(\frac{J}{mol\ K})$
r: Polymer chain size (m)
s: Helix elongation parameter
S: Fresnel sine integral
S_{ent}: Entropy $(\frac{J}{K})$

t: Time (s)
T: Temperature (K)
T_{tor}: Torque ($N\ m$)
v: Excluded volume of a monomer (m^3)
V: Volume (m^3)
w: Number of ways of arranging a system
β: Stretched exponential parameter
δ": Oscillating phase shift
ϕ^*: Overlap concentration
γ: Strain
η: Viscosity ($Pa\ s$)
Π: Osmotic pressure (Pa)
ρ: Density ($\frac{kg}{m^3}$)
σ: Shear stress (Pa)
σ_s: Helix initiation parameter
τ: Relaxation time (s)
ν: Number of elastically effective chains in a network
ω: Angular frequency ($\frac{rad}{s}$)
ξ: Blob size (m)

Chapter 1

Introduction

Biological materials, or biomaterials for short, are a wide class of materials generally used in life sciences and medicine. This class of materials comprises specific metals (specific kinds of steel, silver, and cobalt), ceramics (numerous oxides, phosphates, and other compounds), polymers (teflon and other organic chemicals), natural materials (lipid and protein-based materials), as well as composites between them (1). These materials also have the benefit that they do not harm or otherwise destroy biological tissues with which they may come in contact, generally making them more environmentally friendly than other kinds of materials. They are frequently used to replace bones and other soft tissue in medicine, in scientific research (e.g. agar plates for cell growth), as well as for various other kinds of uses (for example, biologically produced silk used in optical devices (2)).

Protein-based biomaterials are of increasing interest in biomaterials research. Collagen, a protein found in mammals, has long been used for clinical purposes due to its high tensile strength, hydrophilicity, and enhancement of surrounding tissue regeneration (3). Other, novel protein biomaterials have also begun to attract attention, from elastic elastomeric based biomaterials, such as elastin, gluten, and resilin, to telechelic protein materials (those who interact with each other only at the ends of their strands) since they have

been shown to be of use as cellular scaffolds on which cells may grow (4–11). Of particular interest for this work, the telechelic triblock protein CRC has already been shown to function effectively as a cellular scaffold (11, 12), while the newly created elastomeric protein W6, composed of 6 repetitive W units, has different properties that may also allow it to be of use in such a manner. Proteins, their constituents, and the particular structures that they form will be discussed in detail in chapter 2

Though largely the subject of those studying life sciences, these protein materials also possess very interesting physical properties that may have an effect on cells grown upon them when used as cellular scaffolds. Numerous groups have already proven that by varying the physical properties of a specific protein-based substance, the differentiation of stem cells grown on scaffolds made of these materials may be controlled (13–18). These papers demonstrate that it is likely that a stem cell will differentiate into specific types of cells by sensing the mechanical properties of its environment. This would explain why, for example, stem cells in muscle tissue will differentiate into muscle cells while stem cells in bone marrow will differentiate into bone cells. If CRC and W6 are to be used as cellular scaffolds as well, it is therefore of importance that the physical characteristics of materials composed of these proteins be determined in order to effectively make use of them in a laboratory setting.

The manner in which these proteins react, dissolve, or combine with other materials to form composites may determine the properties of the cellular scaffolds which they compose. One particular way to prepare these proteins is to use them to form a gel. Gels are materials composed of a network of interacting polymers. They may be formed within a solvent, an aqueous solvent, or no solvent at all. Hydrogels are gels whose networks are dissolved in an aqueous solvent. The study of their physical properties is particularly complex, and has long been of interest to materials scientists (19–21). Proteins that naturally form a network, such as elastomeric pro-

teins and telechelic proteins, create hydrogels because the solvents in which they are dissolved are aqueous. Thus, the physics of gels is of importance in understanding the physical characteristics of protein hydrogels.

Of particular interest in materials science are the relations between the stress of a material due to an applied strain. Two ideal cases exist: that of the Newtonian fluid and that of the perfectly elastic solid. For a perfectly elastic solid, the strain, γ, creates a stress, σ, via the relation $\sigma = G\gamma$, where G is known as the *stress relaxation modulus*. The resultant stress, σ, of a Newtonian fluid due to a strain, γ, is expressed by the relation $\sigma = \eta\frac{d\gamma}{dt}$, where *eta* is the viscosity. Gels have unique physical properties in that they act as both Newtonian fluids and perfectly elastic solids when placed under strain. Substances that behave in such a manner are labelled *viscoelastic* materials. Whereas a Newtonian fluid cannot be sculpted into a shape, viscoelastic liquids such as Maxwell fluids can temporarily be sculpted into a specific form. Over time, however, the energy added to the system to create this system becomes dissipated, resulting in a loss of the shape. Unlike viscoelastic liquids, viscoelastic solids tend to store strain energy elastically. Once the imposed strain is no longer imposed on the object, a viscoelastic solid regains its former shape. Viscoelastic substances have complex physical properties that can be difficult to model. Examples of these materials include mayonnaise, honey, and lava, all of which are difficult to describe as either completely solid or completely liquid.

Attempts to describe viscoelastic materials has resulted in the creation of a theoretical field of study known as *rheology* (9, 22). As gels can form via proteins interacting either physically or chemically with each other, they are said to be either physically crosslinked, chemically crosslinked, or both. A chemically crosslinked gel has special properties when deformed: because forcing a polymer to be a specific length decreases the number of possible conformations, it will tend to resist such a deformation in order to maximize the number of possible conformations. On the other hand, physically

crosslinked gels resist deformation in the same way as chemically crosslinked gels, with the added fact that their physical associations may break at any time due to thermal fluctuations. A discussion of both kinds of gels is made in chapter 3. To obtain rheological data from such complex materials, scientific researchers choose a certain amount of strain to apply to a material, and measure the amount of mechanical stress required to produce this strain. The corresponding experimental field to rheology is called *rheometry*. The topics of rheology and rheometry will be discussed more thoroughly in chapter 3.

In chapter 4, CRC proteins and protein networks will be described and discussed in greater detail. In addition, the production, purification, and preparation of CRC networks in their hydrogel form will be elaborated upon. Concentration measurements for all protein samples, as well as tests to determine their structure will also be discussed. Various rheological tests on CRC hydrogels and their results will be presented and characterized with regards to both gel and rheological theory.

CRC hydrogels typically tend to self-assemble: a process whereby merely dissolving CRC molecules in an aqueous solvent causes them to enter into a hydrogel network. This is not the sole means of creating a hydrogel network from CRC molecules, as will be demonstrated in chapter 5. Here, a method of chemically modifying CRC hydrogels with the compound 1-ethyl-3-(3-dimethyl aminopropyl)carbodiimide hydrochloride will be discussed. The resultant changes to the rheological properties of the CRC hydrogels are demonstrated with rheometric data and linked to gel theory.

A description of W6 proteins, hydrogels, and methods of preparation for the system will be talked about in chapter 6. The results of rheometric tests performed on W6 gels are presented and discussed here, with references to gel theory and rheological theory used to explain them.

The final chapter summarizes the conclusions from the previous three chapters and discusses possible future work for CRC and W6 hydrogels. An appendix provides a description of the preparation and composition of im-

portant solutions used in this work, as well as a brief discussion on reverse osmosis and deionized water.

Chapter 2

Proteins

Proteins are one of the most basic biomolecular assemblies, comprising a large fraction of the biological materials both inside and outside of cells. Their functions range from signal transmission in the form of hormones, to the enzymatic breaking down of chemicals, to forming the scaffolds on which cells may grow (23). The protein's functions themselves depend strongly on their three dimensional, structural arrangement in space (23). This chapter will focus on their structural assembly and the physics behind it.

2.1 Amino Acids

Polymers are molecules composed of various base units, or monomers, chemically bonded together. Proteins are polymers that utilize various kinds of amino acids as monomeric units (24). Each amino acid consists of a carboxyl group located on one side (called the C-terminus), an amino group on the other (the N-terminus) and a carbon atom linking these two groups (the *alpha*-carbon). In addition to linking the carboxyl and amino groups, this *alpha*-carbon possesses a side chain (the residue, or R-group) that is different for every kind of amino acid, as in Figure 2.1. It is this side chain that distinguishes the individual amino acids and helps to form a protein's

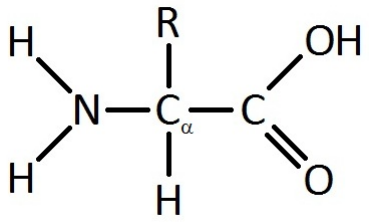

Figure 2.1: Schematic diagram of an amino acid with the α-carbon labelled as C_α

structure. The various kinds of amino acids are presented in Figure 2.2 with the respective properties of their side chains and standardized abbreviations denoted beside them. The amino acids with electrostatic side chains all exist as charged molecules at physiological pH (~7.0) with the sole exception of histidine, which oscillates between charged and uncharged. These amino acids tend to form ionic bonds with other electrostatically charged amino acids or molecules (25). The amino acids in the polar side chain group are partially charged at physiological pH, forming hydrogen bonds with aqueous solvents or other partially charged molecules. Amino acids with hydrophobic side chains tend to bond via hydrophobic interactions or van der Waals forces with other non-polar molecules.

There exist certain amino acids that possess special properties thanks to their side chains. These amino acids include cysteine, selenocysteine, proline, and glycine. Cysteine has a sulfhydryl group that is fairly reactive, frequently bonding covalently to other nearby cysteine groups via a disulfide bridge (25). Selenocsyteine has the same structure as cysteine, save that the sulphur atom is replaced with selenium. This amino acid is only produced in environments rich in selenium, rare in most kinds of cells due to the element's high reactivity (23). Glycine is the simplest structurally of the amino acids because of its hydrogen atom as a side chain. This offers the amino acid the most structural flexibility as it is not hindered by a bulky side chain, allowing it to bend with greater ease(25). Proline is the sole amino acid with a ring

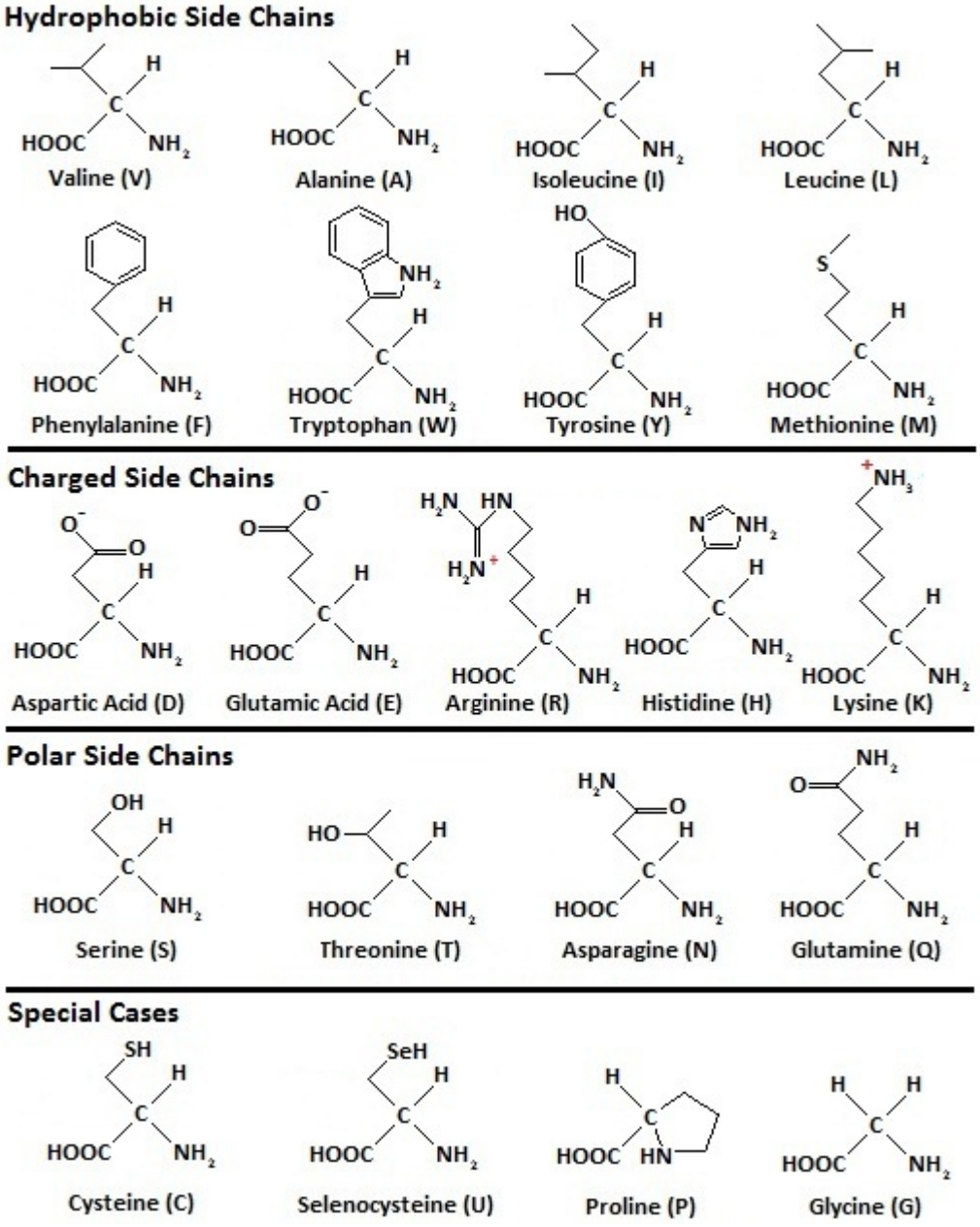

Figure 2.2: Schematic diagrams of all naturally occurring amino acids. The name of the amino acid is given beneath each, as is their standard, one letter abbreviation (given in brackets). All are organized according to the electrostatic properties of their side chains.

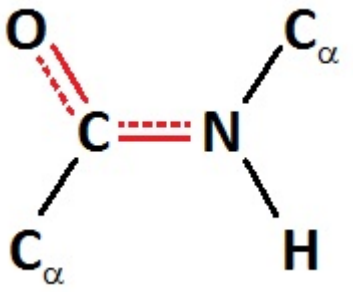

Figure 2.3: The peptide bond between two amino acids. The red, dotted bonds represent the temporary bonds formed between the atoms.

group along its backbone (25). The special properties of glycine and proline are of particular importance in the structure of protein molecules, and will be elaborated on later.

2.2 Peptide Bonds

Proteins are formed by covalently linking the C-terminus of one amino acid with the N-terminal of another, known in biochemistry as peptide bonds. Proteins are sometimes referred to as polypeptides, due to the multiple peptide bonds that link the amino acids. This process removes the -OH group from one amino acid and a H atom from the other, resulting in a bond between the amino acids and the creation of a H_2O molecule. These bonds are especially rigid, not allowing any rotation about the N-C bond. This occurs because of sp^2-hybridization of the electrons in the N-C bond and that of electrons from the bond between the O and C atoms. The hybridization in the N-C bond allows "delocalization" of the electrons, creating temporary bonds that oscillate in their positions as in Figure 2.3 (23). In this quantum orbital hybridization, the electron clouds from the three atoms overlap, allowing electrons to transfer between them. This causes the resulting bond to be planar, allowing it to be very rigid.

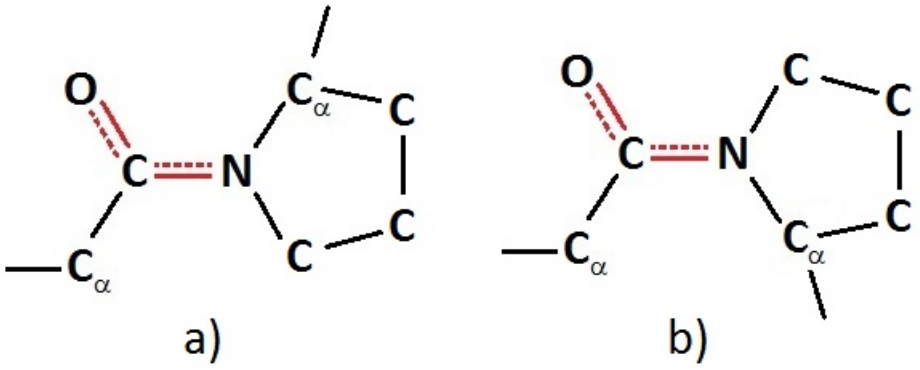

Figure 2.4: Diagram of the most probable bond conformations for proline. Diagram *a*) is the *trans* conformation, and *b*) is the *cis* conformation.

The conformation of the peptide bond in Figure 2.3 demonstrates the C_αs in the *trans* position to one another, or the position where both are farthest from one another. This is the most energetically favoured state as both the C_α atoms are large, creating steric effects between the two if they are found closer. The sole exception to this rule is proline, whose unique ring structure formed between the C-terminus and C_α atom replaces the hydrogen atom normally bonded to the C-terminus with another carbon. This results in higher energy states for proline in both the *trans* position, as mentioned before, and the *cis* position, where the C_{alpha} atoms are closest together, as in Figure 2.4 (23).

While rotations around the N-C bond are generally energetically unfavoured, rotations about the C-C_α bond (or rotations of ψ degrees) and the C_α-N bond (or rotations of ϕ degrees) are frequently encountered, as in Figure 2.5. These rotations are, energetically, of the same order of magnitude as the thermal energy at room temperature (23). Rotations about these axes are therefore quite common, and help make a protein more flexible.

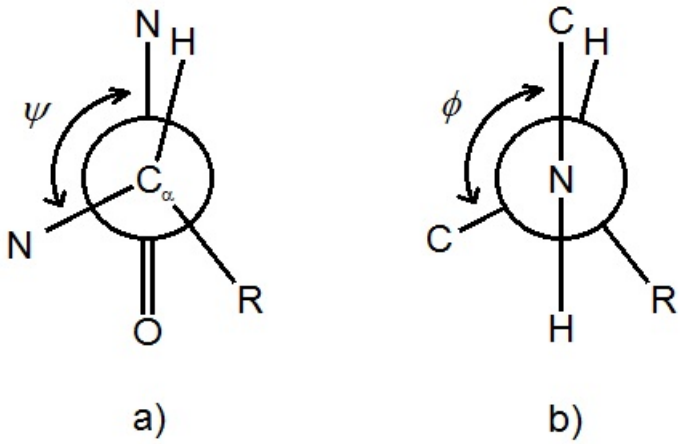

Figure 2.5: a) Newman projection about an amino acid's C_α-C bond, showing a rotation of ψ. b) Newman projection about an amino acid's N-C_α bond, showing a rotation of ϕ.

2.3 Primary and Secondary Structure

The linear sequence of amino acids in a given protein is its primary structure (26), as shown in Figure 2.6. This sequence is also referred to as the main chain, and the order helps to determine the higher order structures of a protein (23). For naturally occurring proteins, this is the sequence hard-coded and expressed by a cell's DNA (25).

A protein's secondary structure is the localized geometric arrangement of amino acids that form within a region of the protein. The secondary structure is strongly influenced by a protein's primary structure, specifically because of the nature of, and interactions between, the side chains of the individual amino acids. The most common of these structures are the alpha-helix (α-helix) and β-sheet structures (27, 28).

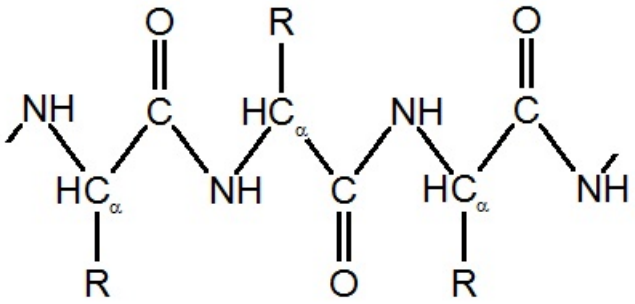

Figure 2.6: A number of amino acids bonded together into a protein. This represents the primary structure of the protein.

2.3.1 Helices

A helix is a single stranded, spiral structure that can be either right-handed or left-handed. The N-terminal of a helix is defined by the amino acid group at the end of a helix whose amine is bonded to another amino acid that does not participate in the helix. Likewise, the C terminal is defined by the amino acid at the other end of the helix. Right-handed helices grow in a counter-clockwise direction from the C-terminus to N-terminus, while left-handed helices form in a clockwise direction from the C-terminus to N-terminus (27, 29). These helices are stabilized by hydrogen bonds between the carboxyl group of one amino acid with the amino group of another amino acid a further distance down the polypeptide chain (23, 27). The hydrogen bond may not form between the carboxyl group and the closest amine group as they are too close to one another, but may form with any amine group further along the backbone. The most common bond occurs between a carboxyl group and an amine group 4 amino acids away, often called the α_R-helix, where the R denotes the right-handedness. The geometry of these helices results in an average of 3.6 residues per turn, creating a slight shift in the position of every fourth residue (27). This occurs because many of the allowed

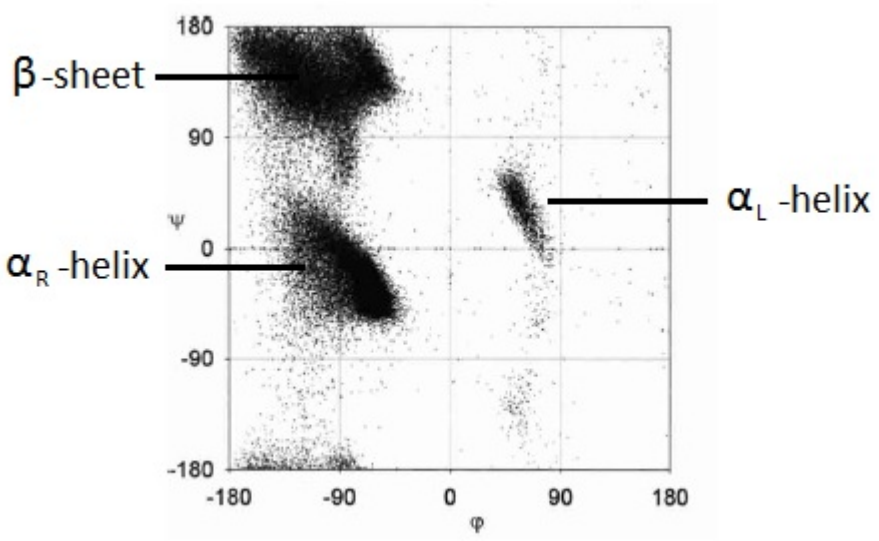

Figure 2.7: A Ramachandran plot of ϕ versus ψ for amino acids from various proteins. The bond angles resulting in various secondary structures are indicated in the figure. Reprinted from *Protein Science*, **12**, Ho, *et al*,"Revisiting the Ramachandran plot: Hard-sphere repulsion, electrostatics, and H-bonding in the α-helix", pp. 2508–2522 (2003) with permission from Elsevier

rotations about C-C_α and C_α-N, or ψ and ϕ as mentioned in section 2.2, are energetically unfavourable as the residues on the polypeptide chain are too close to one another (23). Thus, only specific values of ψ and ϕ will result in a stable helix.

The actual protein bond angles are typically shown in a graph of ϕ versus ψ, known as a Ramachandran map. This map is a plot of measured bond angles, ϕ and ψ, for amino acids in various proteins. A typical Ramachandran map is given in Figure 2.7. Figure 2.7 shows a large number of bond angles occurring in certain regions. It is these angles of ϕ and ψ that are required to produce the various secondary structures. In Figure 2.7, the most common secondary structures are associated with the necessary bond angles required to create them.

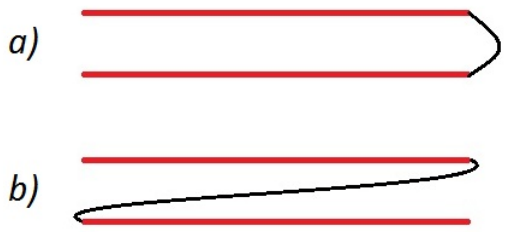

Figure 2.8: Examples of two possible conformations of two adjacent strands (shown in red) in a β-sheet. a) shows an anti-parallel conformation, while b) shows a parallel conformation.

2.3.2 Pleated Sheets

Another major kind of secondary structure is the beta-sheet (β-sheet), or pleated sheet. This structure consists of multiple parallel, zig-zag patterns of amino acids that form a wavy sheet of protein (28). Stability is introduced by hydrogen bonds that form perpendicular to the protein chains (25, 28). This formation can be induced by alternating hydrophobic and hydrophilic amino acids in a protein's secondary structure, forcing the hydrophobic residues to be along one side of the pleated sheet, and the hydrophilic along the other (30). It should be noted that this is not the only means of creating a pleated sheet, as will be discussed in section 2.3.3.

The adjacent strands that compose β-sheets may form either parallel, or anti-parallel arrangements, as in Figure 2.8. Parallel arrangements occur when the N- and C-terminals of the strands are aligned, while anti-parallel conformations occur when the N-terminal of one strand is alongside the C-terminal of an adjacent strand (23, 28). The unique, elongated structure of the β-sheet allows it to resist tensile stresses applied to it (25).

In two anti-parallel, adjacent strands found in some β-sheets, the sequence of amino acids linking the duo is a structure known as a β-turn (23). This structure is a hairpin turn constructed from two amino acids whose peptide bond is found at an angle of 90° to the main chains of the adjacent strands.

Though this structure is most often found in β-sheets, it can be found in other protein structures as well.

2.3.3 Residues and Secondary Structures

Another important factor in both α-helix and β-sheet formation is the kind of residues present in the chain. In fact, it is the side chains themselves that determine the range of possible positions for the amino acid on a Ramachandran plot. Glycine's lack of a side chain (instead of a side chain it possesses a hydrogen atom) allows it to have a very large range of the angles ϕ and ψ (23). This means it has a higher probability of being found in the regions on a Ramachandran plot that disallow both helix and pleated sheet formation.

Of the other unique amino acids, proline's inclusion of a main-chain N in a ring structure in conjunction with its side chain (refer to Figure 2.2) discourages hydrogen bonding with the N due to steric forces. This occurs despite the residue placing its angles within the range necessary for α-helices (23). Though the former property makes it unsuitable for placement inside a helix, it is commonly found at the N-terminus of helices due to the slightly negative charge of the side chain. Interestingly enough, it is frequently the presence of proline's ring structure at the end of a helix that a transition from a helical secondary structure to an entirely different kind occurs in nature (23).

Of the other amino acids, those with hydrophobic side chains tend to be found most often in β-sheets. These particular amino acids tend to have at least one C atom in their side chains. As these C atoms are particularly large, there are relatively few angles of ϕ and ψ that allow enough room for the side chains. The main exception to this occurs in the region on a Ramachandran plot corresponding to the required angles of ϕ and ψ for pleated sheet formation (23). Of these hydrophobic side chains, only that found on alanine is small enough to allow for a more even probability of being found in either the pleated sheet, or helical secondary structure (23).

In addition, the large size of the polar side chains of tyrosine and tryptophan mean they have small dipoles and big hydrophobic components, leading them to favour β-sheet formation like the other hydrophobic residues (23). One other polar amino acid, cysteine, can only make weak hydrogen bonds with water due to the presence of a S group on its side chain. This makes it more hydrophobic than polar, again causing it to favour the angles of ϕ and ψ that encourage pleated sheet formation (23).

β-turns in pleated sheet structures are often dominated by polar and charged residues (23). Their hydrophilic nature allows them to favour hydrogen bonding with the surrounding aqueous solution (a common solvent for proteins). Thus, though they are not likely to be found in the β-sheet core structure, they are often needed to create the necessary conditions for the strands to bend in such a way that they are adjacent to one another.

Polar and charged amino acids are usually found in α-helical structures. The region of the helix that they are most likely to be found is strongly dependent upon their charge. N-terminals in helices tend to be very positively charged, and so amino acids with negatively charged side chains tend to be found at this end (23). Conversely, the C-terminals are very negatively charged, encouraging those amino acids with positively charged residues to be found there. In nature, methionine and leucine are commonly found between these two regions on α-helices (23). This region screens the hydrophobic side chains of methionine and lecuine from the solvent by placing the main chain between them.

2.3.4 Free Energy Interactions

To further understand secondary structures and why they form, it is necessary to talk about their Helmholtz free energy of formation and about entropy in the system. The Helmholtz free energy of a system is defined as

$$F = E - TS_{ent} \tag{2.1}$$

where F is the free energy of a system, E is the internal energy of a system, T is the temperature, and S_{ent} is the entropy in a system (23, 31). This free energy only occurs for an isochoric system (one with constant volume). Though other kinds of free energy exist (see section 2.5), for the purposes of this exercise the Helmholtz free energy will simply be referred to as the free energy. It is important to remember Boltzmann's definition of entropy, where

$$S_{ent} = k\ln(w) \tag{2.2}$$

where k is Boltzmann's constant, and w is the number of ways of arranging a system (31). Equation 2.2 is a powerful tool when combined with the expression for the free energy in equation 2.1, as it allows us to state that the more ways a system can be arranged, the less free energy it must have.

In order to predict the folding of a protein into its secondary structure, it is important to consider that this structure must be the most probable configuration of amino acids on the main chain. The probability, P_a, of a system being in a certain state, a, (or in our case, for a protein chain to adopt a particular conformation) is given by

$$P_a \propto \exp[\frac{-F_a}{kT}] \tag{2.3}$$

(23). Equation 2.3 can be used for any kind of free energy, F_a, whether it is Helmholtz free energy, Gibbs free energy, or others, which will be discussed later. Thus, in order for a secondary structure, such as an α-helix, or β-sheet to form, it must have a minimum of free energy compared to other conformations, corresponding to a higher number of possible states.

To further investigate how the free energy affects secondary structure, consider an unstructured protein chain with N identical amino acids, also called a coil. Assume now that n of these N amino acids may form an α-helix. As the amino acids in a helix form hydrogen bonds with other amino acids 4 positions away, and the last three amino acids cannot form any more

hydrogen bonds as there are no more monomers in the α-helix, there must be $n-2$ hydrogen bonds. If this structure were to suddenly form a helix, its free energy of formation would be

$$\Delta F_\alpha = F_\alpha - F_{coil} \tag{2.4}$$

where F_α is the free energy of the α-helix, and F_{coil} is the free energy of the unstructured coil (23). If the free energy of formation of a hydrogen bond is f_H, then the free energy of formation becomes

$$\Delta F_\alpha = (n-2)f_H - nTS_\alpha \tag{2.5}$$

where S_α is the entropy loss in the system by an amino acid being fixed in a position in the α-helix (23). Rearranging equation 2.5, and placing it in equation 2.3 gives

$$\begin{aligned} \exp\left[\frac{-\Delta F_\alpha}{kT}\right] &= \exp\left[\frac{2f_H}{kT}\right]\exp\left[\frac{n(f_H - TS_\alpha)}{kT}\right] \\ &= \exp\left[\frac{-f_{INIT}}{kT}\right]\exp\left[\frac{-f_{EL}}{kT}\right]^n \\ &= \sigma_s s^n \end{aligned} \tag{2.6}$$

where $f_{INIT} = -2f_H$ is commonly called the free energy of helix initiation, $f_{EL} = f_H - TS_\alpha$ is known as the free energy of helix elongation per residue, σ_s is the helix initiation parameter, and s is the helix elongation parameter (23). Equation 2.6 is known as the Zimm-Bragg model, and is commonly used to determine whether a chain of identical amino acids will form a helix from a coil by studying the parameters σ_s and s. The energy f_{INIT} is independent of the size of the amino acid chain and is always positive since the free energy of a hydrogen bond is large and negative for most amino acids (23). This results in the term σ_s being much less than 1, and in turn itself independent of the size of the chain, n. The energy f_{EL} is a useful tool to determine whether a

section of n amino acids will form a coil. A negative f_{EL} will result in a large value for s, indicating that a helix will likely form, while a positive energy results in a small s, and therefore higher probability of staying in the coil state.

Experimental estimations of these factors have been made by many scientists for the various amino acids (see the series of papers *Helix−coil stability constants for the naturally occurring amino acids in water*) (32, 33). It is from these values that scientists may determine the suitability of specific amino acids for use in *alpha*-helical designs. For example, values of s for alanine have been calculated at ~2, while proline has a value of s ~0.2 (23, 34).

2.4 Self-assembly of tertiary and quaternary structures

The interactions of the various secondary structures along a protein's main chain comprise what is called a protein's tertiary structure (23, 25). These third-order structures can be hydrophobic, hydrophilic, or both, depending on the natures of the secondary structures comprising them. It is these complex structures that describe a protein's form and function, resulting in what are known as fibrous proteins, water-soluble globular proteins, and membrane proteins. Fibrous proteins are usually used by cells as structural scaffolds, and include the proteins that form hair and silk (23). Water-soluble globular proteins form large structures that utilize a mix of helices and β-sheets to form an irregularly shaped mass (23). Membrane proteins are those found embedded in the membranes of various parts of the cells. They are used to transport specific molecules into and out of a cell's various regions, such as between the mitochondria and cellular cytoplasm, or between the cytoplasm and its exterior environment (23).

Fibrous proteins are of importance for this work, and will be elaborated upon here. Typically, these proteins have high periodicity, formed via mul-

tiple secondary structures of the same type separated by various random sequences with some or no regular structure (23). One particular kind of fibrous protein are the α-structural fibrous proteins, composed of multiple helices separated by various, unordered sequences. These kinds of proteins can form what are called coiled-coils, as proposed by Crick in 1953 (29). Coiled-coils are interacting α-helices that have a slightly more regular structure; coiled-coil helices turn every 3.5 residues, whereas normal α-helices turn every 3.6 residues (29). This periodicity is important when considering their interactions with other proteins of the same time, forming what is called a quaternary structure.

Quaternary structures are formed when different proteins interact with each other via electrostatic, hydrophobic, or Van der Waals forces to form more complex structures. They are frequently found in biological systems, either helping to reinforce structures within a cell, or to perform specific functions that would not be possible for just one of the proteins acting alone (23, 25). Though the following discussion will focus on the quaternary structures of fibrous proteins, particularly coiled-coils, it is important to note that quaternary structure is common in all kinds of proteins, including water-soluble globular proteins and membrane proteins.

For coiled-coil fibrous proteins, there are two main methods of interaction: either via a double-helix or triple-helix (see 2.9) (23). A double-helix involves two coiled-coils interacting with each other, while a triple-helix describes three coiled-coils associating. Other higher orders of associations between coiled-coils are possible, but much more unlikely due to the increasing distance between the interacting secondary structures (23). A further discussion of how these coiled-coils interact is given in the next section.

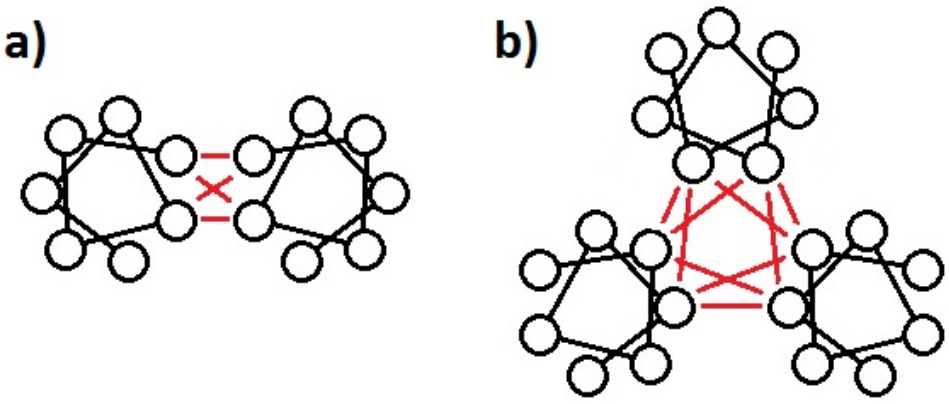

Figure 2.9: Two possible ways of coiled-coils to interact. Amino acids are represented by the black circles, black lines denote covalent bonds, and red lines represent non-covalent associations between the coiled-coils. *a*) a double-helix, *b*) a triple-helix.

2.5 Amphiphilic Coiled-Coil Helices

In order to continue, it is important to describe the idea of amphiphilicity. A structure is said to be amphiphilic when it possesses both hydrophobic and hydrophilic regions. Amphiphilicity allows proteins with hydrophobic regions that otherwise would be insoluble in aqueous solvent to be soluble due to the presence of hydrophilic regions on other parts of the protein. Many coiled-coils are amphiphilic molecules, with some groups of residues being hydrophilic, and others being hydrophobic.

The most common form of coiled-coil exists with seven repeating amino acids, commonly referred to as a heptad repeat. The seven positions of this are represented by the first seven letters of the alphabet, *a*, *b*, *c*, *d*, *e*, *f*, and *g*, as in Figure 2.10. The structure is forced to form as described previously in sections 2.3.1 and 2.3.3.

One kind of coiled-coil α-helix is the leucine zipper. In one particular

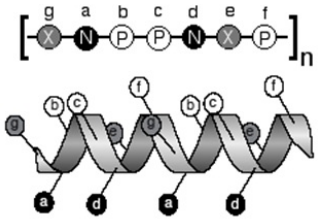

Figure 2.10: The repeating heptad pattern of a coiled-coil α-helix. From *Science*, **281**, Petka *et al.*, "Reversible Hydrogels from Self-Assembling Artificial Proteins", pp. 389–392 (1998). Reprinted with permission from AAAS.

example of this motif, two of the seven repeating positions (a and d) are held by a leucine, an amino acid with a hydrophobic residue. These leucines are present in all repeats of the heptad pattern on the leucine zipper. This positioning of hydrophobic residues results in a hydrophobic strip along one face of the coiled-coil α-helix.

The remaining heptad positions of this leucine zipper are held by hydrophilic amino acids with specific residues. The b, c, and f positions are held by polar amino acids, while the d and g positions are held by charged amino acids (refer to Figure 2.10 for the positions). When the leucine zipper forms its α-helical structure, the resulting geometry creates electrostatically charged areas flanking each side of the hydrophobic leucine strip and a hydrophilic surface on the remaining part of the structure. When many of these proteins are dissolved in a polar solvent, the hydrophobic leucine strips tend to aggregate to shield the hydrophobic portions from the polar surroundings. These interactions form quaternary structures with a hydrophobic leucine inner core and a hydrophilic outer surface, similar to the structure shown in Figure 2.9 b). When this occurs, the leucine zipper domains involved are said to be a "bundle".

The electrostatic residues that flank the leucine strips also interact intermolecularly by dissolved charged ions. This creates a weak, electrostatic interaction between the surfaces of different molecules in a bundle. Depend-

ing on the arrangement of the positively and/or negatively charged strips, either an attractive or repulsive potential can be induced between the two interacting areas. These electrostatic interactions between charged residues on hydrophobically interacting leucine zippers are known as "salt bridges".

Leucine zippers will only form these bundles if the Helmholtz free energy associated with it is at a minimum in the bundled state (35, 36). Recall that the Helmholtz free energy, F, occurs for isochoric systems according to the equation

$$F_{Free} = E - TS_{ent} \tag{2.7}$$

where E is the total internal energy of the system, T is the temperature of the system, S_{ent} is the entropy of the system, and F is the Helmholtz free energy (23). For leucine zippers forming a trimeric complex, there is no change in volume, so the change in the Helmholtz free energy (ΔF) may be calculated via the equation

$$\Delta F_{Free} = \Delta F_{\Phi} + \Delta F_{EL} - T\Delta S_{TR} - T\Delta S_{CF} \tag{2.8}$$

(35). Here, ΔF_{Φ} is the change in free energy resulting from hydrophobic associations in the trimer, ΔF_{EL} is the change in free energy from electrostatic interactions, ΔS_{TR} is the change in entropy resulting from the loss of translational and rotational freedom, and ΔS_{CF} is the change in entropy resulting from fixing the side chains. As previously stated, a minimum in the Helmholtz free energy is favoured due to the probability distribution given by equation 2.3. Fixing the coiled-coils into a trimeric bundle will always result in decreases in both kinds of entropy from equation 2.8, meaning in order for the trimeric bundles to form, the losses in free energies must be greater than that of the entropies. One other important relation that may be extracted from equation 2.3 is the relation of the free energy to the thermal energy of the system. If the thermal energy is greater than the energy of association for the leucine zippers, the probability of coiled-coil associations

drops, while thermal energy less than the energy for association enhances coiled-coil interactions.

2.6 Elastomeric Proteins

Proteins that deform only under high strains are known as elastomeric proteins. Elastomeric proteins are chemically cross-linked with each other to form covalently-bonded, structured networks, distinguishing them from their self-aggregating, physically cross-linked counterparts. These networks are typically large, comprising many individual components. In addition, these elastomeric protein networks are able to absorb large amounts of energy and then release it, retaking their original form.

To see how this is accomplished, consider a polymer with average end-to-end distances r. It is important to note that there exists a certain volume around each monomer where any other monomers pay a high energy cost to enter. This volume is called the excluded volume, and exists due to steric repulsion forces. Assuming this polymer has N monomers and is in an athermal solvent (one for which the solvent molecules are as attracted to the monomers as the monomers are to each other), the excluded volume of each monomer is given by $v \approx b^3$. The distance b is called the Kuhn length, a measure of the effective bond length of the N bonds that compose a polymer (22). Next, we apply what is known as the Flory theory where the total free energy of the system is calculated as the sum of the internal free energy, $F_{int} = kTv\frac{N^2}{r^3}$, and entropic free energy, $F_{ent} = kT\frac{r^2}{Nb^2}$ (37). Here, k is the Boltzmann constant and T is the temperature. The internal energy is obtained by excluding monomers from a certain space (i.e. the excluded volume parameter), while the entropic energy is the amount of energy required to keep the polymer chain at a size r. The total free energy is then

$$F = F_{int} + F_{ent} \approx kT\left[\frac{vN^2}{r^3} + \frac{r^2}{Nb^2}\right] \tag{2.9}$$

Figure 2.11: A polymer chain being stretched by a force f on both sides. The circles are blobs of diameter ξ.

(22). The average end-to-end distance, r, of the polymer chain is the length that will minimize the free energy. Setting $\partial F/\partial r = 0$ and solving for r, we obtain

$$r \approx v^{1/5} b^{2/5} N^{3/5} \approx b N^{3/5} \tag{2.10}$$

where we have used the fact that in an athermal solvent, $v \approx b^3$ (22).

Consider this same polymer being stretched by a force, f, being applied to each end of the polymer in opposite directions. Polymers are known to be fractal objects up to a certain length scale. This means the physics remains the same when either a smaller or bigger fraction of the polymer of interest is considered. Taking this into account, we may write

$$\xi \approx b g^{3/5} \tag{2.11}$$

where ξ is called the blob size, and g is the number of monomers in said blob (22). Above the length scale of these blobs, the chain reacts to the force, f, by stretching, which changes the size of the end-to-end distance of the polymer, r. At the blob size, however, the polymer chain is only affected by a nearly negligible force, allowing the blob to be modelled as a polymer with the same size as one who is not under any force, as in Figure 2.11. The free energy required for stretching requires about kT amount of energy for each tension blob. As there are $\frac{N}{g}$ blobs,

$$F \approx kT \frac{N}{g} \approx kT \frac{r_f}{\xi} \approx kT \left[\frac{r_f}{r}\right]^{5/2} \tag{2.12}$$

where r_f is the new, extended length of the polymer, and r is the equilibrium length of the polymer not under any force (22). Since $r_f > r$, the amount of energy required to keep the polymer in this state is very high. If the force applied to the polymer were suddenly removed, the probability of the polymer staying stretched to a length r_f is very low, as in equation 2.3. Since there are a fewer number of conformational states in the stretched polymer when compared to the unconstrained polymer, the entropy of this state is low making it unfavourable. This results in the polymer "snapping" back to a smaller average end-to-end distance, giving it a higher entropy and lower free energy.

Elastomeric proteins are those proteins that display the tendencies above, but possess more complicated secondary structures. Due to the covalent bonds, a force applied to the network in one direction will be distributed amongst all components within the network (22). For example, if the network is stretched to twice its original length in the $\hat{x}$-direction, each polymer molecule in the network will be stretched to twice their original length along the $\hat{x}$-direction. Thus, when a stress is applied, the number of conformational arrangements available to each individual elastomer in the network decreases drastically, while the free energy increases. When this stress is removed, the individual elastomers within the network will tend towards smaller end-to-end distances to increase the entropy, causing elastic recoil (5).

Some notable elastomeric proteins include elastin, resilin and gluten. Elastin is an elastomer found in all vertebrate species that allows for the elastic properties present in most organs and tissues (4). This process is necessary, for example, in the vessels and arteries leading to the heart where there are great changes in blood pressure. The elastomeric proteins present in these vessels allow them to stretch elastically at high pressure, then snap back into place as the blood pressure lowers (4). Elastin is also found in the lungs of all animals, allowing their expansion on air intake and subsequent contraction on exhalation with no need for extra muscular input on

the latter.

Resilin is typically only found in arthropods (notably insects), and is known as one of the most efficient elastomeric proteins found in the natural world (5, 38). These properties allow it to be used in the wings of certain insects such as grasshoppers, dragonflies and damselflies (39, 40). The presence of resilin in the joints of the damselfly wings and the leg muscles of fleas and froghopper insects allow the storage of energy once the muscle is compressed (41, 42). The release of this energy provides extra power to the insects, whether it is for flight or leaping.

Gluten is an elastomeric protein typically found in cereal species, such as barley, wheat, and rye (6). This protein is thought to be used to provide a source of necessary elemental building blocks (such as carbon, nitrogen, and sulfur) to aid with germination and subsequent growth of produced seeds, with its elastomeric properties being more an unintended consequence of the amino acid sequence than biological necessity (43). These unintentional elastomeric properties and the tendency of gluten molecules to form disulfide bonds with each other allow for the formation of viscoelastic networks in aqueous solution. A material is said to be viscoelastic when it possesses both elastic properties and viscous properties, a concept which will be elaborated upon in section 3.2. It is these viscoelastic properties that give the many varieties of dough made from gluten their unique attributes, such as their ability to stretch before baking.

Chapter 3

Gels and their Mechanical Properties

3.1 Gel Theory

Gels are solutions whose solute constituents create an interacting network that spans the length of the material. This network may form through either transitional or permanent crosslinks between the solute molecules, where crosslinks are covalent or physical associations between different molecules. Many of them possess properties between those of a solid or a liquid, making them viscoelastic in nature. In the following treatment, only polymer-based gels are considered.

3.1.1 Polymer Chain Statistics

To describe polymeric gels, it is necessary to introduce some basic concepts of polymer physics. An "ideal" polymer chain is distinguished from a "real" polymer chain in that the ideal case assumes that more than one monomer may occupy the same place in space (44). This means for an ideal chain, there are no interactions between monomers, and therefore no excluded volume

interactions (see section 2.6 for a more detailed discussion of excluded volume interactions). The problem of ideal chains statistics will be discussed below and as the ideal case is approximately that of the real one, the latter will only be used as needed (see section 3.1.3).

Ideal Chain Statistics

Consider a polymer composed of N Kuhn monomers of length b, where the Kuhn length is as described in section 2.6. If p of these chains are considered, their mean square end-to-end distance, $< r^2 >$, is then

$$< r^2 >= \frac{1}{p} \sum_{i=1}^{p} \vec{\mathbf{r}}_i^2 \tag{3.1}$$

where $\vec{\mathbf{r}}_i$ is the end-to-end vector distance of the ith polymer (22, 45). This ith polymer can be described as the sum of the N Kuhn monomers of vectorial length b_j, or

$$\vec{\mathbf{r}}_i = \sum_{j=1}^{N} \vec{\mathbf{b}}_j \tag{3.2}$$

For this individual polymer chain, the square end-to-end distance is

$$\begin{aligned} r_i^2 &= \vec{\mathbf{r}}_i \cdot \vec{\mathbf{r}}_i \\ &= \sum_{j=1}^{N} \left[\vec{\mathbf{b}}_j \cdot \vec{\mathbf{b}}_j + 2 \sum_{k=1}^{j-1} \vec{\mathbf{b}}_k \cdot \vec{\mathbf{b}}_j \right] \end{aligned} \tag{3.3}$$

where the dot product between the two vectors $\vec{\mathbf{b}}_j$ and $\vec{\mathbf{b}}_k$ is

$$\vec{\mathbf{b}}_k \cdot \vec{\mathbf{b}}_j = b^2 \cos\theta_{kj} \tag{3.4}$$

with θ_{kj} the angle between the two vectors. The square end-to-end distance is a useful means of determining the actual size of a polymer. As there is an equal probability that the vector $\vec{\mathbf{r}}$ will move in one of two opposite direc-

tions, the average of $< \vec{\mathbf{r}} >= 0$. Thus, the square end-to-end distance is more useful as its root provides a magnitude which may be used in calculations.

To evaluate the second sum in equation 3.3, consider that there is no restriction on the direction of either of the Kuhn monomers $\vec{\mathbf{b}}_k$ or $\vec{\mathbf{b}}_j$. This means that there is an equal probability that the angle between the two is either $\cos\,\theta_{kj}$ or $\cos\,(\theta_{kj} + \pi) = -\cos\,\theta_{kj}$. Thus, the second sum in equation 3.3 must be equal to 0. This leaves the first sum in equation 3.3. The angle between $\vec{\mathbf{b}}_j$ and itself is 0, making the cosθ term equal to 1. Therefore, equation 3.3 can be rewritten as $r_i^2 = Nb^2$, and equation 3.1 is then

$$\begin{aligned} < r^2 > &= \frac{1}{p}\sum_{i=1}^{p} Nb^2 \\ &= Nb^2 \end{aligned} \tag{3.5}$$

The result of equation 3.5 can be used to determine the entropy present in a network of ideal chain polymers. Ideal chains grow in a random walk pattern, meaning that there is an equal probability that monomer $i + 1$ attached to monomer i will branch off in any direction. Polymers that grow via random walk patterns follow Gaussian statistics. In one dimension, the probability distribution function, P_x, of an ideal chain polymer can be written as

$$P(N, r_x) = \frac{1}{\sqrt{2\pi < r_x^2 >}} \exp\left(-\frac{r_x^2}{2 < r_x^2 >}\right) \tag{3.6}$$

This probability can be extended to the three dimensions has a probability

distribution function, P, of the form

$$\begin{aligned} P(N, \vec{r}) &= P_x P_y P_z \\ &= \left(\frac{1}{2\pi < r_x^2 >}\right)^3 \exp\left(-\frac{r_x^2}{2 < r_x^2 >}\right) \cdot \\ &\quad \left(\frac{1}{2\pi < r_y^2 >}\right)^3 \exp\left(-\frac{r_y^2}{2 < r_y^2 >}\right) \cdot \\ &\quad \left(\frac{1}{2\pi < r_z^2 >}\right)^3 \exp\left(-\frac{r_z^2}{2 < r_z^2 >}\right) \end{aligned} \tag{3.7}$$

because the probability in all directions is equal. As the probability of an ideal chain going in either the x, y, or z direction is equal, and the sum of mean square displacements for x, y, and z must equal the total mean square displacement of Nb^2, we may write $< r_x^2 >=< r_y^2 >=< r_z^2 >= \frac{Nb^2}{3}$. Assuming ideal chain statistics, we may use this result in equation 3.6 to give

$$P(N, \vec{r}) = \left(\frac{3}{2\pi N b^2}\right)^{3/2} \exp\left(-\frac{3r^2}{2Nb^2}\right) \tag{3.8}$$

(22).

The entropy and free energy of an ideal chain can be computed by relating the probability distribution function from equation 3.8 to the number of ways of arranging the system, w, via the equation

$$P(N, \vec{r}) = \frac{w(N, \vec{r})}{\int w(N, \vec{r}) \mathrm{d}\vec{r}} \tag{3.9}$$

Recalling equation 2.2 from section 2.3.4, the entropy of an ideal polymer

chain can be written using equation 3.9 as

$$\begin{aligned} S_{ent}(N, \vec{r}) &= k \ln P(N, \vec{r}) + k \ln \left[\int w(N, \vec{r}) \mathrm{d}\vec{r} \right] \\ &= -\frac{3k\vec{r}^2}{2Nb^2} + \frac{3}{2}k \ln \left(\frac{3}{2\pi N b^2} \right) + k \ln \left[\int w(N, \vec{r}) \mathrm{d}\vec{r} \right] \\ &= -\frac{3k\vec{r}^2}{2Nb^2} + S_{ent}(N, 0) \end{aligned} \tag{3.10}$$

where k is the Boltzmann constant, and $S(N, 0)$ is the amount of entropy independent of the end-to-end vector, $\vec{r}$.

3.1.2 Gel Types

The point at which a solution's solute molecules first form a network spanning one end of a substance to the other is called the gel point. It is at this the point at which a gel is said to have formed (22, 46). Gels can utilize many different kinds of molecules as a solvent and may be formed through colloids, though here we will only consider polymeric solute molecules. The polymeric components of the substance that are not yet a part of this spanning network of interacting molecules are termed the sol. The physical traits of these systems depend on the type of gel formed and can be quite varied.

The number of possible crosslinks that a polymer can make with other polymer molecules in its surroundings determines whether or not a solution with these polymers as solute molecules may form a gel. This number is called the *functionality*, f, of the polymer. If a polymer could only interact with two or fewer other polymers at most (i.e. $f < 3$) the result will be a solution of longer polymeric molecules. These molecules could not form a network that spans the material and is therefore cannot be called a gel. If $f \geq 3$, the polymers present may form branches, where one polymer can associate with multiple other polymers. This branching is necessary for gel formation, and so is assumed to be the case in all gels discussed.

Gels can be either physical or chemical in nature. Physical gels are those

that form via a physical process, such as electrostatic interactions or entanglements. This can create either a strong or weak physical gel. A physical gel is said to be strong when, at a specific set of physical conditions, the network it creates does not melt or flow. This occurs because of the strong physical interactions amongst the constituents that do not allow the gel to easily change its shape. Examples of strong physical interactions include intertwined double and triple helices and entanglements between polymers. Weak physical gels are formed via weak interactions amongst the constituents, such as hydrogen bonding, electrostatic interactions, or hydrophobic interactions. These interactions form reversible crosslinks that break and reform on a finite timescale.

Chemical gels are different from physical gels in that they form via covalent bonds between molecules. These gels are always strong. Regardless of the methods used to crosslink the gels, the resultant networks always display the same behavior, as will be described in the following section.

3.1.3 Chemically Crosslinked Gels

Chemically crosslinked gels form strong networks through their covalent bonds. This is reflected in their physical characteristics since they act as viscoelastic solids. To understand chemical gels, it is necessary to first consider what can be called a "dry" network. This network of polymers is assumed not to be in solution; thus, a "dry" network is not a gel. Models for chemical gels, however, assume a dry network as a basis, using the results of the theory to formulate important concepts. The models are then extended to assume that such a network is "swollen" by a solvent, thereby affecting certain physical properties, and allowing more information to be gleaned. In the following discussion of chemical gels, the theory of rubber elasticity is first used to describe the dry network of polymers, followed by the thermodynamic changes that occur once this network is dissolved in a solvent to form a chemical gel.

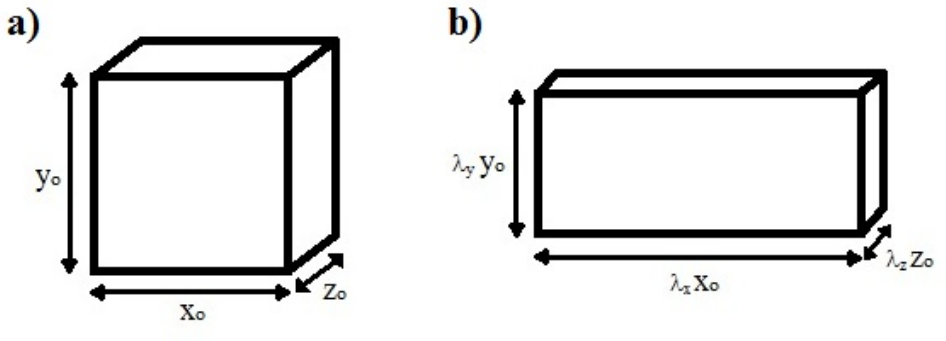

Figure 3.1: A chemically crosslinked material **a)** in an undeformed state with initial dimensions x_o, y_o, and z_o, and **b)** in a deformed state with new dimensions $\lambda_x x_o$, $\lambda_y y_o$, and $\lambda_z z_o$.

Theory of Rubber Elasticity

The theory of rubber elasticity can be described by the $affine\ network\ model$, which assumes ideal chain statistics (see section 3.1.1 for a description of ideal chains). To understand this model, suppose that a material of chemically crosslinked polymers is deformed such that it will stretch along one direction, and compress in all other directions, as in Figure 3.1. If its initial dimensions are x_o, y_o, and z_o, then its dimensions in the deformed state are $\lambda_x x_o$, $\lambda_y y_o$, and $\lambda_z z_o$, where λ_i is some constant numerical factor. As the material is composed of a network of polymers, any deformation occurring to the material as a whole can be assumed to occur in the same way for the polymers composing it. If one individual polymer is considered, the change in its initial dimensions r_{ox}, r_{oy}, and r_{oz} can be related to its new dimensions (r_x, r_y, and r_z) by the factors λ_i, or

$$r_x = \lambda_x r_{ox} \tag{3.11a}$$

$$r_y = \lambda_y r_{oy} \tag{3.11b}$$

$$r_z = \lambda_z r_{oz} \tag{3.11c}$$

If the assumption is made that the polymer chains are ideal, then the entropy of one ideal polymer chain is given by equation 3.10, with $\vec{r}^2 = r_x^2 + r_y^2 + r_z^2$. The change in entropy of a single, ideal chain upon deformation is given by

$$\begin{aligned}\Delta S_{ent}(N, \vec{r}) &= S_{ent}(N, \vec{r}) - S_{ent}(N, \vec{r}_o) \\ &= \left(-\frac{3k(r_x^2 + r_y^2 + r_z^2)}{2Nb^2} + S(N,0)\right) \\ &\quad - \left(-\frac{3k(r_{ox}^2 + r_{oy}^2 + r_{oz}^2)}{2Nb^2} + S(N,0)\right) \\ &= -\frac{3k}{2Nb^2}\left[(\lambda_x^2 - 1)r_{ox}^2 + (\lambda_y^2 - 1)r_{oy}^2 + (\lambda_z^2 - 1)r_{oz}^2\right]\end{aligned} \tag{3.12}$$

From equation 3.12, the change in entropy for the entire network is therefore the sum of the entropic contributions of every individual network strand, or

$$\Delta S_{network} = -\frac{3k}{2Nb^2}\sum_{i=1}^{n}\left[(\lambda_x^2 - 1)(r_{oix}^2) + (\lambda_y^2 - 1)(r_{oiy}^2) + (\lambda_z^2 - 1)(r_{oiz}^2)\right] \tag{3.13}$$

where n is the number of ideal chains in the network. Recall that for an ideal chain, the mean square end-to-end distances of each component are related by $< r_o ix^2 >=< r_o yi^2 >=< r_o iz^2 >= \frac{Nb^2}{3}$. For n ideal chains of the same composition, the equation

$$< r_{ox}^2 >= \frac{1}{n}\sum_{i=1}^{n} r_{oix}^2 \tag{3.14}$$

must hold by definition of the mean square end-to-end distance. Therefore, equation 3.13 may be rewritten as

$$\begin{aligned}\Delta S_{network} &= -\frac{3k}{2Nb^2}\left[(\lambda_x^2 - 1)(n\frac{Nb^2}{3}) + (\lambda_y^2 - 1)(n\frac{Nb^2}{3}) + (\lambda_z^2 - 1)(n\frac{Nb^2}{3})\right] \\ &= -\frac{nk}{2}(\lambda_x^2 + \lambda_y^2 + \lambda_z^2 - 3)\end{aligned} \tag{3.15}$$

As discussed in section 2.6, the entropy is an important factor in determining the free energy of a polymer, or in this case a polymer system. The Helmholtz free energy of a deformed polymer network is related to the entropy by equation 2.1, which in the case of a deformed network of ideal polymers can be written using equation 3.15 as

$$\begin{aligned}\Delta F &= F_{deformed} - F_{undeformed} \\ &= (E_o - TS_{deformed}) - (E_o - TS_{undeformed}) \\ &= -T\Delta S \\ &= \frac{nkT}{2}(\lambda_x^2 + \lambda_y^2 + \lambda_z^2 - 3)\end{aligned} \tag{3.16}$$

The relative deformations of the material (λ_x, λ_y, and λ_z) are not independent of one another, as an elongation along one axis will cause a relative reduction in the other two. If the volume of the new, deformed state is assumed to be exactly the same as that of the undeformed state, the relation between the deformation constants is

$$\lambda_x \lambda_y \lambda_z = 1 \tag{3.17}$$

If the deformation is along the $\hat{x}$-direction, then the two other directions should experience the same amount of deformation as the other. This leads to the relations $\lambda_y = \lambda_z = \frac{1}{\sqrt{\lambda}}$, where $\lambda = \lambda_x$. The free energy is then

$$\Delta F = \frac{nkT}{2}\left(\lambda^2 + \frac{2}{\lambda} - 3\right) \tag{3.18}$$

The free energy of an ideal chain network can also be related to the force applied to it. If the force, f_x is assumed to occur in one direction (say the

$\hat{x}$-direction), the equation for the force is obtained by

$$\begin{aligned} f_x &= \left(\frac{\partial \Delta F}{\partial L_x}\right) \\ &= \left(\frac{\partial \Delta F}{\partial (\lambda L_{ox})}\right) \\ &= \frac{1}{L_{ox}} \frac{\partial \Delta F}{\partial \lambda} \\ &= \frac{nkT}{L_{ox}} \left(\lambda - \frac{1}{\lambda^2}\right) \end{aligned} \tag{3.19}$$

where L_{ox} is the initial size of the material along the $\hat{x}$-direction and L_x is the final size of the material along the $\hat{x}$-direction. The component of stress, σ_{xx}, applied along the $\hat{x}$-direction to the surface with normal $\hat{x}$, can also be determined via

$$\sigma_{xx} = \frac{f_x}{L_y L_z} = \frac{nkT}{L_{ox} L_y L_z} \left(\lambda - \frac{1}{\lambda^2}\right) = \frac{nkT\lambda}{L_{ox} L_{oy} L_{oz}} \left(\lambda - \frac{1}{\lambda^2}\right) \tag{3.20}$$

where the fact that the deformation along the $\hat{y}$-direction and $\hat{z}$-direction is equal to $\frac{1}{\sqrt{\lambda}}$. Assuming this material has rectangular dimensions, the volume is defined as $L_{ox} L_{oy} L_{oz}$, and the total stress, σ, is

$$\sigma = \frac{nkT\lambda}{V} \left(\lambda - \frac{1}{\lambda^2}\right) \tag{3.21}$$

Equation 3.21 is useful in determining what is called the "stress relaxatiom nodulus" (or shear modulus), G, of the ideal chain network. This value determines the relative strength of a material, and is found via the ratio of stress to relative deformation, or

$$G = \frac{\sigma}{\left(\lambda - \frac{1}{\lambda^2}\right)} = \frac{nkT}{V} = \frac{\rho \Re T}{M_c} \tag{3.22}$$

where ρ is the density of the polymer, $\Re$ is the ideal gas constant, and M_c

is the molecular mass of a polymer chain. Equation 3.22 is a surprising result in that as the temperature increases, so does the shear modulus. This means that a chemically cross-linked material will actually stiffen at higher temperatures, requiring more of a force (or stress) than at a lower temperature to induce the same deformation. This can be understood by considering that at higher temperatures a molecule will have more thermal and therefore more kinetic energy. This thermal energy allows a polymer to increase its resistance to being sculpted into a specific shape; this occurs because at higher kinetic energies, a polymer is harder to keep "still". Thus, it will want to spring back to a size that lets it move around more. It should also be noted that this stress relaxation modulus is independant of time due to the mutual independence of its components. This important characteristic differentiates a chemically crosslinked network from a physical one, as will be seen in section 3.1.4.

Another important quantity present in equation 3.22 that will be elaborated upon in section 3.1.4 is the number of elastically effective chains in the network, $\frac{\rho\Re}{M_c}$. This is the number of polymer chains that contribute towards the elasticity of the network. In the affine network theory of rubber elasticity, it is assumed that all of the polymer chains are contributing towards the elasticity of the network.

In reality, the affine network model of rubber elasticity can only be an approximation due to entanglement effects (45, 47). Entanglements occur when one polymer chain gets wrapped around another. When a stress is applied to such a system, the entanglements themselves will contribute to resisting the deformation as neither polymer may physically pass through the other. Thus, the modulus for such a system must be higher, and is typically represented by the approximation

$$G \cong G_x + G_e \approx \rho\Re T\left(\frac{1}{M_x} + \frac{1}{M_e}\right) \tag{3.23}$$

where G_x is the contribution of the crosslinks in the network to the shear

modulus, G_e is the entanglement contribution to the shear modulus, M_x is the molecular weight of the chain length between crosslinks, and M_e is the minimum molecular weight in order for entanglements to be observed (48). From equation 3.23, it can be seen that as the distance (or molecular weight) between crosslinking sites increases, the contribution of entanglements increases. This follows from the idea that the crosslinks restrict the motion of a polymer in a network. With less polymer crosslinking sites, there is more freedom for the chain to move about dynamically, making it more likely it will be entangled.

Solvent Swelling

As mentioned previously, chemical gel networks are inadequately described by the theory of rubber elasticity alone. Any model of a chemical gel must take into account solvent interactions with the crosslinked network. Depending on the kind of solvent used, when a solvent is considered in relation to a crosslinked network, it can be thought of as "swollen" in that solvent molecules permeate the polymer network, taking up volume inside it, and ultimately pushing the network molecules apart. In the following discussion, the polymer molecules that compose the network are considered to be the solute molecules. In addition, it will be assumed that the solute molecules behave as real chains in that the chains have excluded volume interactions (see section 2.6 for a more detailed description of excluded volume interactions).

The solvent used most often in protein polymer networks is what is known as a good solvent. A solvent is called a good solvent when the interactions between the solute molecules and solvent molecules are attractive. As this attraction is governed by physical interactions, such as hydrophobic or electrostatic associations, the electrostatic or hydrophobic nature of the solute (or in this case network molecules) will determine whether a solvent is deemed "good" or not. Athermal solvents, as described in section 2.6, are solvent molecules that are exactly the same as the solute network. This means that

athermal solvents are good solvents in the limiting case where the solvent particles are very attracted to the solute network (22).

When polymer molecules are dissolved in a solvent, the volume fraction, ϕ, of polymer chains to solvent plays an important part in the physical characteristics of the resulting solution. A solution with very few chains and a lot of solvent is called a dilute solution. In a dilute solution, the polymer molecules will behave as though they were completely isolated from one another. A solution where the concentration of polymer molecules is just high enough that the chains overlap and interact is called a semi-dilute solution. It is useful to define the overlap concentration, ϕ^*, as the volume fraction at which polymer chains begin to interact as though they were closely packed by

$$\phi^* \approx \frac{Nb^3}{r^3} \tag{3.24}$$

where N is the number of Kuhn monomers in the polymer, b is the Kuhn length of the Kuhn monomer, and r is the average end-to-end distance of a polymer in these conditions. As the polymers are real chains, they have excluded volume interactions (22, 49). This allows the result in equation 2.10 for the chain length, r, from section 2.6 to be used in eq 3.24 to give

$$\phi^* \approx \frac{Nb^3}{[bN^{3/5}]^3} \approx N^{-4/5} \tag{3.25}$$

Equation 3.25 shows that as the number of monomers in a polymer increases, the overlap concentration decreases.

Another important physical characteristic of chemical gels is the osmotic pressure, Π. When a good solvent is used in a solution of solute molecules, the solvent will be attracted to the solute. This causes swelling of the molecules due to what is called the osmotic pressure. The osmotic pressure of a solution is defined mathematically as the difference in free energy of a pure solvent, and the resultant solution once solute molecules have been added. Expressed

mathematically,

$$\Pi = -\frac{\partial \Delta F}{\partial V}|_n \tag{3.26}$$

where ΔF is the change in free energy, V is the volume, and n is the number of solute molecules (22, 49). For good solvents and semidilute solution conditions, the osmotic pressure can be written as

$$\Pi \approx \frac{kT\phi}{Nb^3}\left(\frac{\phi}{\phi^*}\right)^z \approx \frac{kT\phi^{z+1}}{b^3}N^{\frac{4z}{5}-1} \tag{3.27}$$

For a semidilute solution, however, the osmotic pressure must be independent of the size of the polymer. This implies the exponent for N must be zero, or $z = \frac{5}{4}$. Thus, the final osmotic pressure is

$$\Pi \approx \frac{kT}{b^3}\phi^{9/4} \tag{3.28}$$

demonstrating a 9/4 dependence of the osmotic pressure on the volume fraction. Furthermore, the osmotic pressure may be related to the concentration of the polymers in solution via the relation $c = \frac{m}{V} = \frac{M}{\aleph_A}\frac{n}{V} = \frac{M}{\aleph_A N b^3}\phi$, where $\aleph_A$ is Avogadro's number, M is the molecular weight of the polymer, and n is the number of solute molecules in solution. From this, equation 3.28 may be used to show the relation between osmotic pressure and concentration as

$$\Pi \propto c^{9/4} \tag{3.29}$$

Equation 3.29 predicts that, for a semidilute solution of polymers in a good solvent, the osmotic pressure is dependent upon the concentration of a substance via a power law.

One final property of chemical gels can be attained through the concentration dependence of the osmotic pressure and consideration of the effect of solvent on the polymer network. Recall that the shear modulus for a material is given by the ratio of the stress, σ, to the relative deformation of the

material, as described in section 3.1.3. As stated before, the osmotic pressure is caused by solvent swelling the solute molecules, or in this case the polymers forming the chemically crosslinked network. This causes the size of the network to increase. From rubber elasticity theory, however, it is known that the polymer network has an entropic resistance to increasing in size. This resistance is governed by the shear modulus. Thus, when a solvent is used to solubilize a chemically crosslinked polymer network to form a chemical gel, the osmotic pressure will try to make it to grow in volume while the elastic properties will attempt to discourage it. As time passes, the osmotic pressure and shear modulus will equilibrate, resulting in a constant volume (50). At this point, the shear modulus will exactly equal the osmotic pressure, and we can say

$$\Pi = G \propto c^{9/4} \tag{3.30}$$

(49, 50). Therefore, for a chemical gel, the shear modulus should demonstrate a power law dependence on the concentration of polymers in the gel.

3.1.4 Physical Crosslinking and Self-Assembly

Other than chemically crosslinking polymers, polymers may form gels by physical associations. These associations may be either weak, or strong (as mentioned in section 3.1.2). As mentioned before, strong physically crosslinked networks are those that form via entanglements. These types of networks are very similar to chemically crosslinked networks in that the entanglements function somewhat like crosslinks, and so they will not be elaborated upon here. The problem of weak, physical gels, however, will be addressed in the following sections.

Physical Interactions

Physical gels composed of polymers may be formed via three kinds of interactions: nodular domains, helical structures, and microcrystallites. Of

particular interest are helical structures, where associations between polymers only occur between helical regions on the chain. These associations are termed bundles, and the site on the polymer at which they occur are called associating sites (8, 48, 51). In aqueous solution these associating regions may be hydrophobic: the hydrophilic solution forces the hydrophobic regions of various molecules to cluster together in an effort to shield them from their environment (9).

Much like the chemical gels mentioned in section 3.1.3, the weakly crosslinked, physical gels addressed here are affected by entanglements and solution conditions. Semidilute solution conditions will be assumed because at very high concentrations, entanglements are the dominating factor in determining gel properties, meaning such a gel would be a strong gel and not a weak gel. At the opposite end of the spectrum, if the polymer concentration in solution was low enough to create dilute solution conditions, the polymers would not interact with one another enough to form a network. Thus, in the following discussion, semidilute solution conditions must be assumed.

The main property governing the interactions of these is the thermoreversibility of their associations. To demonstrate this, consider a weak, physically crosslinked polymer network. Next, assume that there is only one possible physical association between the polymers in the material, whether it is hydrophobic, electrostatic, or some other association. As the crosslinks between polymers are not permanent, there is some time at which such an association will possess enough thermal energy to overcome the energy of the physical association. This causes the physical crosslink to break. If the entire polymer network is considered, the average time at which breaking occurs is called the relaxation time, τ, and is given by

$$\tau = \frac{1}{\beta(T)} \tag{3.31}$$

where $\beta(T)$ is called the breaking function. Tanaka and Edwards have de-

termined this function can be given by the formula

$$\beta(T) = \omega_o \exp\left(-\frac{W}{kT}\right) \tag{3.32}$$

where ω_o is the characteristic frequency of thermal vibration, and W is the amount of energy needed to cause the polymers to dissociate (8, 52). Equation 3.32 demonstrates the dependence of the breaking on the thermal conditions, kT, and so the relaxation time must vary with kT via the relation $\tau \propto \exp\left(\frac{W}{kT}\right)$. At high kT, the polymers have more thermal energy, and so more of them are likely to have enough energy to cause their physical crosslinks to break. Thus, the relaxation time should be lower, reflecting the higher number of dissociations occurring. For low kT, the polymers have less thermal energy, and so are less likely to break their physical associations, reflected by a longer relaxation time.

The relaxation time has important consequences when a stress is applied to a material composed of weak, physical crosslinks. As these crosslinks are time-dependent, the shear modulus must also be time-dependent. Consider the same physically crosslinked network under stress mentioned before. At shorter times than the relaxation time ($\tau >> t$), the physical crosslinks of the polymers have not yet dissociated, so stresses placed on such materials are still distributed throughout the network via the crosslinks (53). This distribution of strain energy throughout the network occurs in exactly the same manner as for a chemical gel because the material makes no distinction between physical and chemical crosslinks. Thus, at short time scales, the shear modulus, $G_{physical}(t \to 0)$, should approach what is known as the plateau modulus, G_∞. This modulus is that of the chemically crosslinked network. For longer times ($\tau < t$), the average crosslink within the network has dissociated. This means the energy stored by polymers in the stretched state, as described in section 3.1.3, must use a new mechanism to rid themselves of the entropic energy and return to a low energy, low average mean square end-to-end length. This is done by viscous friction between the poly-

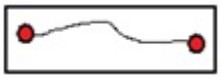

Figure 3.2: A model of a simple telechelic molecule with two reactive end groups (in red), and an unreactive center group.

mers and their surrounding environment. As the polymers lengths shorten to reduce their entropic energy, they collide with the solvent particles and polymers surrounding them. This allows the entropic energy to be dissipated as friction with a polymer's surroundings. In addition, because the elastic (entropic) energy is proportional to the shear modulus, the latter must also decrease with time. Weakly, physically crosslinked materials can therefore be described as viscoelastic liquids: materials that store elastic energy on small time scales, while dissipating the same energy as viscous friction on longer ones.

Telechelic Gels

A telechelic polymer is a linear polymer with two reactive end groups and an unreactive chain, as in Figure 3.2. The term itself was first proposed by Uraneck, *et at* in the 1960s for telechelic, organic chemicals that form gels. (54). Typically, the functional groups at the ends of the polymer are the same, though there exist "heterotelechelic" polymers that have end groups with different functionality (55). In order for telechelic molecules to form gels, their functionality must be greater than 2, as described in section 3.1.2, else they would only form very long polymers. As there are only two associating sites on a telechelic molecule, in order for gelation to occur each site must be able to associate with more than one other polymer. Thus, telechelic polymers that form gels always possess associating sites that bind with two, or more, associating sites.

The two reactive ends of telechelic polymers act as physical association sites, allowing them to be crosslinked into physical gels. This unique loca-

tion for the association sites allow for different kinds of structures within such a network. Consider, for example, a material composed of telechelic molecules in semidilute solution with associating sites that bind to one another. One possible arrangement for a telechelic polymer in these conditions is to have both its associating sites physically crosslink with the associating sites of different molecules within the solution, contributing towards network formation. Another possibility would be for only one association site of this molecule to crosslink with another molecule, causing the molecule to only slightly contribute to network formation. Perhaps the associating sites of a single molecule will react with either themselves or nothing at all, contributing nothing towards network formation (8–10).

The various structures of telechelic polymers in solution allow for different physical characteristics than normal, weakly crosslinked physical gels. At semidilute solution conditions, the last two structures are more unlikely, and so can be ignored. Assuming the first two structures occur, the number of elastically effective chains in the network, ν, can be calculated from the relation

$$\nu = n\left(\frac{e^{W/kT}}{1+e^{W/kT}}\right) \tag{3.33}$$

where n is the total number of telechelic polymers in the network (8, 48). The top term in equation 3.33 is a measure of the number of associations between sites on different polymers, while the bottom considers both associations between sites on different polymers, and sites that are not associating with anything at all (8, 51). This implies a two-state case: either the polymers are a part of the network through the $e^{W/kT}$ term, or they do not contribute at all, represented by the 1. The consequence of equation 3.33 is that only ν associations will contribute towards the elasticity of the network. This means that the shear modulus for telechelic molecules must be modified from

equation 3.22 to give

$$G = \nu kT = nkT \left(\frac{e^{W/kT}}{1 + e^{W/kT}} \right) \tag{3.34}$$

assuming no entanglement contributions.

In addition, telechelic molecules only possess one relaxation time for each kind of network forming association that its end groups can make. As telechelic molecules only have 2 association sites, if even one single crosslink between end groups breaks the polymer no longer contributes to the network, for the reasons described above. If the polymers had possessed more than one association site, the breaking of one crosslink would not affect the network as much because the polymer would still belong to the network through its two or more other association sites. This would allow it to continue to store any applied stress energy as elastic energy. In the case of telechelic molecules, it is therefore an all-or-none case, as described by equation 3.33.

There are two simple models that can be used to describe viscoelastic liquids: the Maxwell model and the Kelvin-Voigt model. In the Maxwell model, materials are treated as though they possessed a component that stores elastic energy in series with another component that dissipates energy through viscous friction. Such materials are called Maxwell fluids. In the Kelvin-Voigt model, an elastic component is placed in parallel with the viscous dissipation component. Annable, *et al*, have shown that self-assembling gels composed of telechelic molecules are well described by the Maxwell model (8, 9). The viscous component dissipates the energy that the elastic component stores, leading to a single, average relaxation time for the system. That telechelic polymer gels are described by a Maxwell model follows from the relations obtained above in equations 3.32, 3.33, and3.34. The reason telechelic molecules follow the Maxwell model as opposed to the Kelvin-Voigt model is that the same component that stores stress energy is the same component that dissipates it via viscous friction. If the molecule were to follow the Kelvin-Voigt

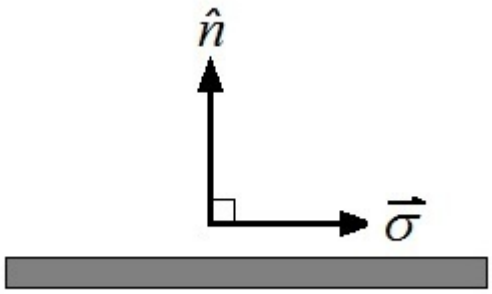

Figure 3.3: A shearing stress, σ, being applied to the surface of a material with a normal vector in the $\hat{n}$ direction.

model, there would have to be two separate components that only function in one specific way: one that stores elastic energy and one that dissipates it. As telechelics store energy via the same component through which they dissipate energy (i.e. their free ends), they must follow a Maxwell model. For a more detailed discussion of Maxwell fluids and their properties, refer to section 3.2.1.

3.2 Rheological Theory

3.2.1 Basic Rheology

Rheology is the study of how matter flows and deforms. Typically this is accomplished by subjecting a material to mechanical *shearing* forces or stresses of some kind. To shear a material is to apply a stress or force to a surface in a direction perpendicular to that surface's normal vector, as in Figure 3.3.

Consider a material between two plates separated by a distance y. If the top plate is subjected to a shear stress (σ) causing it to move while the bottom plate remains immobile, the material touching the top plate will move a distance Δx in the same direction due to frictional forces. This will create a deformation gradient, as in Figure 3.4. The *strain* (γ) of the sample

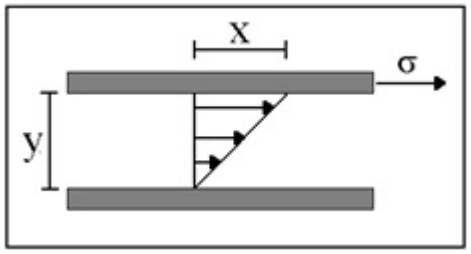

Figure 3.4: A material between two plates separated by a distance y. If the top plate is subject to a stress, σ, both the plate and the material touching the top of the plate will move a distance Δx.

is defined as

$$\gamma = \frac{\Delta x}{y} \tag{3.35}$$

while the *strain rate* ($\dot{\gamma}$) is

$$\dot{\gamma} = \frac{d\gamma}{dt} \tag{3.36}$$

If the material is a perfectly Newtonian fluid, we may say that

$$\sigma = \eta \cdot \dot{\gamma} \tag{3.37}$$

where η is said to be the *viscosity* of the liquid. If the material is a solid, we may say that

$$\sigma = G \cdot \gamma \tag{3.38}$$

where G is the *shear modulus* of the material (9). In reality, some materials exist in a phase that cannot be definitely called either solid or liquid, displaying instead qualities of both. These materials are said to be *viscoelastic*.

All deformed materials possess what is called a strain history. This term describes how the deformation of a material at time t is dependent upon all previous deformations it has undergone. Keeping this in mind, the total stress placed upon a material may be calculated. When a material is subject to different kinds of individual step strains, $\delta\gamma_i$, over a period of time t_i, the

overall stress on the material may be defined as a linear superposition by

$$\sigma(t) = \sum_i G(t - t_i)\delta\gamma_i = \sum_i G(t - t_i)\dot{\gamma}_i \delta t_i \tag{3.39}$$

where $\gamma_i^{\cdot}$ is the strain rate from equation 3.36, $G(t - t_i)$ is the relaxation modulus of the material, and t_i is the time at which even i occurs. This relation may be changed to an integratal

$$\sigma(t) = \int_{-\infty}^{t} G(t - t')\dot{\gamma}(t')dt' \tag{3.40}$$

which takes into account all strain deformations of the material over a time t' to determine the stress on the material ($\sigma(t)$) at time t (22, 56, 57).

Viscoelastic Fluids

Consider a Maxwell fluid, as described in section 3.1.4, with a spring and a dashpot in series as in Figure 3.5. If a stress, σ, is applied to this system at time $t = 0$, the stress on each component, σ_i, will be equal while the components of strain, γ_i will not. This may be written as

$$\sigma = \sigma_S = \sigma_D \tag{3.41a}$$

$$\gamma = \gamma_S + \gamma_D \tag{3.41b}$$

$$\sigma(t) = G(t)\gamma \tag{3.41c}$$

where the subscripts S and D represent the spring and dashpot, respectively, $G(t)$ is the time dependant relaxation modulus, and γ is the overall strain of the system. From equations 3.37, 3.38, 3.41a, and 3.41b, we can write

$$\sigma(t) = G(t)\gamma_S = G(t)(\gamma - \gamma_D(t)) = \eta\frac{d\gamma_D}{dt} \tag{3.42}$$

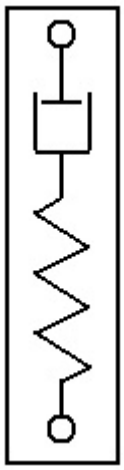

Figure 3.5: Schematic diagram of a Maxwell fluid: a dashpot and spring in series. Certain kinds of telechelic polymer gels have been found to act as Maxwell fluids.

which is a differential equation with stress relaxation modulus $G(t)$. The solution to this differential equation is

$$\gamma = \gamma_D = Ae^{-\frac{G_M t}{\eta}} \tag{3.43}$$

where A is a constant of integration, and G_M is a constant term. If no stress was applied to the system prior to the stress at $t = 0$, then the strain on the dashpot at that time was $\gamma_D(0) = 0$, and

$$\gamma = A \tag{3.44}$$

Substituting 3.44 into 3.43 and using 3.42 and 3.41c, equation 3.43 can be rearranged to obtain

$$G(t) = G_M e^{-\frac{G_M t}{\eta}} = G_M e^{-\frac{t}{\tau_M}} \tag{3.45}$$

where the relaxation time is defined as

$$\tau_M = \frac{\eta}{G_M} \tag{3.46}$$

The relations expressed in equations 3.45 and 3.46 are the expected response of any material that acts as a Maxwell fluid to stresses. From this, we should expect that any such material, including networks composed of telechelic polymers (see section 3.1.4), will only possess one relaxation time, τ_M, as defined above.

For the Kelvin-Voigt model, the two components (the elastic spring and the viscous dashpot) are in parallel. When a strain (γ) is applied to the system, the strain of each component should be equal to that strain ($\gamma = \gamma_S = \gamma_D$), while the overall stress of the system will be a linear combination of the stresses of each component ($\sigma = \sigma_S + \sigma_D$). As the spring has its strain related to the stress by $\sigma = G_S\gamma$, where G_S is a constant stress relaxation modulus, and the dashpot's strain is related to the stress via $\sigma = \eta\frac{d\gamma}{dt}$, where η is the viscosity, the overall stress on the system is then

$$\sigma(t) = G_S\gamma + \eta\frac{d\gamma}{dt} \tag{3.47}$$

If a constant stress (σ_o) is applied and placed in equation 3.47, the resultant stress relaxation modulus ($G(t)$) can be derived to be

$$G(t) = G_S + \eta\delta(t) \tag{3.48}$$

where $\delta(t)$ is the Dirac delta function.

It has been known for some time, however, that many telechelic gel systems demonstrate deviations from the standard Maxwell model (58–60). In particular, research by Berret, *et al* that has focused on fluorocarbon-based telechelic systems and that by Tsitsilianis, *et al* on hydrophobic polystyrene end-capped telechelics have demonstrated so-called stretched exponential be-

havior (60–64). This behavior is expressed by the relation

$$G(t) = G_\infty \exp\left[-\left(\frac{t}{\tau}\right)^\beta\right] \tag{3.49}$$

where t possess the same definitions as in equation 3.45, G_∞ is the stress relaxation modulus at short time scales, τ is a relaxation time, and β is a constant for a particular system with values of $0 < \beta \leq 1$. The case of $\beta = 1$ corresponds to the standard Maxwell model.

3.2.2 Complex Rheology

One interesting way of studying viscoelastic materials is through *oscillatory shear*. Consider a material undergoing an oscillating strain $\gamma(t)$ at a driving frequency ω, or

$$\gamma(t) = \gamma_o \sin(\omega t) \tag{3.50}$$

applied to an object. For a perfect, Newtonian fluid, equation 3.37 implies that the stress needed to cause such a strain is given by $\sigma(t) = \sigma_o \cos(\omega t) = \sigma_o \sin(\omega t + \frac{\pi}{2})$. The strain is therefore out of phase with the stress by $\frac{\pi}{2}$ for a Newtonian fluid. Perfectly elastic solids follow equation 3.38, thus oscillating stresses are in phase with oscillating strains.

While this is true for Newtonian fluids and elastic solids, a viscoelastic material's response to a stress is more complex in that the strain is out of phase with the stress by a constant δ. This can be written as

$$\sigma(t) = \sigma_o \sin(\omega t + \delta) \tag{3.51}$$

for a viscoelastic material (56). Replacing equation 3.50 into equation 3.40 gives

$$\sigma(t) = \int_{-\infty}^{t} G(t - t')\gamma(\dot{t'})dt' = \gamma_o \omega \int_{-\infty}^{t} G(t - t')\cos(\omega t')dt' \tag{3.52}$$

This relation may be further simplified by defining some time $t'' = t - t'$ and placing it into equation 3.52

$$\sigma(t) = \gamma_o \omega \int_0^\infty G(t'') \cos[\omega(t - t'')] dt'' \tag{3.53}$$

Using the trigonometric relation $\cos(\alpha - \beta) = \cos(\alpha)\cos(\beta) + \sin(\alpha)\sin(\beta)$, equation 3.53 becomes

$$\begin{aligned}
\sigma(t) &= \gamma_o \omega \int_0^\infty G(t'') [\sin(\omega t)\sin(\omega t'') + \cos(\omega t)\cos(\omega t'')] dt'' \\
&= \gamma_o \sin(\omega t)\omega \int_0^\infty G(t'')\sin(\omega t'') dt'' + \gamma_o \cos(\omega t)\omega \int_0^\infty G(t'')\cos(\omega t'') dt'' \\
&= \gamma_o G'(\omega)\sin(\omega t) + \gamma_o G''(\omega)\cos(\omega t)
\end{aligned} \tag{3.54}$$

where $G'(\omega)$ is called the *storage modulus*, and $G''(\omega)$ is called the *loss modulus*. The storage modulus is a measure of the elastic energy stored by a viscoelastic material under stress, while the loss modulus is a measure of the amount of energy dissipated by such a material. It can be seen from this relation that the storage and loss moduli are respectively the sine and cosine Fourier transforms of the stress relaxation modulus $G(t)$ times ω. Thus, they may be written as

$$G' = \omega \int_0^\infty G(t)\sin(\omega t) dt \tag{3.55a}$$

$$G'' = \omega \int_0^\infty G(t)\cos(\omega t) dt \tag{3.55b}$$

These moduli can also be used to define what is called the *complex modulus*, G^*, via the relation

$$G^* = G' + iG'' \tag{3.56}$$

Recall that the oscillatory stress of a viscoelastic material is out of phase with the strain by a factor δ. The storage and loss modulus may then be

written in terms of this constant as

$$G' = \frac{\sigma_o}{\gamma_o}\cos\delta \tag{3.57a}$$

$$G'' = \frac{\sigma_o}{\gamma_o}\sin\delta \tag{3.57b}$$

where σ_o is the amplitude of the oscillating stress, and γ_o is the amplitude of the oscillating strain.

For chemical gels, the storage and loss moduli should be essentially independent of the angular frequency. This independence arises from the relations derived in section 3.1.3. As can be seen in the equations in this section, there is no dependence of the shear modulus on time. Thus, when the modulus is integrated with respect to time in equation 3.40 and the Fourier transform is applied to the resulting equation, the resultant complex modulus and its components (G' and G'') should be independent of angular frequency.

Though chemical gels should only possess the storage modulus component due to their elastic storage capabilities, in reality a loss modulus component is also measured. This component is a measure of the relative amount of energy dissipated throughout the chemical gel via loose ends.

Complex Viscoelastic Fluid Models

The storage and loss moduli for a Maxwell fluid composed of a polymer network can be determined by performing the sine and cosine Fourier transforms on the stress relaxation modulus from equation 3.45. This gives, for the storage and loss moduli

$$G'(\omega) = G_\infty \frac{\omega^2\tau^2}{1+\omega^2\tau^2} \tag{3.58a}$$

$$G''(\omega) = G_\infty \frac{\omega\tau}{1+\omega^2\tau^2} \tag{3.58b}$$

where ω is the angular frequency, τ is the average relaxation time of the material, and G_∞ is the modulus of a chemical gel with polymers of the same size as those used in the physical gel. These equations can be used to determine the relaxation frequency, which is the inverse of the average relaxation time. At this frequency, the moduli are given by $G' = \frac{1}{2}G_\infty = G''$. Therefore, the characteristic relaxation time can be determined at the point where the moduli are equal, called the crossover modulus.

The temperature dependence of the relaxation time will also have an effect on the crossover modulus of a telechelic polymer system. As the temperature of the material increases, the relaxation time must decrease. This causes an increase in the relaxation frequency, meaning the point at which the moduli are equal will shift to higher frequencies. A decrease in temperature will have the opposite effect, causing a shift in the crossover modulus towards lower frequencies. A linear concentration dependence for the relaxation time was determined by Annable, *et al* for telechelic polymer solutions. This linear relationship could be explained by considering that at higher concentrations, there are more telechelic polymers through which to distribute a strain placed upon the system. This means there is less energy distributed through each individual physical crosslink, and therefore less elastic stretching of individual polymers. This reduced elastic stretching means smaller elongations on average, making it less unfavourable for the polymers to be in such a stretched configuration. This places less strain on the physical crosslink associations, reducing the number that break, and thereby increasing the relaxation time. In addition, the increase in polymer concentration allows more energy to be stored in the system elastically, then dissipated as more polymers will be stretched by the stress. Thus, an increase in both G' and G'' should also be observed. Most real proteins, however, demonstrate more complex rheological behavior, as will be shown in succeeding chapters.

The Kelvin-Voigt possesses a different stress relaxation modulus from the Maxwell model, as given by equation 3.48. Taking the Fourier sine and cosine

transforms on equation 3.48 gives

$$G'(\omega) = G_S \tag{3.59a}$$

$$G''(\omega) = \eta\omega \tag{3.59b}$$

The relations given by equations 3.59a and 3.59b are relatively simple: G' is a constant term with respect to ω, while G'' possesses a simple, linear relation with respect to ω. It is clear that the Maxwell models and Kelvin-Voigt models possess very different properties that should be readily visible given experimental data.

Performing the sine and cosine Fourier transforms on the stretched exponential model (equation 3.49) using Wolfram Mathematics software results in non-analytical results, complicating modelling of both G' and G''. For the case $\beta = \frac{1}{2}$, however, much simpler functions are obtained for both moduli

$$\begin{aligned} G'(\omega) = G_\infty & \frac{\sqrt{\frac{\pi}{2}}\left(1 - \mathrm{C}\left(\frac{1}{\sqrt{2\pi\omega\tau}}\right)\right)\sin\left(\frac{1}{4\omega\tau}\right)}{2\sqrt{\omega\tau}} \\ & - G_\infty\sqrt{\frac{\pi}{2}}\left(\frac{\left[\left(1 - \mathrm{S}\left(\frac{1}{\sqrt{2\pi\omega\tau}}\right)\right)\cos\left(\frac{1}{4\omega\tau}\right)\right]}{2\sqrt{\omega\tau}} + 1\right) \end{aligned} \tag{3.60}$$

$$\begin{aligned} G''(\omega) = G_\infty & \frac{\sqrt{\frac{\pi}{2}}\left(1 - \mathrm{C}\left(\frac{1}{\sqrt{2\pi\omega\tau}}\right)\right)\sin\left(\frac{1}{4\omega\tau}\right)}{2\sqrt{\omega\tau}} \\ & + G_\infty\frac{\sqrt{\frac{\pi}{2}}\left(1 - \mathrm{S}\left(\frac{1}{\sqrt{2\pi\omega\tau}}\right)\right)\cos\left(\frac{1}{4\omega\tau}\right)}{2\sqrt{\omega\tau}} \end{aligned} \tag{3.61}$$

where $C(\alpha) = \int_0^\alpha \cos(\frac{\pi x^2}{2})dx$ and $S(\alpha) = \int_0^\alpha \sin(\frac{\pi x^2}{2})dx$ are the Fresnel integrals.

3.2.3 Rheometry

While rheology is the theoretical approach to determining the viscoelastic properties of a material, rheometry is the experimental side, though both

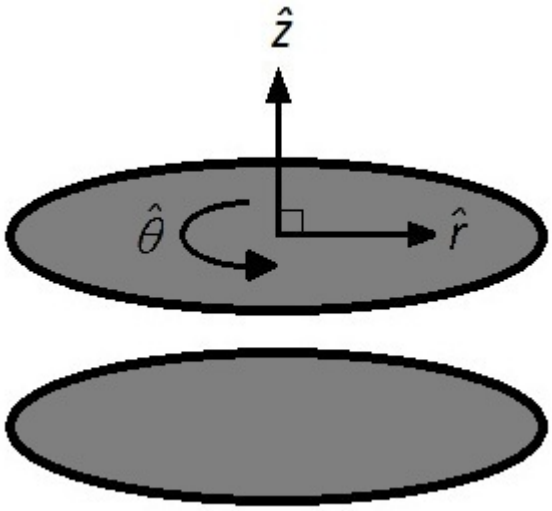

Figure 3.6: Schematic diagram of the plate-plate geometry which can be used to apply a stress in the $\hat{\theta}$-direction.

terms are sometimes used interchangeably in an experimental setting. Typical rheometry experiments involve applying a stress or a strain to a material using a specific geometry to measure the opposing response. This technique allows either strain to be measured as a function of stress, or vice-versa. These measurements make it possible to calculate the storage and loss moduli (G' and G'', respectively) for the material.

To determine the complex modulus components, the material must be subject to an oscillatory shearing stress as in section 3.2.2. One possible means of applying this stress is via a plate-plate geometry, as in Figure 3.6. If a material is placed between the two plates, a shear stress may be applied by moving the top plate in the $\hat{\theta}$-direction while keeping the bottom plate immobile (65).

The relations derived in section 3.2.2 are simplified derivations for scalar quantities. In reality, stresses and strains must be expressed as tensors to consider all possible deformations on a three-dimensional object. We may

define the *stress tensor*, $\boldsymbol{\sigma_{ij}}$, as

$$\boldsymbol{\sigma_{ij}} = \begin{vmatrix} \sigma_{xx} & \sigma_{xy} & \sigma_{xz} \\ \sigma_{yx} & \sigma_{yy} & \sigma_{yz} \\ \sigma_{zx} & \sigma_{zy} & \sigma_{zz} \end{vmatrix} \tag{3.62}$$

where each component, σ_{ij}, represents a force in the i-direction being applied to a surface with a normal in the j-direction (66). It is important to note that these tensors are symmetric, so $\sigma_{ij} = \sigma_{ji}$. This tensor symmetry is called the Cauchy rule (66). From the geometry of Figure 3.6, if a force is applied in the $\hat{\theta}$-direction, the stress tensor, when converted to cylindrical coordinates, may be reduced to

$$\boldsymbol{\sigma_{ij}} = \begin{vmatrix} 0 & 0 & 0 \\ 0 & 0 & \sigma_{\theta z} \\ 0 & \sigma_{\theta z} & 0 \end{vmatrix} \tag{3.63}$$

where $\sigma_{\theta z}$ is the stress component in the θ-direction being applied to the surface with $\hat{z}$-normal.

It is possible to use the *double dot product* to help determine the "magnitude" of a tensor. This mathematical technique involves the deconstruction of a matrix into two multiplying vectors that are then scalar multiplied together to create a scalar value. In mathematical terms, for an $n \times n$ matrix $\mathbf{A} = \vec{b}\,\vec{c}$, where $\vec{b}$ is an $n \times 1$ matrix, and $\vec{c}$ is an $1 \times n$ matrix, the double dot product is defined as

$$\mathbf{A} : \mathbf{A} = (\vec{b}\,\vec{c}) : (\vec{b}\,\vec{c}) = (\vec{b} \cdot \vec{c})(\vec{b} \cdot \vec{c}) = (\vec{b} \cdot \vec{c})^2 \tag{3.64}$$

The magnitude of a tensor is defined as

$$|\mathbf{A}| = \sqrt{\frac{1}{2}\mathbf{A} : \mathbf{A}} \tag{3.65}$$

Equation 3.65 which allows us to calculate the magnitude of the stress tensor

from equation 3.63, giving

$$|\boldsymbol{\sigma_{ij}}| = \sqrt{\frac{1}{2}\boldsymbol{\sigma_{ij}} : \boldsymbol{\sigma_{ij}}} = \sigma_{\theta z} \tag{3.66}$$

The strain may also be represented by a three-dimensional tensor, $\boldsymbol{\gamma_{ij}}$, defined as

$$\boldsymbol{\gamma_{ij}} = \begin{vmatrix} \gamma_{rr} & \gamma_{r\theta} & \gamma_{rz} \\ \gamma_{\theta r} & \gamma_{\theta\theta} & \gamma_{\theta z} \\ \gamma_{zr} & \gamma_{z\theta} & \gamma_{zz} \end{vmatrix} \tag{3.67}$$

where the component γ_{ij} is the deformation in the j-direction of the surface with a normal in the i-direction, and cylindrical coordinates are used for convenience (66). As the stress is only occurring at the upper plate in the $\hat{\theta}$-direction, the only deformation that occurs must also be in the $\hat{\theta}$-direction on the surface with normal $\hat{z}$, or $\gamma_{\theta z}$. Using equations 3.64 and 3.65 on 3.67 gives

$$|\boldsymbol{\gamma_{ij}}| = \gamma_{\theta z} \tag{3.68}$$

From subsection 3.2.2 and equation 3.54, the stress and strain components may be expressed as

$$\sigma_{\theta z} = \gamma_{\theta z}[G'\sin(\omega t) + G''\cos(\omega t)] \tag{3.69}$$

where an oscillatory stress is assumed, and G' and G'' are the storage and loss moduli, respectively. Equation 3.69 indicates that, using the plate-plate geometry, we may arrive at a simple relationship between the stress and strain on a material, allowing G' and G'' to be easily measured.

It is difficult for rheometers to measure the exact stress being applied to the material in a plate-plate geometry as it is a function of radius (as will be shown). Instead, the torque, T_{tor}, is measured due to its relationship to the applied stress and the simplicity with which it is measured. For circular

disks of radius R, this relation is

$$T_{tor} = 2\pi \int_0^R r^2 \sigma(r) dr = 2\pi \int_0^R r^2 G^* \gamma dr \tag{3.70}$$

where $\sigma(r)$ is the applied stress on the material at radius r (56). The strain of a material in this geometry at a distance r from the middle with an angular displacement θ is

$$\gamma = \frac{\theta r}{h} \tag{3.71}$$

where h is the distance between the two plates (56). The maximum strain possible on the material occurs at the maximum disk radius, R, providing the relation $\gamma_R = \frac{R}{r}\gamma$ and its derivative as $dr = \frac{R}{\gamma_R} d\gamma$. Replacing these in equation 3.70 gives

$$T_{tor} = 2\pi \int_0^{\gamma_R} \left(\frac{R}{\gamma_R}\right)^3 G^* \gamma^3 d\gamma \tag{3.72}$$

The Leibnitz rule is given by

$$\frac{d}{d\alpha} \int_{a(\alpha)}^{b(\alpha)} f(x,\alpha) dx = \int_{a(\alpha)}^{b(\alpha)} \frac{\partial}{\partial \alpha} f(x,\alpha) dx + \frac{db(\alpha)}{d\alpha} f(b(\alpha),\alpha) - \frac{da(\alpha)}{d\alpha} f(a(\alpha),\alpha) \tag{3.73}$$

(56). Applying equation 3.73 to equation 3.72 after rearrangement and differentiation with respect to γ_R gives

$$G^* = \frac{T_{tor}}{2\pi R^3 \gamma_R} \left[3 + \frac{d \ln T_{tor}}{d \ln \gamma_R}\right] \tag{3.74}$$

The complex modulus of viscoelastic materials is a function of both angular frequency and strain. It has long been known that at low strain amplitudes, the complex modulus no longer depends upon the strain. The range of strains at which the complex modulus is independent of strain is called the *linear viscoelastic region*. At these strains the $\frac{d \ln T_{tor}}{d \ln \gamma_R}$ term in equation 3.74 simplifies to 1 as the torque is independent of the strain. This leads to

the much simpler expression for the complex modulus

$$G^* = \frac{2T_{tor}}{\pi R^3 \gamma_R} = \frac{2Th}{\pi\theta R^4} \tag{3.75}$$

where only the amount of strain at radius R must be measured for an applied torque, T_{tor}, to determine G^* (56). Making use of the relations presented in equations 3.57a and 3.57b, equation 3.75 may be used to give expressions for the storage and loss moduli, giving

$$G' = \frac{2T_{tor}h}{\pi\theta R^4}\cos\delta \tag{3.76a}$$

$$G'' = \frac{2T_{tor}h}{\pi\theta R^4}\sin\delta \tag{3.76b}$$

where δ is the phase difference between the stress and strain response.

Controlled Stress Rheometry

There are two ways to measure the storage and loss modulus of a sample: by controlling the stress and measuring the strain or vice-versa. Rheometers that measure the strain as a function of stress are known as controlled stress rheometers (56). The most common means of controlling the applied stress is actually done by controlling the torque applied to a sample via what is called a drag cup motor, which is described as follows (56, 67). For the plate-plate geometry, the top plate is attached to a long, cylindrical shaft while the bottom plate is held in place. The top part of the cylindrical shaft is attached to an air bearing, which supports either a copper or aluminum cup. A torque is applied by generating a rotating magnetic field around the cup, which will attempt to follow the created field (56, 67). The torque created is proportional to the square of the voltage (56). The strain can be measured using a variety of methods including an optical lever, capacitance transducers, or optical encoders (56). The latter is the most common, and uses a light source to shine through a disc composed of various transparent and opaque

areas, allowing precise measurement of the angular position, θ. For oscillating torques, the phase difference δ may be calculated by determining the time difference between the oscillating maxima of θ and the torque.

When using controlled stress rheometers, it is important to precisely determine the instrument inertia. Torque induced on the drag cup is countered by air bearing friction, rotor inertia and reluctance torque in addition to the viscosity of the sample, with the largest effect being the rotor inertia for samples with low viscosity (56). The torque applied, T_{app}, differs from the actual torque experienced by the sample, T_{exp} via the relation

$$T_{exp} = T_{app} - I \cdot \ddot{\theta} \tag{3.77}$$

where I is the motor inertia, and $\ddot{\theta}$ is the second derivative of the angular displacement with respect to time (68). The correction on the torque can then be determined via subtracting the inertial term, which can be done with the software. Determination of the motor inertia can be found via a standardized test using air as the sample medium: the motor inertia is found by subtracting the calculated torque experienced by the air (determined by the strain) from the torque applied to the air at a certain angular acceleration.

To control strain on a sample using a controlled stress rheometer, typically the software attempts several low torque (and therefore stress) values and measures the strain. An algorithm allows the rheometer to approach the stress required in order to obtain the strain by reducing the torque by a small interval if the measured strain is too high, and increasing the torque by a small interval if it is too low. Thus, before a measurement of the moduli may be taken, controlled stress rheometers must spend a small amount of time approaching the desired strain.

Chapter 4

CRC

4.1 The System

CRC is a *de novo* protein designed with three parts: two leucine zipper blocks (the C-blocks, one on each end), and a modular, random coil (the R-block). The leucine zippers are of the type described in section 2.5, possessing hydrophobic leucines at the a and d positions on the α-helix (see Figure 4.1 for the amino acid sequence). The R random coil block is designed so that it is able to dissolve in aqueous solution via multiple glutamic acids. It also does not possess any preferred secondary or tertiary protein structure. These properties allow for the insertion of integrin binding domains (the X sequence) into the R block, as in Figure 4.1 (12). Of particular interest are RGDS binding domains, which previous studies have shown allow cells to bind to CRC protein hydrogels (11).

CRC molecules associate via the hydrophobic leucine strips located on their C blocks. This association is further strengthened by the presence of salt bridges that form between the positively-charged glutamic acids of one C block and the negatively-charged lysines on the other, as described in section 2.5. The charged residues in the R-block exclude it from interfering in any hydrophobic interactions the C blocks may make with one another. This

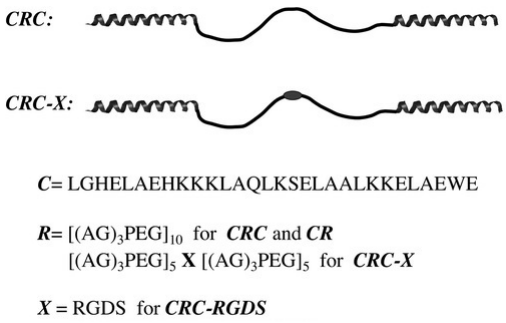

Figure 4.1: The structure and amino acid sequence of the main domains of CRC and CRC-X molecules. Reprinted with permission from *Biomacromolecules*, **10**, Fischer *et al*, "Biofunctional Coatings via Tageted Covalent Cross-linking of Associating Triblock Proteins", pp.2408–2417 (2009). Copyright (2009) American Chemical Society.

type of system tends to self-assemble into trimeric bundles, as in Figure 4.2. The hydrophobic strips located on the leucine zipper C block allow these gels to bind with other hydrophobic surfaces, as also seen in Figure 4.2. It is possible to hypothesize that the insertion of an RGDS binding domain into CRC molecules will not affect this gel formation in any way as they are located in the middle of the R block, a domain which does not play a role in gel formation.

4.2 Methodology

4.2.1 Protein Expression

Large-scale CRC and CRC-RGDS protein expression was performed using a New Brunswick Scientific Bioflo 110 bioreactor using standard protocol (see reference (12) and appendix A.1). To verify that protein was expressed, a sodium dodecyl sulfate polyacrylamide gel electrophoresis (SDS-PAGE) was performed after each run using samples collected during the bioreactor process. The optical densities (ODs) of each were measured, and the samples

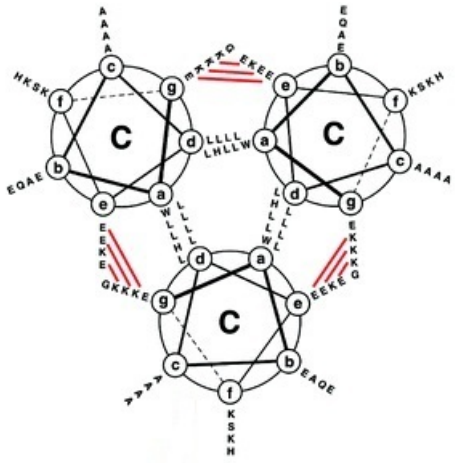

Figure 4.2: CRC molecules crosslinked into a network. From Petka *et al.*, Science, **281**, 5375, (1998). Adapted with permission from AAAS

diluted with 8 M urea and mixed until an OD of 4 was obtained. Note that the OD is the absorbance of a sample using light at a wavelength of 600 nm, where absorbance will be defined in section 4.3.1. The electrophoresis process was the same as that first mentioned by Cleveland, *et al*, save three 5 minute rinses with DI water were done, followed by 1 hour of staining, and overnight destaining, again in DI water (69). It should be noted that although the molecular weights of CRC and CRC-RGDS are 17900.6 g/mol and 18317 g/mol, respectively, the proteins themselves tend to run much higher on a SDS-PAGE gel, perhaps due to excessive negative charge (12). A sample SDS-PAGE containing both pre-induction and post-induction samples is demonstrated in Figure 4.3.

4.2.2 Protein Purification

All the cell pellets from one bioreactor run are gathered and resuspended in Buffer B for a total volume of ~1.5 L of solution. For a discussion on buffers used in protein purification, please refer to section B.2.1. The solution was

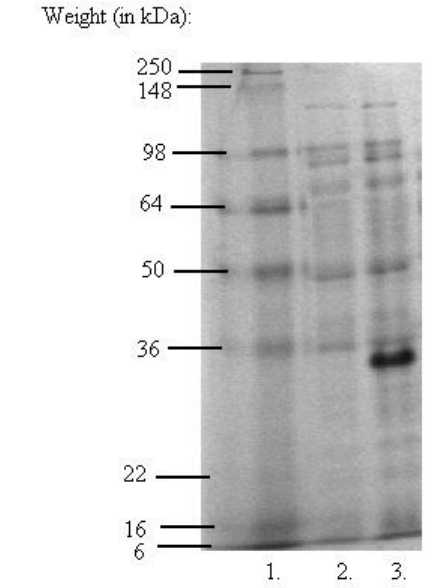

Figure 4.3: A sample SDS-PAGE of the CRC bioreactor run # 21 pre-induction and post-induction samples. The appearance of the dark band in the post-induction sample indicates protein expression.

then refrozen in a −20°C freezer to help lyse intact cells. One-sixth (~250 mL) of this lysate solution was then diluted with ~225 mL Buffer B, and well stirred to break up any remaining, intact cells. To begin separating the protein from undesirable cell components, such as organelles and DNA, the lysate is centrifuged for 20 minutes at high speeds. The resulting supernatant liquid is collected.

GE IMAC Sepharose resin (~100 mL) was placed on a Pharmacia XK50 column. The resin was then bound to nickel, as per the instructions from the manual. The column was prepared for purification by equilibrating the pH of the column to pH 8 by washing through ~300 mL of Buffer B. Half of the supernatant liquid collected from centrifugation was then run through the column. The six histidine residues (His-tag) present in the CRC and CRC-RGDS amino acid sequences allowed the protein to bind to the nickel present on the column, while those proteins lacking the His-tag were more likely to flow through (70–72). This occurs because histidine possesses an imidazole group as a residue, a factor which has previously been found to enhance binding (73). Further washes with ~200 mL of Buffer B, and ~800 mL of Buffer C (same composition as Buffer B, save pH is at 7.0) washed out weakly bound protein. Protein was then extracted from the column (or eluted) and collected by pumping through ~200 mL elution buffer. Samples were taken at each step of the column purification process and ran on a SDS-PAGE gel. A sample SDS-PAGE containing all the washes and elutes for a particular protein batch is provided in Figure 4.4.

Following elution, the protein solution was concentrated in Millipore tangential flow concentrators, following the procedure outlined in the instruction manual. The resulting protein solution was then sealed in treated Spectra/Por 1 dialysis membranes by Spectrum Labs. These specific dialysis membranes have molecular weight cut-offs of 6000 to 8000 Da, well below the molecular size of CRC (17900.6 Da) and CRC-RGDS (18317 Da) to ensure that there is little loss of protein. Sealed bags of protein were then

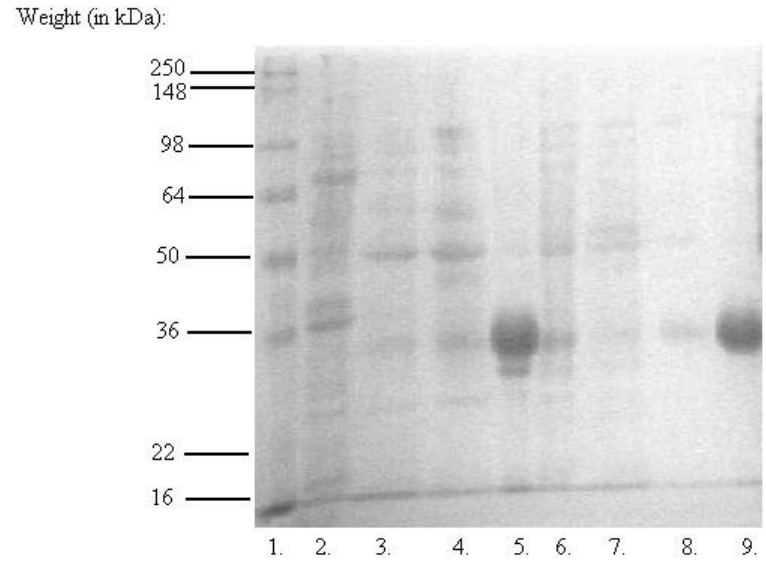

Figure 4.4: A sample SDS-PAGE showing the load fractions, wash fractions, and elute fractions collected for CRC samples # 4-I and # 7. Lane 1 contains a protein standard, SeeBluePlus 2.

placed in a continuous flow dialysis system that continually pumped in fresh reverse osmosis (RO) water. The pores in the dialysis membranes allowed osmotic pressure to force the salts (urea, tris, sodium phosphate, and imidazole) dissolved in solution into the surrounding water. The water was allowed to pour out of the top of the system to allow the resulting aqueous solution to be continually diluted.

After leaving the protein in the dialysis system for 2 days, precipitate and a highly concentrated gel appeared in the bag. Low pH resulting from the RO water causes the protein to precipitate out of solution, and experiments performed indicate that it would not redissolve in solution. This made it unfit for use as undissolved protein possesses different properties than dissolved protein, and so it was deemed necessary to re-solubilize it. To do so, the resulting gel was placed in a 50mL tube and deionized water with sodium phosphate and sodium azide was added for a final concentration of ~10 mM sodium phosphate, 0.2 mg/mL sodium azide in solution. The gel was then heated in a 65°C heat bath and vigorously shaken until the gel was nearly completely dissolved. The resulting solution typically contained precipitate, which was removed by a combination of centrifugation and syringe filtration with a 0.2 μm filter. The cleared solution was then replaced in the Spectra/Por 1 dialysis bags and the aforementioned dialysis system for one more day to remove remaining sodium phosphate and sodium azide. The final solution was frozen in a -80°C freezer and placed into a lyophilizer to remove the frozen water by sublimation (74). Dried samples were collected from the lyophilizer and stored in a 4°C freezer, until use.

4.2.3 Hydrogel Preparation and Rheometry

Samples were prepared by weighing the mass of protein required for a specific weight/weight (w/w) concentration of protein to total mass into a 2mL Eppendorf microcentrifuge tube. The average purity of samples was found from multiple testing to be around ~90%, so this concentration was assumed

when preparing samples. The mass of 50 mM sodium phosphate, 0.2 mg/mL sodium azide in aqueous solution required to obtain the desired protein concentration was calculated via the formula

$$m_{sol} = 0.90(m_{pro}) \left(\frac{100\%}{[CRC]_{\%}} - 1 \right) \tag{4.1}$$

where m_{sol} is the mass of the solution required, m_{pro} is the mass of protein weighed out, and $[CRC]_{\%}$ is the desired (w/w)% concentration of protein in hydrogel. The resulting solution was then heated in a 65°C heat bath and stirred occasionally until fully dissolved and well mixed. The actual concentration of the resulting protein hydrogel was then determined according to the protocol outlined in section 4.3.1.

An Anton-Paar MCR 301 rheometer was obtained to perform all rheometry results. This rheometer uses a drag cup motor and optical encoder to measure torque, θ, and δ, as explained in section 3.2.3. The rheometer utilized disposable, 25 mm diameter, circular top plates and specialized bottom plates, both designed by Dr. James Harden. These plates were sand-blasted to create a rough surface. This rough surface was used to minimize the amount of slippage that could occur between the plates and the samples as slip between the two causes a lower stress to be observed for a certain strain. Samples were loaded onto the plates as per operating instructions. A procedure was performed before each test to determine the height between the two plates. This procedure uses a normal force sensor which measures deflections in the air bearing and a resultant difference in capacitance, allowing the normal force to be calculated. Thus, the height between the two plates can be determined by slowly lowering the rheometer's top plate until a normal force is detected. At this point the height of the upper plate is slowly increased until no more normal force is measured. This point is set as the zero height point. When loading a sample onto the rheometer, an excess amount of material is used. Then, the rheometer is lowered to a distance

of 1 mm between the upper and lower plates. Excess sample is squeezed out from between the two plates when this is done, necessitating its removal via a scoop. Standardizing the height ensures the sample volume is similar between different samples.

Uncertainty in sample measurements for any rheometer cannot be determined exactly from numerical estimations as the biggest variation between samples is caused by loading. As CRC is a fairly liquid-like substance it tends to flow, though its high viscosity means an exact volume cannot be pipetted onto the rheometer's bottom plate. Thus, it is difficult to add the same amount of material to the plates every time. This necessitates edge trimming with a scoop, removing any excess sample that may affect rheometry. Though this excess material removal does help ensure the amount of materials loaded are fairly similar, they are not exactly the same and cannot be measured, resulting in an unknowable contribution to uncertainty.

In addition to this complication, samples typically possess different amounts of trapped gases within their networks. The more gases present in a network, the lower their rheological properties will be, though their elimination from a network once loaded onto the rheometer is impossible. While centrifugation was performed to eliminate trapped gases from the samples before being loaded onto the rheometer, small amounts of air were still trapped during the loading procedure. Measurements of the amount of gases trapped are impossible once a sample has been loaded and tested as removing a sample from the rheometer to determine the relative volume of gases cause the sample to trap even more air withing its network. This trapped gas effect cannot be accurately quantified, and thus also contributes an unknown quantity to uncertainty between samples.

When the upper plate of the rheometer is lowered onto a sample, there is a chance that an air pocket or multiple air pockets will exist between the sample and the upper plate. Air pockets between the sample and plates allow for lower torques to cause higher strains, due to less surface area contact

between the instrument and samples. This results in lower rheometric data results. This cannot be observed as the upper plate is not transparent, and so it cannot be guaranteed that this does not occur for samples. Thus, air pockets will also contribute an unknowable contribution to variations between measurements. Thus, the actual uncertainty between measurements of samples cannot accurately be determined.

4.3 Concentration and Circular Dichroism

It is possible to use spectroscopic techniques to determine quantitative and qualitative information about the concentration and structure of proteins within a hydrogel. Techniques used to derive information from CRC hydrogels include ultraviolet absorption spectroscopy for concentration determination and circular dichroism spectroscopy for structural data.

4.3.1 Concentration Determination

While most amino acids absorb light at around 200 nm, it has long been known that 280 nm light is strongly absorbed by the amino acids phenylalanine, tryptophan, and tyrosine, and is weakly absorbed by cystine (two disulfide-linked cysteines). This occurs because the electrons within the aromatic rings of phenylalanine, tryptophan, and tyrosine all require less energy to attain an excited state than most amino acids due to resonance within the rings (75).

The spectroscopic technique itself was first developed by the mathematicians Pierre Bouguer and Johann Heinrich Lambert and later developed into its present form by German physicist August Beer into Beer's Law (76, 77). Consider light incident on a solution containing solute molecules that absorb light of a specific wavelength. The intensity of the light after passing through

the solution (I) is then related to the initial intensity (I_o) by

$$I = I_o \cdot 10^{-\epsilon c d} \tag{4.2}$$

where c is the concentration of the solution, d is the distance within the solution the light travelled before exiting, and ϵ is known as the *extinction coefficient* of the solute (77). This extinction coefficient is characteristic for every substance, has units of $M^{-1}cm^{-1}$ and depends upon the wavelength of light being considered. To simplify calculations, the absorbance, A, is typically derived as

$$A = -log_{10}\left(\frac{I}{I_o}\right) = \epsilon \cdot c \cdot d \tag{4.3}$$

(77). It is also useful to obtain the concentration in units of mg/mL, which may be obtained using the molecular weight, MW, and (4.3) to form

$$c = \frac{A \cdot MW}{\epsilon \cdot d} \tag{4.4}$$

A blank measurement of the absorbance value of the solvent without solute allows any contribution of the solvent to the 280 nm absorbance to be eliminated.

The 280 nm extinction coefficient of tryptophan, tyrosine, and cystine are well known, and are given in Table 4.1 (78, 79). Whenever cysteine appears in a protein's amino acid sequence, it is assumed that half of them have formed the 280 nm absorbing cystine molecule as it is difficult to explicitly determine the cystine quantity, and the contribution of cystines is relatively low compared to that of tryptophan and tyrosine (79). From knowledge of the amino acid sequence of CRC, and therefore the number of cysteine, tryptophan, and tyrosine residues, it is possible to calculate the extinction coefficient for CRC and CRC-RGDS (see Table 4.1). It should be noted that the RGDS amino acid sequence contains no cysteines, tryptophans, or tyrosines, and therefore will not contribute to the calculation for the extinction

coefficient.

Substance	ϵ in $[M^{-1}cm^{-1}]$
Cystine	120
Tryptophan	5690
Tyrosine	1280
CRC (and CRC-RGDS)	13940

Table 4.1: Extinction coefficients for certain amino acids and amino acid complexes

From this information, the concentrations of CRC hydrogels could be determined via 280 nm absorbance (Abs_{280}) measurements of a solution containing the protein in a container of known size. Quartz cuvettes with interior lengths and widths of 1 cm were chosen as containers due to their transparency to light at 280 nm. Most spectrophotometers are only accurate at measuring values of Abs_{280} within the range of 0.1 and 1. As the lowest concentration of CRC hydrogels would produce an Abs_{280} much higher than the maximum limit, samples were diluted in order to reduce their concentration, and therefore their Abs_{280}. In addition, because there is no guarantee before concentration measurements that the CRC hydrogel concentration is homogeneous, two samples were taken from different regions of the hydrogel. This was done so that an average concentration could be calculated to try to eliminate the effects that any heterogeneity would have on the concentration measurement of the hydrogel.

The concentration measuring technique is as follows. Two samples of a specific hydrogel were weighed out (giving m_{gel}) into 1.5 mL tubes using a Mettler AE260 DeltaRange scale. One millilitre of an 8 M urea solution was then weighed into each tube containing the hydrogel samples to denature the protein and cause the gel to dissociate, providing $m_{solvent}$. The resultant solutions were then heated in a 65^oC heat bath and agitated until the gels were completely dissolved and well mixed. Another dilution was made of each sample by weighing 200 μL of the resultant solutions into new 1.5

mL tubes (providing $m_{solution}$) and mixing in an additional 800 μL of 8 M urea. A blank measurement was then made of the solvent using a Thermo Spectronic BioMate 3 spectrophotometer. The Abs_{280} values for each sample were then measured and the concentrations ($c_{solution}$) of the protein in the diluted solutions calculated from (4.4). Using the obtained masses, the weight/weight protein concentration of the gel (c_{sample}) was then determined via the formula

$$c_{sample} = c_{solution} \cdot MW \cdot \frac{m_{gel} + m_{solvent}}{m_{solution} \cdot m_{gel}} \cdot 100\% \tag{4.5}$$

Since two samples were tested, the average concentration is considered to be the hydrogel concentration. This is equal to

$$c_{hydrogel} = \frac{c_{sample1} + c_{sample2}}{2} \tag{4.6}$$

with the uncertainty equal to

$$\Delta c_{hydrogel} = \frac{1}{2}|c_{sample1} - c_{sample2}| \tag{4.7}$$

The reason the uncertainty on the concentration is calculated by differences between sample concentration measurements is that the uncertainty due to the instrument used to measure absorbance at 280 nm is far smaller than variations in concentration within the sample itself. CRC samples are somewhat heterogeneous in their concentration due to the viscoelastic nature of the material. This makes it far more likely that deviations between measurements are due mostly due to differences in concentration between the two samples than to the instrument.

4.3.2 Secondary Structure Determination

The secondary structure of CRC is very important for hydrogel formation, and so it is important to verify that CRC molecules are indeed forming α-

helices. One means of determining a protein's secondary structure is to use a technique called *circular dichroism* (CD). Circular dichroism has been shown to qualitatively demonstrate the existence of secondary structures, specifically α-helix, β-sheet, and random coils, within a protein (80, 81).

Different optically active (or *chiral*) structures will absorb different amounts of L over R circularly polarized light due mainly to differences in their structure (82). The difference between the absorptions of left and right circularly polarized light (A_L and A_R, respectively) at a specific wavelength can give the ellipticity ($\theta(\lambda)$) by

$$\theta(\lambda) = 32.98 \cdot (A_L(\lambda) - A_R(\lambda)) \tag{4.8}$$

where the ellipticity is related to the ellipse's major axis (a) and minor axis (b) by

$$\theta(\lambda) = tan^{-1}\left(\frac{b}{a}\right) \tag{4.9}$$

(82). It is typical to present the CD data as the mean residue ellipticity ($[\theta]_{mrw,\lambda}$) at wavelength λ as

$$[\theta]_{mrw,\lambda} = \frac{100 \cdot \theta(\lambda)}{m \cdot d} \tag{4.10}$$

(82). This form for the ellipticity has the added advantage that it is independent of the concentration of protein and the path length of the solution containment vessel.

The determination of the secondary structures from the mean residue ellipticity is done by qualitative observation of the position and number of minima and maxima. Figure 4.5 shows the various forms the mean residue ellipticity takes for common protein secondary structures.

CD data for two samples of CRC and one sample of CRC-RGDS were taken with a JASCO spectrophotometer. All samples were prepared by weighing out a sample in the dry form into a 1.5 mL tube. Samples were

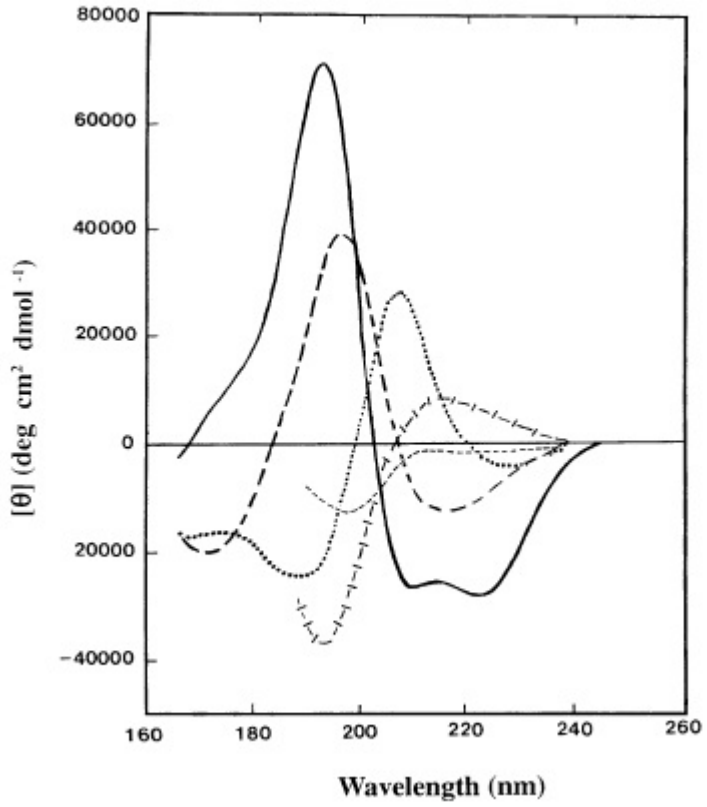

Figure 4.5: CD spectra for various protein secondary structures. Solid-line, α-helix; long dashed line, anti-parallel β-sheet; dotted line, type I β-turn; cross dashed line, extended 3_1-helix or poly (Pro) II helix; short dashed line, irregular structure. Reprinted from *Biochimica et Biophysica Acta* (*BBA*) – *Proteins & Proteomics*, **1751**, Kelly *et al.*, "How to study proteins by circular dichroism", pp. 119–139 (2005), with permission from Elsevier.

dissolved in 10 mM sodium phosphate (pH 7.5) buffer to ensure pH stability. A low concentration of sodium phosphate was used to reduce the amount of circularly polarized light absorbed by the salt. The protein was dissolved at a concentration of 20 μM. CD data for various samples of CRC and CRC-RGDS are presented in Figure 4.6.

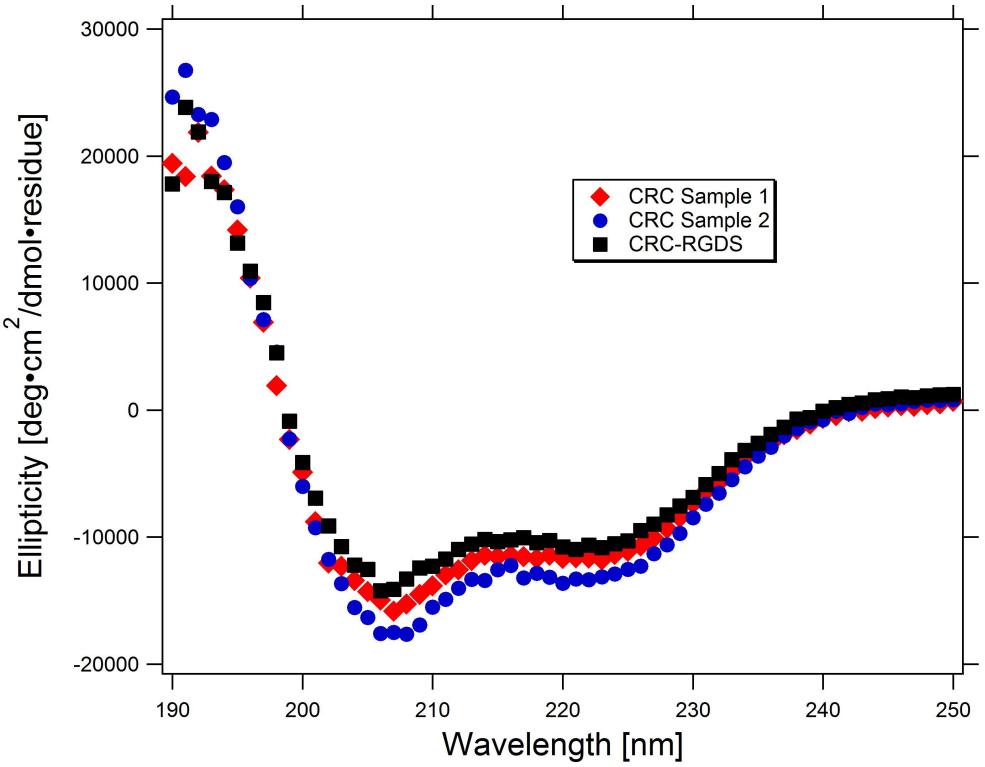

Figure 4.6: Mean residue ellipticity for various samples of CRC and CRC-RGDS.

As can be determined by comparison with the results from Figure 4.5, Figure 4.6 demonstrates that the shape of all plotted CRC and CRC-RGDS mean residue ellipticity data is indicative of α-helices and random coil regions. This reinforces the idea that both CRC and CRC-RGDS possess α-helical end domains in solution.

4.4 Results and Discussion

To study the rheological behavior of CRC gels, the storage and loss moduli (G' and G'', respectively) were measured as functions of angular frequency, ω, on the Anton-Paar MCR310 rheometer. Results for G' and G'' are calculated by Rheoplus software using the relations given by equations 3.76. Only one sample has been tested for each data set as good quality protein was difficult to obtain due to its finite lifetime in aqueous solvent and the large cost and amount of time it takes to produce the amounts of protein required for rheometric tests. As such, no standard deviations, n-values, or p-values could be calculated for each data set. An appropriate strain amplitude was chosen that ensured the 5.3% sample (and therefore all samples of a higher concentration) was within its linear viscoelastic range.

4.4.1 Measurement Uncertainty

A plot of G' and G'' vs. ω within the frequency range 10 rad/s $\leq \omega \leq$ 100 rad/s is shown in Figure 4.7. Nominal sample conditions, such as concentration, pH, and temperature, were identical for both samples, but subject to uncertainties described below.

As explained in section 3.1, the concentration of the gels plays a large role in its strength, and therefore rheology. A small difference in the gel concentration can play a large role in a gel's response to a stress or strain. Due to the manner in which the gels were prepared (i.e. mixed) it is impossible to obtain a homogeneous gel concentration, and so all measurements of this value may vary from the mean concentration. Another possible variable that can cause uncertainty is differences in the loading of samples. This could lead to some air pockets appearing between the gel sample and rheometer, thereby decreasing the measured moduli. The typical uncertainty for rheological measurements is 10-20%, and is assumed for all measurements of both G' and G'' in the following discussion and chapters.

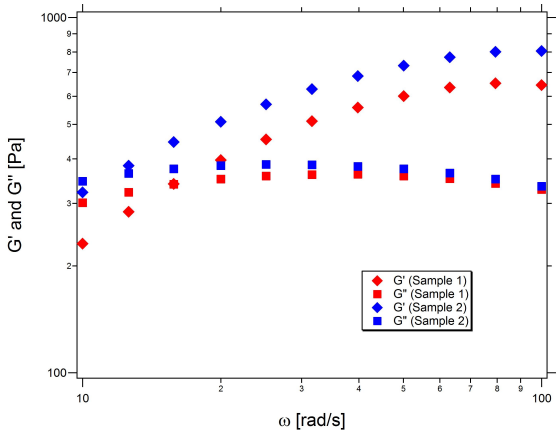

Figure 4.7: G' (◆) and G'' (■) vs. angular frequency, ω, for two 7.5% CRC gels, pH 7.5, at T = 285 K.

4.4.2 Stretched Exponential Behavior

In the first test, a (10.4±0.3)% (w/w) gel was tested at 12°C by measuring the storage modulus, G', and loss modulus, G'', as functions of angular frequency, ω. The data were scaled by dividing the storage and loss moduli (G' and G'') of each set by the intersection point of the moduli ($G' = 992$ Pa $= G''$), and dividing all values of ω by the angular frequency at this intersection point ($\omega = 5.15$ rad/s). The scaled data are plotted in Figure 4.8.

Unlike in ideal telechelic systems, Maxwellian behavior was not observed. Stress relaxation was instead expressed via stretched exponential behavior. Thus, it was first necessary to determine which value of β could accurately model the data. In order to do so, numerical estimations were made using Wolfram Mathematica software. Equations 3.58 were used to model the case $\beta = 1$, while the Fourier sine and cosine transforms were performed on equation 3.49 for the cases $\beta = 0.75$, 0.5, and 0.25 to obtain equations for G' and G'', respectively. The crossover angular frequency was first determined by setting $G'(\omega) = G''(\omega)$ for each value of β and using the software to estimate a possible value for ω where this crossover would occur. The numerical values obtained for ω at each value of β were then used in their respective

equations for G' to obtain the value of the modulus at the intersection point. These modulus values were then used as divisors in order to scale their respective equations. Values of angular frequency were input into the resulting equations to generate data sets for each β. Results are shown in Figure 4.8. As can be readily seen, the stretched exponential model with $\beta = 0.5$ fits the data much more accurately than the estimations using $\beta = 1, 0.75$, or 0.25. In order to quantify the quality of the stretched exponential model with $\beta = 0.5$ as a good fit, it is necessary to calculate the parameter χ^2. This parameter is a means of determining how close experimental data matches model data, with a minimum being desired. χ^2 is calculated via

$$\chi^2 = \sum_{i=1}^{n} \left[\frac{G_{exp}(\omega_i) - G_{model}(\omega_i)}{G_{model}(\omega_1)} \right]^2 \tag{4.11}$$

where $G_{exp}(\omega_i)$ is the experimental storage (or loss) modulus datum at a certain angular frequency, ω_i, $G_{model}(\omega_i)$ is the model storage (or loss) modulus datum at a certain angular frequency, ω_i, and n is the number of data points (in this case, $n = 1$) (83). To ensure a good fit, χ^2 must be a minimum with respect to other possible values for β (83). Model data were calculated for β values of 0.45 and 0.55 and plotted with the $\beta = 0.5$ model data as well as the data points for the 10.4 % gel in Figure 4.9. These values for β were chosen as they are similar to the value of $\beta = 0.5$. χ^2 values were calculated using equation 4.11 for each model, with the data presented in Table 4.2. Table 4.2 demonstrates that the calculated χ^2 data for $\beta = 0.5$ is very near

β	χ^2 for G'_{scaled}	χ^2 for G''_{scaled}
0.45	0.659	0.705
0.5	0.274	0.0763
0.55	0.573	12.1

Table 4.2: Calculated values of χ^2 for various values of β.

a minimum with respect to the other two models. The true value of β likely

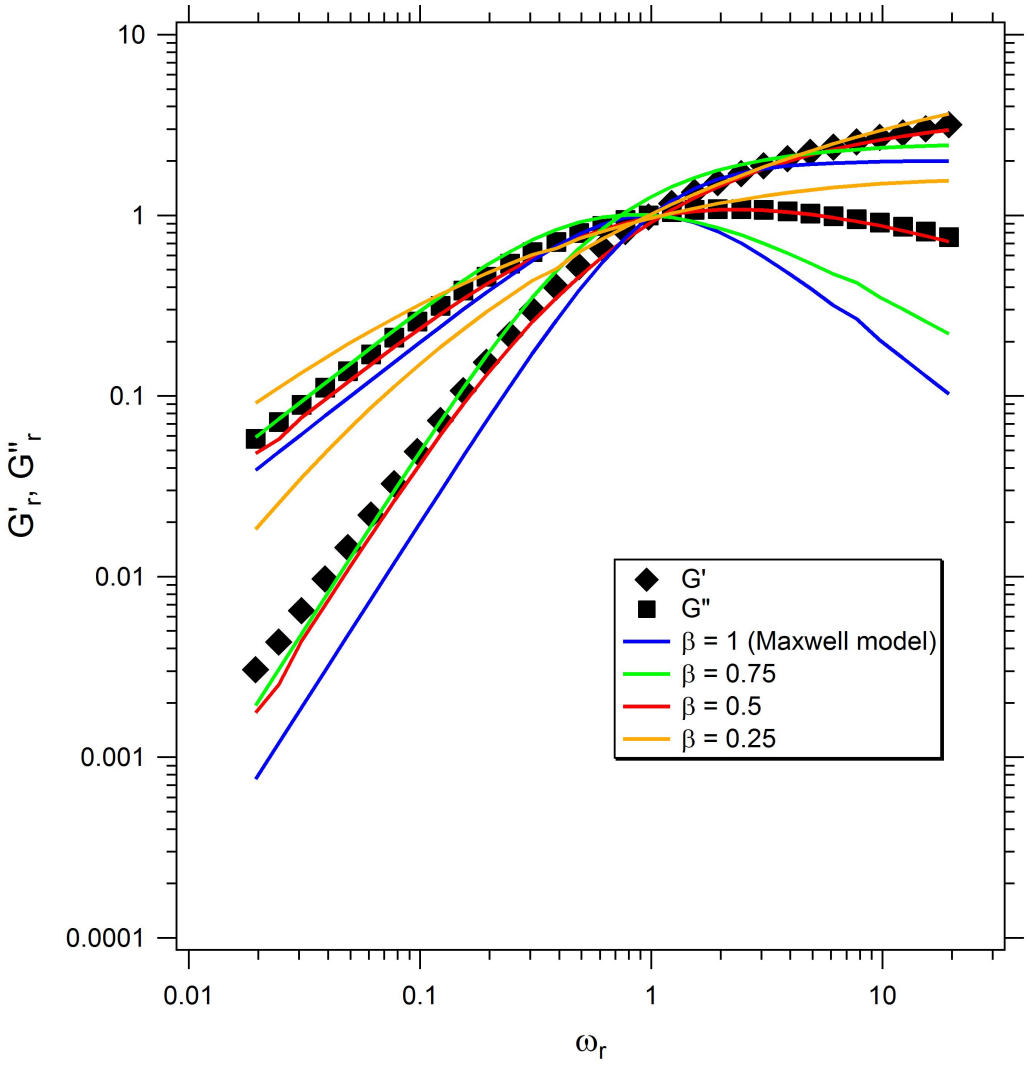

Figure 4.8: G' (◆) and G'' (■) vs. angular frequency, ω, for a 10.4% CRC gel, pH 7.5, at T = 285 K. The data have been fitted to numerical estimations of the stretched exponential model with the blue line representing values for $\beta = 1$ (the Maxwell model), the green line representing the values for which $\beta = 0.75$, the red line for values using $\beta = 0.5$, and the orange line for values representing $\beta = 0.25$.

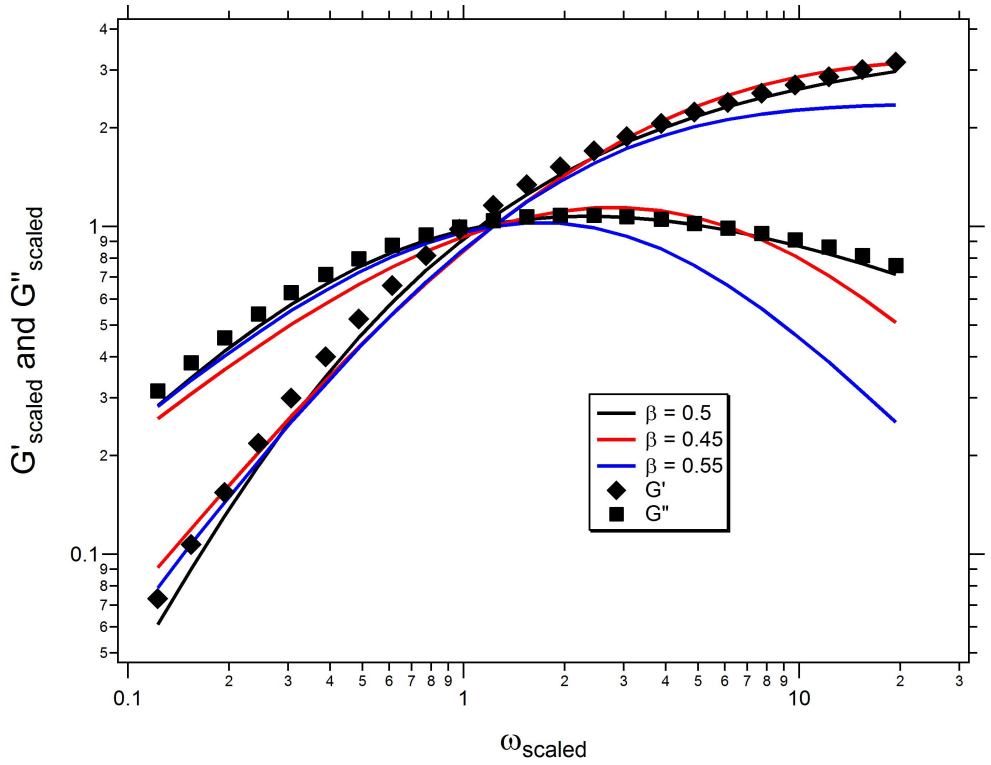

Figure 4.9: G'_{scaled} (◆) and G''_{scaled} (■) vs ω_{scaled} for various values of β. Values of G'_{scaled} and G''_{scaled} for a 10.4 % gel at $T = 285$ K are plotted using ◆and ■, respectively.

lies in the range $0.5 \leq \beta \geq 0.55$, though further work must be done in order to determine the value exactly.

This variation from the Maxwell model is not predicted from the ideal theory, but imitates results obtained by Berret, *et al* and Tsitsilianis, *et al* where the value for β had to be determined numerically (60–64).

One possible reason for the variation from ideal Maxwell behavior in CRC systems is the formation of dimers. Though the end groups of CRC must bundle into trimers in order to form a crosslinked network, a finite number of dimers and unimers do exist in the system. These dimers would not contribute very much to elastic energy storage within the system as they would not be able to distribute the stored energy throughout the network. In addition, when the dimer dissociates it will dissipate energy through viscous friction in exactly the same way as the CRC molecules involved in a trimeric bundle dissipate energy once the trimer disassembles. This results in a lower storage modulus due to less trimeric junctions, and a higher loss modulus due to a larger number of end groups dissipating energy through viscous friction than accounted for in trimeric bundles.

4.4.3 Thermal Dependence

In the thermal dependence tests, the temperature was varied using a Peltier hood to observe the behavior of the gels. The Peltier hood controls temperature via electrical heating to increase temperature, or by running cooling water through the bottom plate to cool the metal and reduce the sample's temperature. In combination, the two can be used to precisely control the temperature of the sample by using a thermometer within the rheometer to measure the temperature of the metal, which must be at the same temperature as the sample since they are in thermal contact. Data points were obtained from a $(10.4 \pm 0.3)\%$ (w/w) gel, and are plotted in Figure 4.10.

The data from Figure 4.10 demonstrates a shift in the relaxation frequency to higher frequencies for higher temperatures. This is as expected

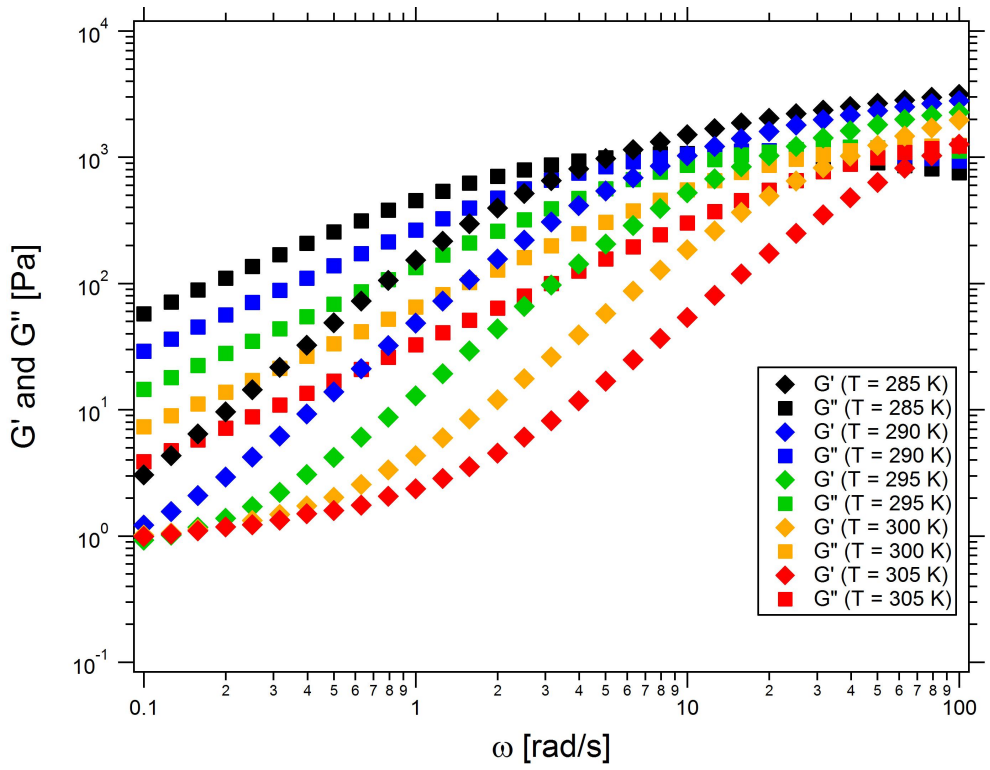

Figure 4.10: G' (◆) and G'' (■) vs. angular frequency, ω, for a (10.4±0.3)% CRC gel in 50 mM sodium phosphate, 0.2 mg/mL sodium azide (pH 7.5) at varying temperatures

from the theory, discussed in section 3.2.2, where higher temperatures increase the thermal energy of the system, allowing for greater dissociations between the physical crosslinks. It also demonstrates that the stretched behavior demonstrated in section 4.4.2 is conserved within this temperature range as the data set for $T = 285$ K displayed in Figure 4.10 is the same as that presented in the previous section.

To fully investigate the temperature dependence of this gel, the crossover angular frequency (ω_r) and crossover moduli (G_r) for each temperature (T) were determined by finding the intersection between the linearly interpolated lines created from the storage and loss moduli bounding the intersection. The data are given in Table 4.3. Note that the uncertainty on the temperature is determined via the reading on the rheometer's thermometer, the uncertainty of the angular frequency is given in the rheometer's manual, while that of τ is calculated from the uncertainty of ω.

T [in K]	G_r [in Pa]	ω [in rad/s]	τ [in s]
(285.00 ± 0.01)	$9.92\text{X}10^{2}$	(5.6 ± 0.2)	(1.22 ± 0.05)
(290.00 ± 0.01)	$1.06\text{X}10^{3}$	(10.3 ± 0.2)	$(6.1 \pm 0.2)\text{X}10^{-1}$
(295.00 ± 0.01)	$1.13\text{X}10^{3}$	(22.6 ± 0.2)	$(2.79 \pm 0.03)\text{X}10^{-1}$
(300.00 ± 0.01)	$1.16\text{X}10^{3}$	(46.5 ± 0.2)	$(1.352 \pm 0.006)\text{X}10^{-1}$
(305.00 ± 0.01)	$1.22\text{X}10^{3}$	(95.4 ± 0.2)	$(6.59 \pm 0.02)\text{X}10^{-2}$

Table 4.3: Crossover modulus and crossover angular frequency for the $(10.4 \pm 0.3)\%$ (w/w) hydrogel sample presented in Figure 4.10 gel at various temperatures.

From these crossover values, the original data were scaled via the formulae

$$G'_{scaled} = \frac{G'(\omega, T)}{G_r} \tag{4.12a}$$

$$G''_{scaled} = \frac{G''(\omega, T)}{G_r} \tag{4.12b}$$

$$\omega_{scaled} = \frac{\omega}{\omega_r} \tag{4.12c}$$

The scaled moduli were then plotted versus the scaled angular frequency, leading to Figure 4.11.

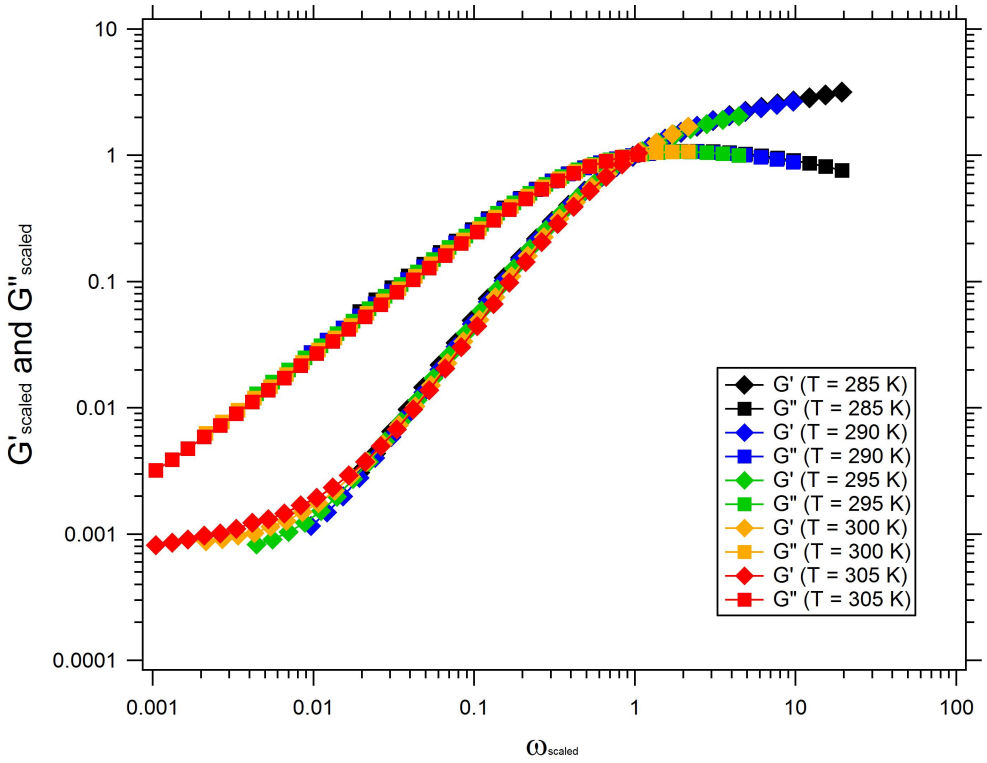

Figure 4.11: G'_{scaled} (◆) and G''_{scaled} (■) vs ω_{scaled} for a $(10.4 \pm 0.3)\%$ (w/w) CRC gel at various temperatures.

As the values of G'_{scaled} and G''_{scaled} agree for all T studied, we can see that CRC protein hydrogels possess the same behavior within the temperature range of 285 K to 305 K. The advantage to this thermal scaling method allows the rheological behavior of the CRC hydrogels to be extended to lower or higher frequencies than is normally possible.

It is also possible to explain the thermal behavior of the hydrogels by associating it with the energy of formation of the physical association represented by the relaxation time, as done by Annable, *et al*, themselves building off the theoretical work of Tanaka and Edwards (8, 51). Using the crossover

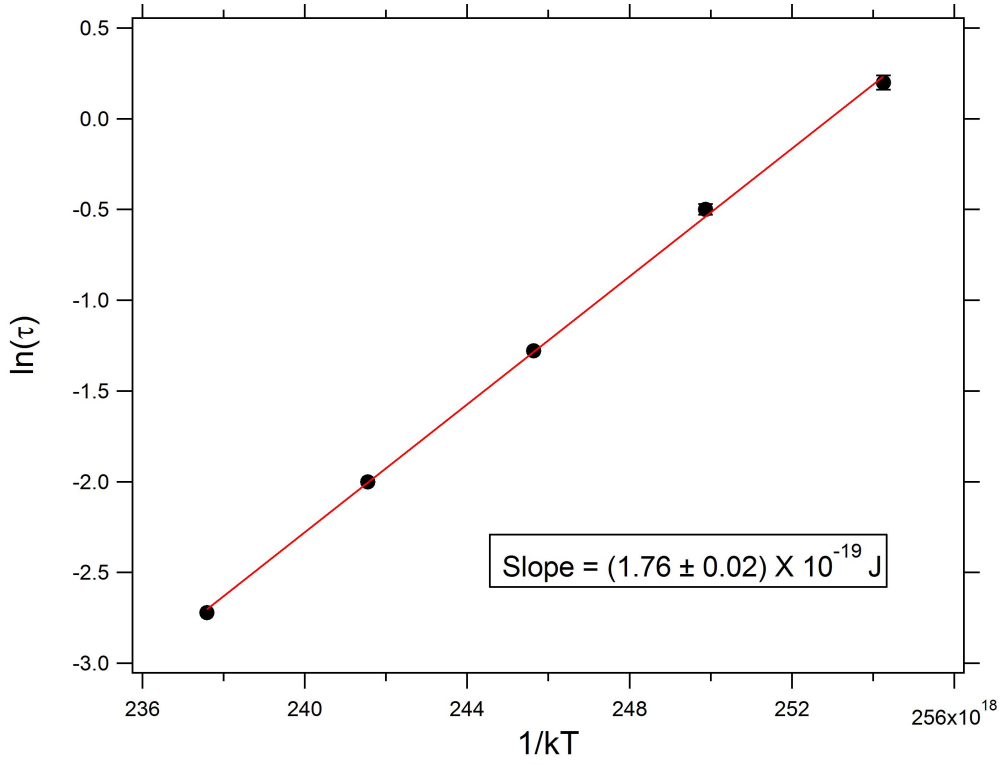

Figure 4.12: ln τ vs. $1/kT$ for various temperatures showing a linear fit for the data. The data is taken from Table 4.3.

angular frequency, ω_r, to find the characteristic relaxation time, τ (see Figure 4.11), and plotting the logarithm of these versus the inverse of the thermal energy, kT, in Figure 4.12 we see a linear relation between the two. Note: the uncertainty on $\ln(\tau)$ was calculated using the relation

$$\Delta \ln(\tau) = \frac{\Delta \tau}{\tau} \tag{4.13}$$

where the $\Delta\tau$ is the uncertainty in τ.

The linear nature of the data indicates a relation that follows an Arrhenius equation of the form

$$\tau \propto e^{\Delta G/kT} \tag{4.14}$$

as proposed by Tanaka and Edwards (51), where ΔG is some amount of energy dependent upon the binding of the telechelic polymers. This indicates an Arrhenius dependence of the relaxation time on the temperature, as expected from the theory for physical gels presented in section 3.1.4. From the linear fit of Figure 4.12, the slope of the graph is estimated as $(1.76 \pm 0.02)X10^{-19}$ J of energy at room temperature.

4.4.4 Concentration Dependence

The rheological dependence of CRC hydrogels on concentration was also studied. Three concentrations ($5.3 \pm 0.1\%$, $7.5 \pm 0.1\%$, and $10.4 \pm 0.3\%$) of CRC in 50 mM sodium phosphate, 0.2 mg/mL sodium azide (pH 7.5) were used to determine the gel behavior over a range of concentrations. The storage moduli (G') and loss moduli (G'') were measured as functions of angular frequency, ω, and the results are shown in Figure 4.13. The uncertainty on the data are approximately equal to the uncertainty on the concentration measurements, giving a maximum approximate uncertainty of $\pm 3\%$ on each modulus measurement.

The data in Figure 4.13 indicate a concentration dependence for the gel's moduli and relaxation time. As expected from the theory presented in section 3.2.2, the moduli increase with increasing concentration. This is due to a higher number of telechelic polymers increasing the amount of elastic energy stored in the system once it is deformed.

Using the same linear extrapolation technique to scale the data as in section 4.4.3, we obtain Table 4.4. The data presented in Table 4.4 can be used to estimate a relationship between the relaxation time and concentration, as plotted in Figure 4.14. A linear relationship is assumed between the relaxation time of the moduli and the concentration, as this is expected from theory for telechelic polymer gels. The slight variation in data points from linear behavior could be attributed to a small sample size where a single point variation could cause a significant difference in statistical analysis. It

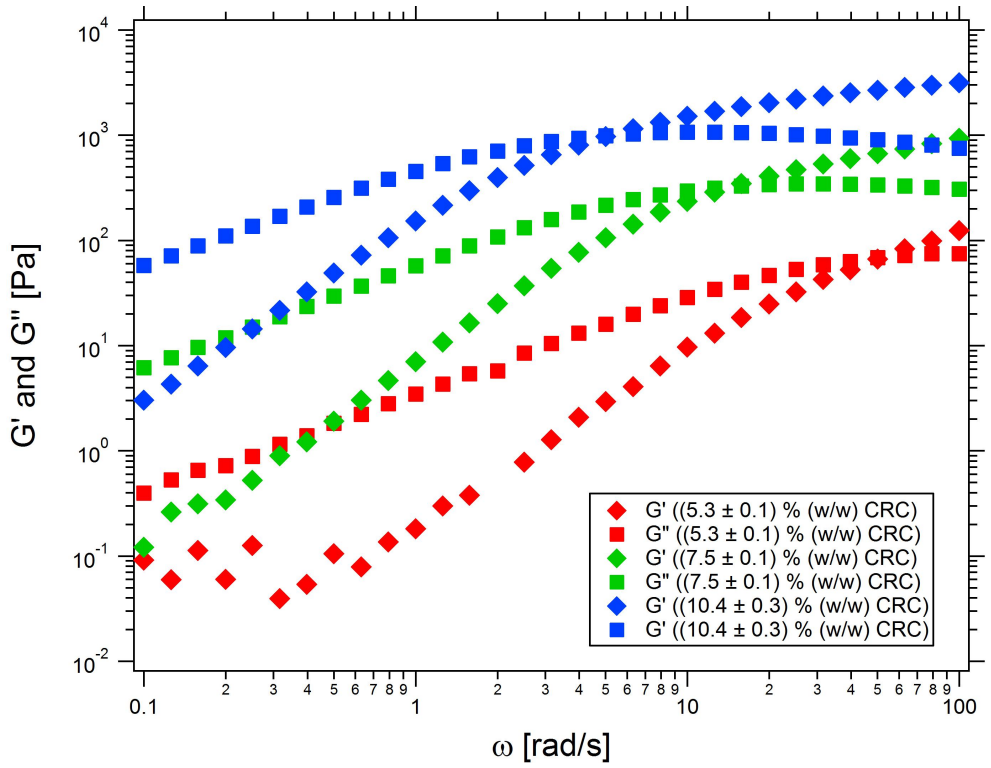

Figure 4.13: G' (◆) and G'' (■) vs. ω for varying concentrations of CRC at T = 285 K.

Concentration	G_r [in Pa]	ω [in rad/s]	τ [in s]
$(5.3 \pm 0.1)\%$	$9.92\text{X}10^2$	(5.2 ± 0.1)	(1.22 ± 0.03)
$(7.5 \pm 0.1)\%$	$3.23\text{X}10^2$	(14.5 ± 0.1)	$(4.35 \pm 0.03)\text{X}10^{-1}$
$(10.4 \pm 0.3)\%$	$1.13\text{X}10^3$	(52.2 ± 0.1)	$(1.204 \pm 0.002)\text{X}10^{-1}$

Table 4.4: Crossover modulus and crossover angular frequency for various CRC hydrogel concentrations at T = 285 K

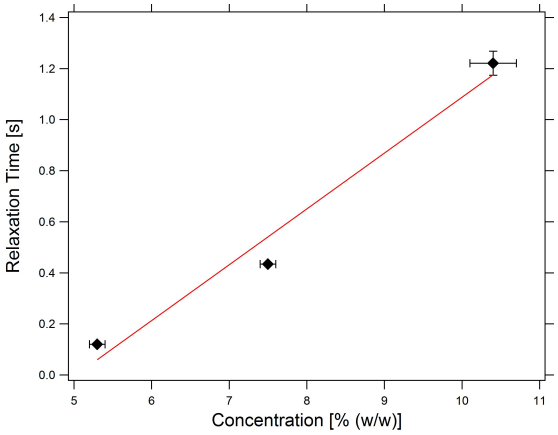

Figure 4.14: The relaxation time, t, plotted as a function of gel concentration. A linear dependence is assumed between the relaxation time and the concentration. The data is taken from Table 4.4

is therefore assumed that if enough samples were tested, the samples would demonstrate a much more linear behavior.

To verify that CRC gels continue to display the same behavior at different concentrations, the data from Table 4.4 were used to plot Figure 4.15. Here, the behavior of the different concentrations seems to cause little variation on the stretched exponential behavior of the gels. This is logical as increasing the overall concentration should only affect the relative amount of elastic energy stored and dissipated, as well as the speed with which the gels can dissipate the energy in terms of viscous friction. Concentration should not have any other effect on the overall mechanism of how the networks store and dissipate the energy. This also demonstrates that at concentrations of 10.4% and below, entanglements don't play a role in the gels. Had entanglements participated in gel properties, no relaxation time would be observed as the energy would be stored by protein molecules crossing over one another, a physical association that can never break.

In order to determine a possible relationship between concentration and modulus data, a plot of G_r vs. $c[\%]$ was made, with the results displayed in

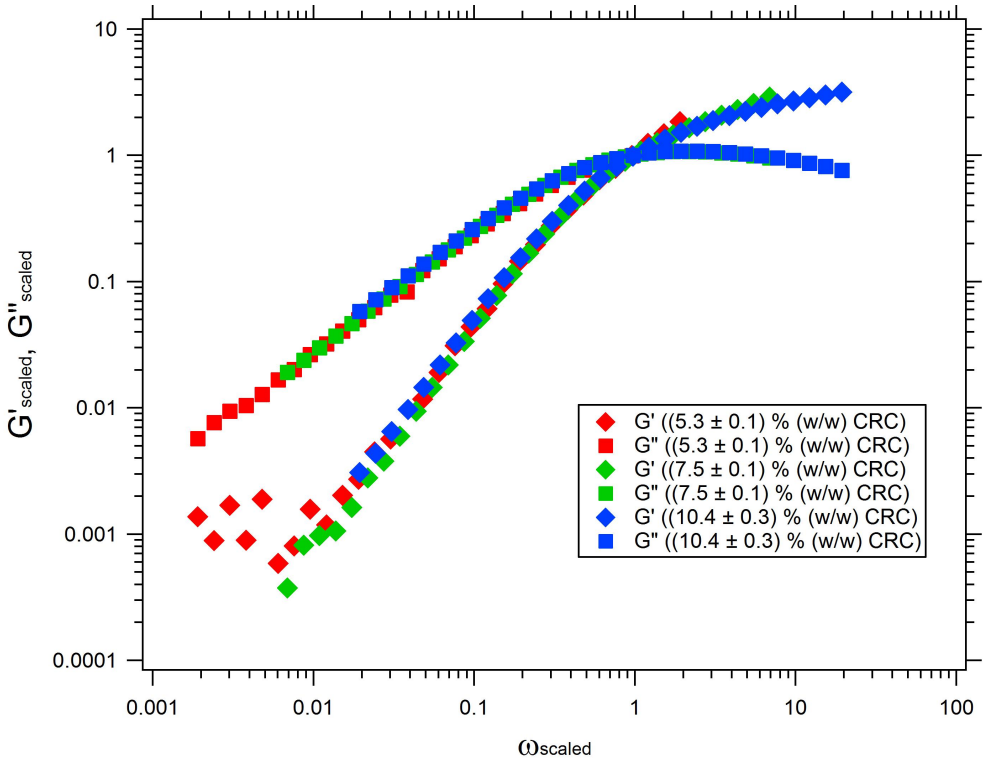

Figure 4.15: G'_{scaled} (◆) and G''_{scaled} (■) vs. ω_{scaled}, for varying concentrations of CRC at T = 285 K

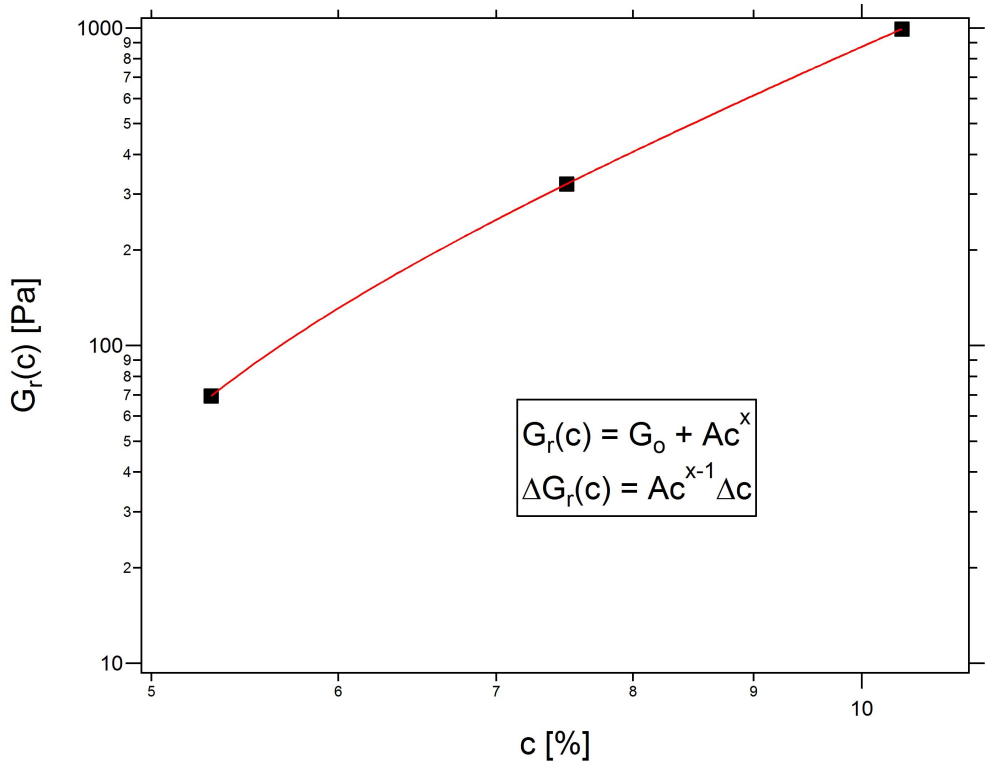

Figure 4.16: G_r vs. c for hydrogels at $T = 285$ K. A power law fit has been assumed between G_r and concentration.

Figure 4.16. A power law fit was found to best fit the data, though with only three data points it is impossible to say with certainty that the moduli should follow this model. From the fit given, an estimation of the uncertainty of the crossover modulus, G_r, due to uncertainty in concentration can be made via

$$\Delta G_r(c) = Ac^{x-1}\Delta c \tag{4.15}$$

where $\Delta G_r(c)$ is the uncertainty in the crossover modulus, c is the concentration (in %), and A and x are constants. Estimations of A and x using iterative software give values of 0.782 and 3.08, respectively. Using these calculated values in equation 4.15 allow an estimation of the uncertainty on

the crossover modulus to be calculated.

4.4.5 Insertion of an Integrin Binding Domain

Another topic of interest with CRC hydrogels is the effect an integrin binding domain, such as RGDS, will have on the gel's rheological properties if placed in the middle R block. The addition of the RGDS might affect the elastic energy present in the protein by increasing the length of the R block. It is far more likely, however, that the insertion of the RGDS domain should have minimal effect due to its location in the R block far away from the physical associations in the C blocks. Two hydrogel samples were prepared in 50 mM sodium phosphate, 0.2 mg/mL buffer at pH 6.5: one composed of 7.7% (w/w) CRC, the other of 7.7% (w/w) CRC protein with the RGDS binding domain, or CRC-RGDS. Each was tested on the rheometer, and the results are given in Figure 4.17.

Slight variations between data in Figure 4.17 can be easily explained by considering the uncertainty between measurements, as expressed in Figure 4.17 by the example error bar. To determine the exact amount of variability between the data sets, the uncertainty for the crossover moduli were determined from equation 4.15. The approximate value of this uncertainty is shown by the error bar in Figure 4.17. Even with this error in consideration, the differences between the data sets still seem to be fairly large. These differences may be due to differences in loading between samples, and likely not any contribution by the RGDS domain. This can clearly be seen by comparing the differences between the data sets of Figure 4.7 with those of Figure 4.17: the differences between the data sets of the former set are much larger than those of the second. This strongly favours the explanation that differences between data sets are likely due to differences in loading and not any contribution the RGDS domain exerts on the rheometry.

This confirms the previously stated hypothesis: as the RGDS domain is located in the random coil (R) block of the protein it should play no

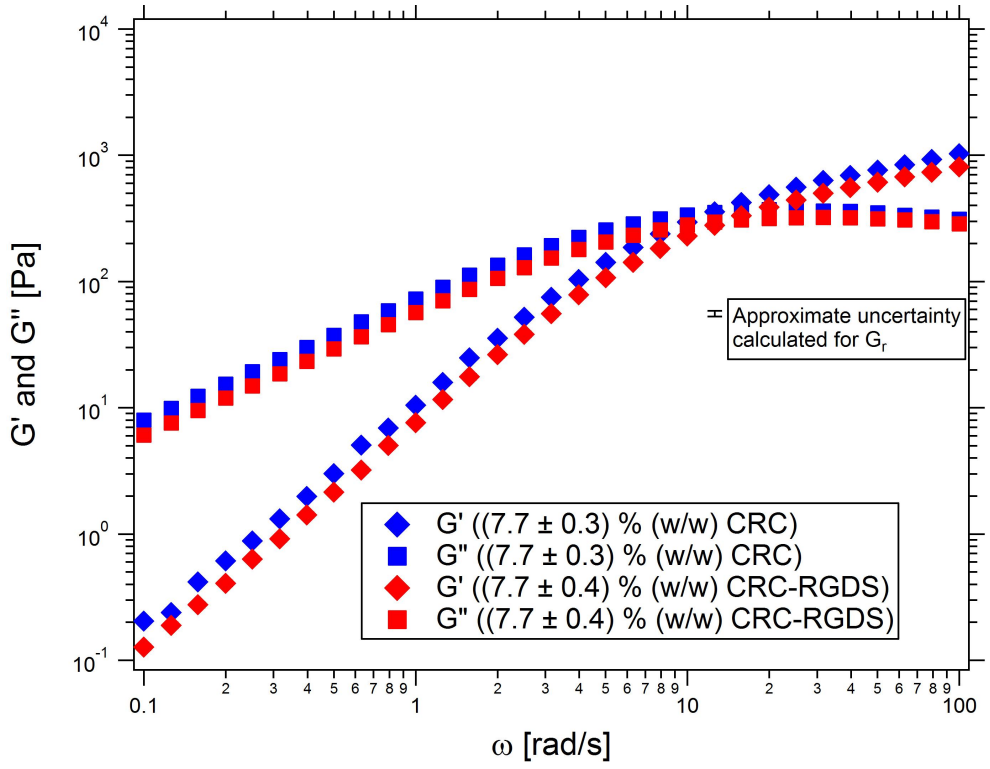

Figure 4.17: G' (◆) and G'' (■) vs. ω, for 7.7% CRC and CRC-RGDS at T = 285 K, with an approximate uncertainty of ~20% displayed by the error bar.

part in the crosslinking interactions of the trimeric bundle. The insertion of the RGDS does not significantly affect the elastic energy of the sample either, indicating that the presence of this domain in the R block will not affect physical crosslinking, and therefore will have no effect on the physical network.

4.4.6 pH Dependence

Another possible variable for CRC gels is sensitivity to pH. As the pH of a solution is a measure of the concentration of H^+ ions or OH^- ions in solution, it is possible that the pH could affect the salt bridges that reinforce the trimeric bundle. A pH of 7.5 is of particular interest because this is the approximate pH of blood in the human body. Various CRC samples were prepared in 50 mM sodium phosphate, 0.2 mg/mL sodium azide buffer at different pH values, 6.5, 7.5, and 8.5.

The prepared gels were subsequently tested on the rheometer, and the resulting data are given in Figure 4.18.

From the data presented in Figure 4.18, it can be concluded that pH variations between the ranges of pH 6.5 and pH 8.5 will have no significant effect on the overall structural properties of CRC hydrogels. This likely occurs because at these pH values, the α-helical interactions are shielded by the salt bridges formed between the lysines and glutamic acids. These salt bridges interact with the ions of the solution, preventing them from interfering with the interactions of the leucine zipper core. Thus, CRC protein networks are unaffected by solutions in the pH range of 6.5 to 8.5.

4.4.7 Conclusion

From the data presented in the previous sections, it can be concluded that CRC hydrogels demonstrate stretched exponential behavior with a value of β in the range $0.5 \leq \beta \geq 0.55$. This value is likely close to a value of

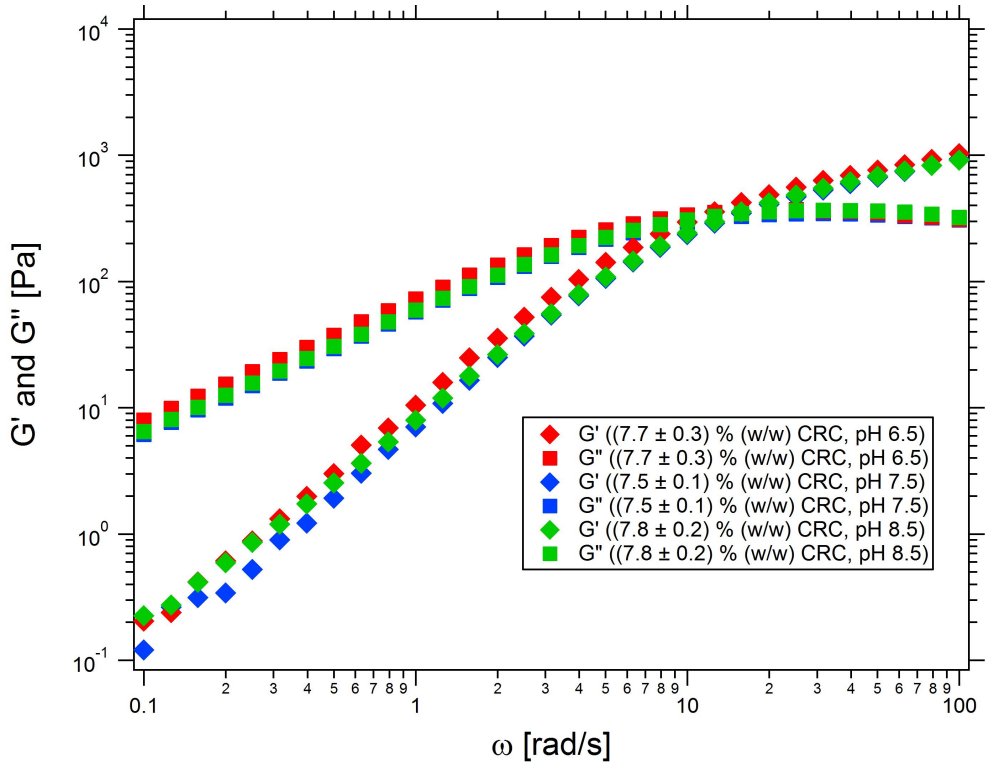

Figure 4.18: G' (◆) and G'' (■) vs. ω, for 7.5% CRC at various pH values. $T = 285$ K

$\beta = 0.5$. This can be related to the appearance of dimers within the system. This behavior remains the same for a range of temperatures (285 K - 290 K), concentrations, and solution pH values. Increasing the temperature of these gels shifts the relaxation frequency to higher values, while increasing the concentration shifts it to lower frequencies. The association energy for the trimeric bundle is estimated to be around $(1.76 \pm 0.02) X 10^{-19}$ J, and the logarithmic relaxation time shows an Arrhenius dependence on the temperature. An increase in protein concentration results in higher modulus values due to increased storage of elastic energy. The addition of an integrin binding domain, RGDS, has no effect on either the relaxation time or modulus properties. Finally, changing the solution pH has no effect on relaxation times or on moduli. All of these can be explained by telechelic polymer theory, as presented in previous sections.

Chapter 5

EDC Crosslinked CRC

5.1 The System

In addition to undergoing self-assembly, CRC protein hydrogels may also be chemically crosslinked using a selective chemical crosslinker. This process irreversibly crosslinks the protein gels, changing the gels from weak, physically crosslinked ones to chemically crosslinked gels. The behavior of the system should then be modelled as an ideal elastic network.

EDC crosslinking

The chemical 1-ethyl-3-(3-dimethyl aminopropyl)carbodiimide hydrochloride, or EDC, is a well-studied zero-length chemical crosslinker used to covalently bond proteins (see Figure 5.1). The term zero-length is used to describe crosslinkers that do not become chemically linked to the final product, thus adding no extra (or zero) length to the final product. EDC functions by first reacting with a carboxylic acid group to form an O-acylisourea which can then react with an amine group to from an amide bond (84, 85).

Leucine zipper bundles are good candidates to form branched polymer networks via EDC crosslinking, if certain conditions are met. If an amino acid with a carboxylic acid containing residue (such as glutamic acid) is

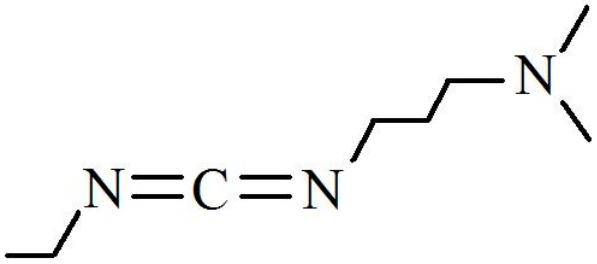

Figure 5.1: An EDC molecule

positioned at every e position of the leucine zipper, and an amine containing residue (such as lysine) is positioned at every g position, they can be easily crosslinked together due to their relative proximity in the trimeric bundle. The number of chemical crosslinks possible for a CRC molecule depends on the number of lysines available in a leucine zipper: there are only three lysines available for crosslinking on the leucine zipper, as opposed to four glutamic acids.

5.2 Methodology

Samples used for crosslinking were made following the protocol outlined in section 4.2.3, with the only exception being that all samples were dissolved in a 50 mM sodium borate, 0.2 mg/mL sodium azide (pH 7.5) buffer solution instead of a sodium phosphate buffer. Sodium phosphate is known to react with EDC while sodium borate does not, making the latter the more desirable buffering salt for crosslinking. For all crosslinked samples, the starting concentration was purposely set higher than the desired testing concentration as the addition of EDC solution to crosslink CRC gels would dilute them.

CRC samples were loaded into a 1 mL syringe and transferred to two separate 2 mL syringes with leur-locks. The syringes were then briefly heated and shaken to remove air bubbles from the gel samples loaded. One syringe

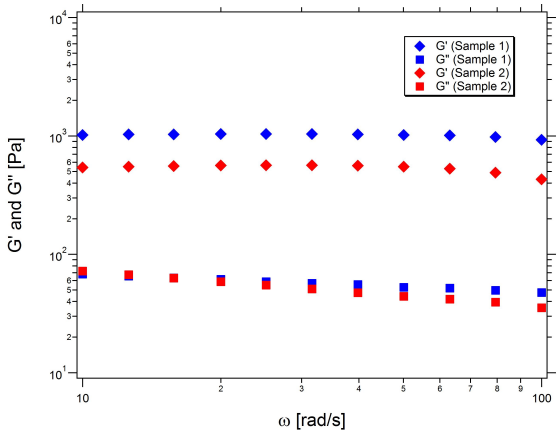

Figure 5.2: G' (◆) and G'' (■) vs. ω for two 5% CRC, 50 mg/mL EDC sample at a pH of 7.5 and temperature of 295 K.

was then attached to a leur-lock trijunction, with one end containing a rubber stopper. A sample of CRC was loaded into the system and the desired amount of EDC to add was calculated for each sample. This EDC was dissolved in the same buffer as the CRC, and was loaded into the system via a Hamilton syringe. The sample was quickly mixed using two syringes attached to the leur-lok system, and then loaded onto the rheometer plates.

5.3 Results and Discussion

As in chapter 4, only one CRC hydrogel sample was tested to obtain each data set. The reasons for this are the same as explained in section 4.4. There are therefore no calculations for standard deviation, n-values, or p-values obtained for each set of data.

A plot of G' and G'' vs. ω for two different samples, each nominally with 5% CRC, 50 mg/mL EDC at $T = 295$ K is given in Figure 5.2.

The uncertainty for this data set should be larger than it was in Chapter 4 as the volume of CRC protein gel measured before crosslinking cannot be obtained with great accuracy. This is due to the estimation required by

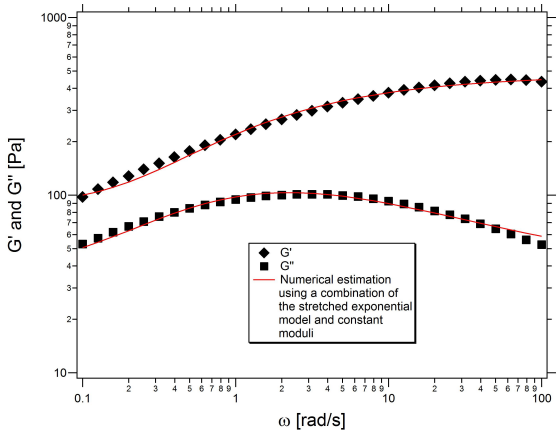

Figure 5.3: G' (◆) and G'' (■) vs. ω for a 5% CRC, 50 mg/mL EDC sample at a pH of 7.5 and temperature of 285 K. A numerical estimation was made combining a constant modulus with the stretched exponential model with $\beta = 0.5$.

combining the inaccurate volume measurement made by using the scale on the syringe with the approximate volume measured for the trijunction. Thus, when EDC containing buffer is added to the system the amount added could easily cause the protein concentration to be much higher or lower than required. This is in addition to the uncertainty introduced by differences in concentration and the manner in which samples are loaded onto the rheometer, as explained in section 4.4.1.

5.3.1 Gel Behavior

First, the rheological behavior of a 5% CRC, 50 mg/mL sample at pH 7.5 and a temperature of 12°C was characterized by measuring the storage modulus, G', and loss modulus, G'' as functions of angular frequency. Results are presented in Figure 5.3. As can be seen, EDC crosslinked CRC gels are not entirely independent of angular frequency, as might be expected for a chemically crosslinked gel (see section 3.2.2). One possible explanation for this is that not all of the telechelic polymer ends are chemically crosslinked, and in

fact are still partially governed by physical crosslinks. The rheology moduli data should therefore be expressed as linear combinations of the chemical gel components and physical gel components.

As discussed in section 4.4.2, CRC gels display a stretched exponential behavior with $\beta = 0.5$. The model for EDC crosslinked CRC modulus behavior should also take this into account. A series of equations for both storage and loss moduli may then be written as

$$\begin{aligned} G'(\omega) &= G_\infty \frac{\sqrt{\frac{\pi}{2}}\left(1 - \mathrm{C}\left(\frac{1}{\sqrt{2\pi\omega\tau}}\right)\right)\sin\left(\frac{1}{4\omega\tau}\right)}{2\sqrt{\omega\tau}} \\ &\quad - G_\infty\sqrt{\frac{\pi}{2}}\left(\frac{\left[\left(1 - \mathrm{S}\left(\frac{1}{\sqrt{2\pi\omega\tau}}\right)\right)\cos\left(\frac{1}{4\omega\tau}\right)\right]}{2\sqrt{\omega\tau}} + 1\right) + G'_o \\ &= G_\infty\kappa' + G'_o \end{aligned} \tag{5.1}$$

$$\begin{aligned} G''(\omega) &= G_\infty \frac{\sqrt{\frac{\pi}{2}}\left(1 - \mathrm{C}\left(\frac{1}{\sqrt{2\pi\omega\tau}}\right)\right)\sin\left(\frac{1}{4\omega\tau}\right)}{2\sqrt{\omega\tau}} \\ &\quad + G_\infty \frac{\sqrt{\frac{\pi}{2}}\left(1 - \mathrm{S}\left(\frac{1}{\sqrt{2\pi\omega\tau}}\right)\right)\cos\left(\frac{1}{4\omega\tau}\right)}{2\sqrt{\omega\tau}} \\ &= G_\infty\kappa'' + G''_o \end{aligned} \tag{5.2}$$

where G_∞ is the plateau modulus, κ' and κ'' are short forms for the stretched exponential components, and G'_o and G''_o are contributions from the chemically crosslinked protein molecules. These equations were also numerically determined using Wolfram Mathematica software by estimating the values of G_∞, G'_o, and G''_o and inputting the correct values of ω. The model data are also plotted in Figure 5.3.

The correspondence between the data and the model is quite good, indicating that these gels are indeed a mix between a chemical gel and physical gel as evidenced by the mixed rheological response of the gel. Differences between the model and the data are quite small, less than the expected differences between nominally similar samples (see Figure 5.2). It is there-

fore likely that EDC crosslinking CRC results in some permanent, chemical crosslinks that produce a constant modulus contribution, while uncrosslinked molecules continue to exhibit stretched exponential behavior.

5.3.2 EDC Concentration Dependence

CRC samples crosslinked at a constant concentration and varying amounts of EDC were tested to determine whether the EDC concentration had an effect on either the gel as it crosslinked, or on the resultant crosslinked network.

The rheometric tests were completed by measuring the storage and loss moduli at 1% strain and 10 rad/s as functions of time for various 5% gels. These values were chosen as 1% strain is within the sample's linear viscoelastic range, and at an angular frequency of 10 rad/s there is less chance that slip will occur. The data are presented in Figure 5.4. As can be seen over this 10 hour period, the moduli of the CRC samples with higher concentrations of EDC plateau much quicker than those samples with lower concentrations. This occurs because a higher concentration of crosslinker within the material makes it more likely the trimeric bundles will encounter an EDC molecule and form covalent bonds. As can be seen, the storage moduli for all samples increase with time. This occurs because, as time progresses, more trimeric bundles become chemically crosslinked, increasing the value of the storage modulus, which is a measure of the elastic energy.

Another conclusion may be drawn from these data by comparing the curves for the 10 mg/mL EDC concentration sample and the 50 mg/mL EDC sample. As can be seen, the storage modulus for the former seems to be approaching that of the latter near 10 hours. The storage modulus of the 5 mg/mL EDC concentration sample at 10 hours seems to be approaching that of the 10 mg/mL EDC concentration sample at 6 hours. It is possible that the storage modulus for these concentrations of EDC would all converge to the same value at high enough concentrations. The loss modulus for both the 10 and 5 mg/mL EDC concentrations seem to be approaching the maximum

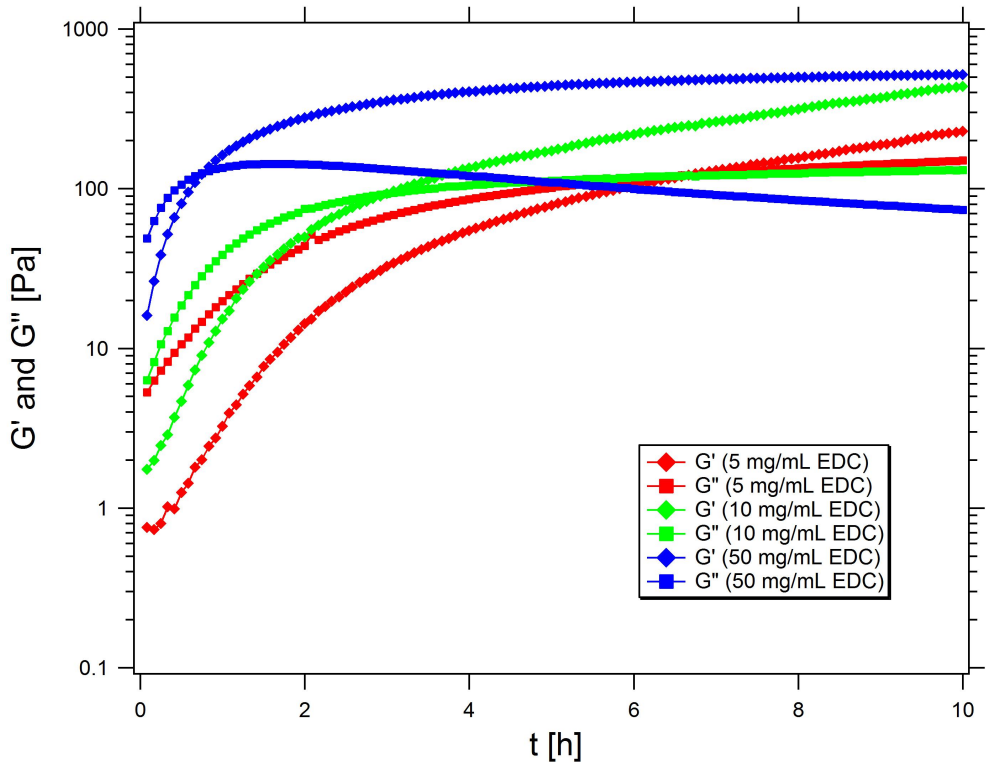

Figure 5.4: G' (◆) and G'' (■) as functions of time for 5% CRC gels with varying EDC concentrations.

loss modulus value of the 50 mg/mL EDC sample. It is possible that, given enough time, these samples would also attain this maximum value, and then begin to drop as well. One possible reason for the drop in loss modulus with time for the 50 mg/mL sample is due to a lower number of free ends able to dissipate elastic energy through viscous friction with the solvent. Given enough time, all the free ends should come into contact with EDC, and therefore be eligible for chemical crosslinking. Thus, as time progresses there are more chemical crosslinks formed than physical ones, leading to lower storage modulus data.

To further compare the effects of varying EDC concentrations on the 5% gels, a plot of moduli versus ω is given in Figure 5.5. From Figure 5.5, it

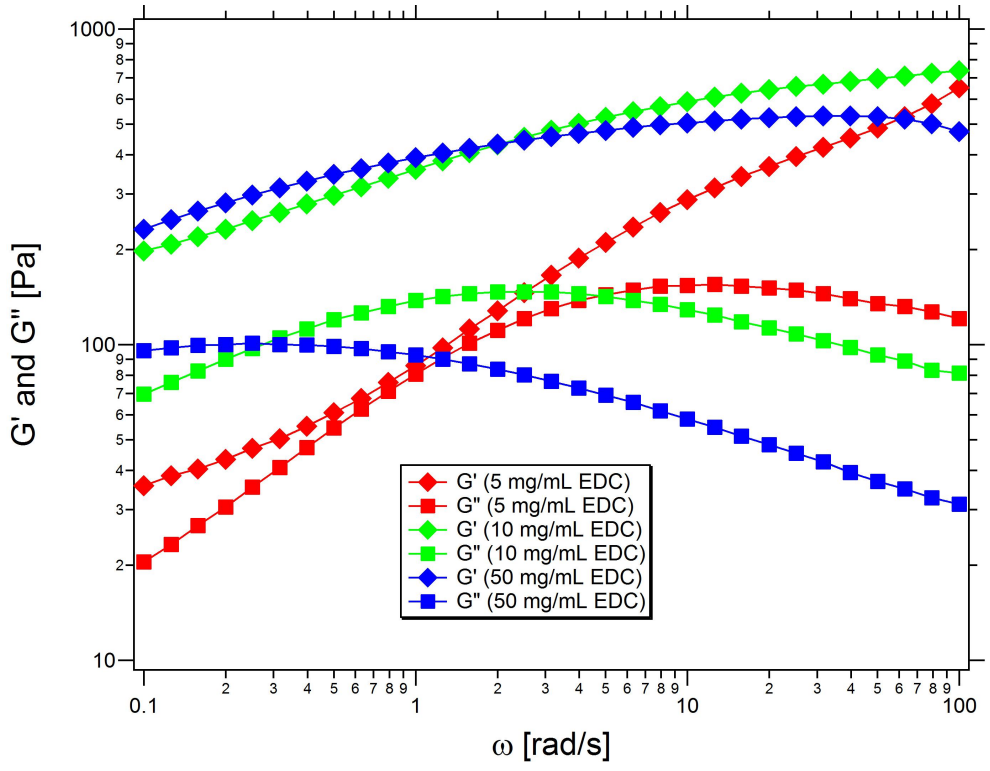

Figure 5.5: G' (◆) and G'' (■) vs. ω for 5% CRC hydrogels with varying EDC concentrations at 295 K.

Gel Sample	G'_{max} [Pa]
5.3% CRC	17.8
5% CRC, 5 mg/mL EDC	652
5% CRC, 10 mg/mL EDC	701
5% CRC, 50 mg/mL EDC	566

Table 5.1: The maximum storage modulus, G'_{max}, for a 5.3% CRC sample and a 5% CRC, 50 mg/mL EDC sample at various temperatures for $0.1 < \omega < 100$ rad/s.

is seen that the behavior of the hydrogels is decreasingly dependent of ω for higher concentrations of EDC. It is also seen that a characteristic relaxation time, τ, can no longer be calculated from any of the samples as there is no crossing over of the storage (G') or loss (G'') moduli within the range of frequencies studied. Both the aforementioned observations lead to the conclusion that after 10 hours and at a minimum concentration of 5 mg/mL EDC, a 5% CRC hydrogel changes from a stretched exponential fluid to a chemical gel. This arises from the fact that stretched exponential fluids have an associated relaxation time with their rheological components, while chemical gels are very weakly dependent on the time, and therefore angular frequency. In the case of CRC, this relaxation time is associated with the lifetime of the self-assembling trimeric bundles, and chemically crosslinking them together prevents the dissociation of the trimers from occurring.

It should be noted that the maximum storage modulus for all three CRC samples with different amounts of EDC is higher than that of the 5.3% sample of CRC without EDC, as presented in table 5.1. From these values it is readily seen that the EDC crosslinked samples are over thirty times as strong as the physically crosslinked CRC sample. This is likely due to the increased number of crosslinks caused by the chemical crosslinking. The physical associations of regular CRC are not permanent, and the energy required to break them is of the order of the thermal energy. Therefore, at room temperature (~295 K) many of the potential trimeric associations of the physically crosslinked

system are dissociated, creating a weaker system that cannot store stress energy. Chemical crosslinking, however, creates far more bonds, allowing many more molecules to participate in energy storage and dissipation. This creates much higher maximum storage moduli than the physically crosslinked sample. Thus, there are still some physical trimeric associations that can dissociate, creating a dependence of the modulus on angular frequency.

5.3.3 Temperature Dependence

The behavior of a fully crosslinked gel was investigated at various temperatures to determine the thermal dependence. The 5% CRC, 50 mg/mL EDC sample was selected since the moduli varied very little with t, implying that the sample was fully crosslinked. The data are shown in Figure 5.6.

Figure 5.6 indicates an inverse relationship between the moduli of a CRC hydrogel and the ambient temperature. From the model proposed in section 5.3.1, the first components are those representing the chemical gel contribution to the moduli. These are proportional to the temperature, and should increase as temperature is raised. This is likely due to a finite fraction of non-EDC crosslinked CRC leucine zippers. As the EDC has not affected them, their interactions must be the same as before. Therefore, the physical associations of EDC crosslinked CRC gels create lower moduli within the frequency ranges studied due to decreases in relaxation time.

5.3.4 CRC Concentration Dependence

The behavior of EDC crosslinked CRC hydrogels at different concentrations is also of interest. Crosslinking time tests were performed for ten hours on a 5%, 7.5%, and 10% CRC hydrogels with 50 mg/mL EDC as in Figure 5.7. An EDC concentration of 50 mg/mL was chosen because, as indicated from the data in Figure 5.4, at 10 hours with this concentration of EDC many of the sites available will crosslink. The curves presented in Figure 5.7 demonstrate

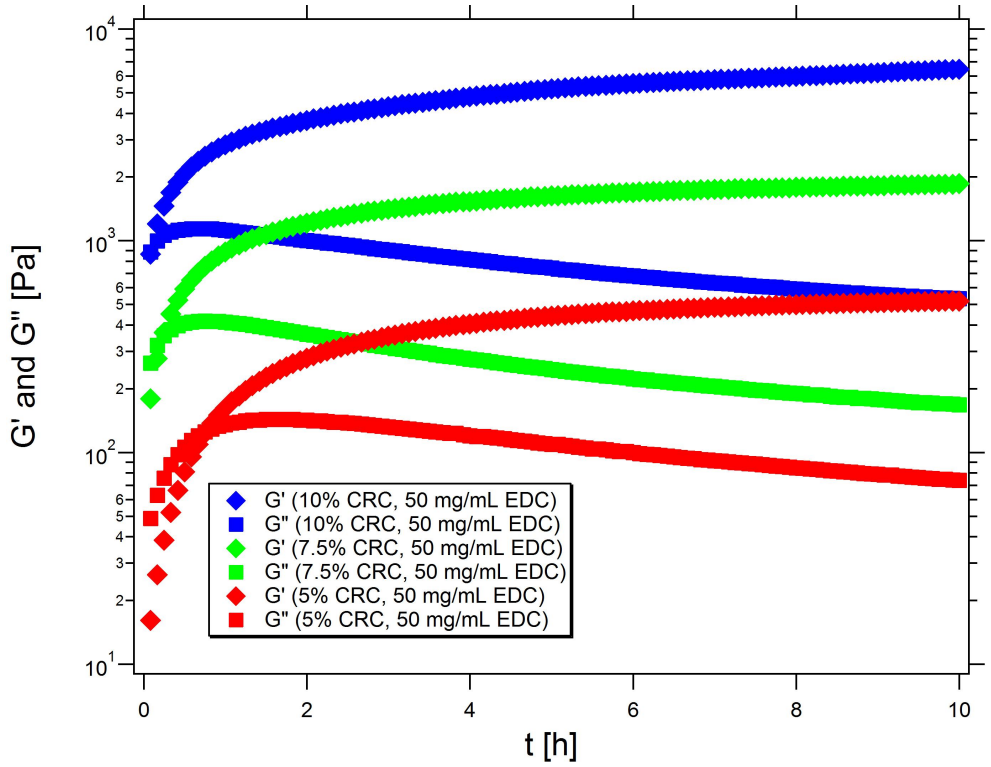

Figure 5.6: G' (◆) and G'' (■) vs. t for a 5% CRC hydrogel with 50 mg/mL EDC.

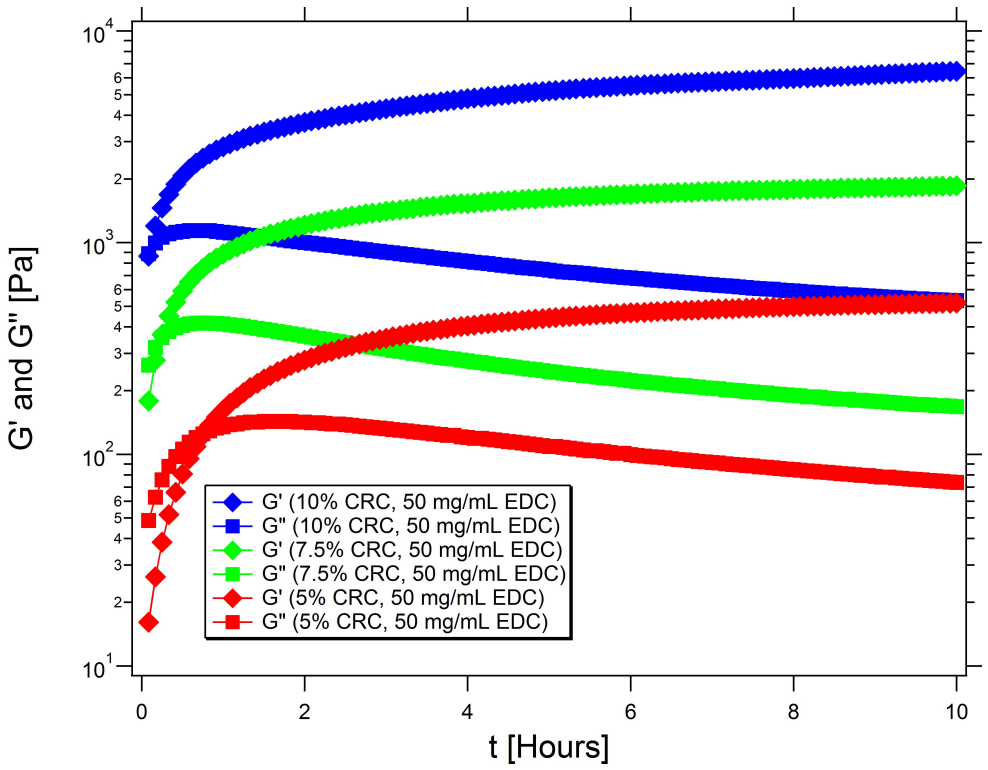

Figure 5.7: G' (◆) and G'' (■) vs. t for hydrogels with 50 mg/mL EDC and varying CRC concentrations at a temperature of 295 K.

very similar behavior with time. At all concentrations shown, the storage modulus overtakes the loss modulus in less than one hour's time. This occurs more quickly at higher concentrations, likely due to the increased number of possible chemical crosslinks. With a larger number of possible crosslinking pairs of glutamic acids and lysines, the rate of reaction increases. Thus, the reaction must occur more quickly for higher concentrations of CRC. This is reflected in a higher storage modulus, representative of increased elastic energy storage in the system due to a larger number of crosslinks.

The shapes of the curves for all three concentrations above the crossover point (the point at which $G' > G''$) are all very similar. This indicates that all three concentrations of CRC are in the same semidilute solution range during and after crosslinking. The largest difference between the three concentrations is the relative strengths of each gel. The 10% CRC sample possesses the strongest storage and loss moduli, while the 5% possesses the weakest. This is due to the increased number of chemical crosslinks at higher concentrations of CRC, allowing more polymers to both store and dissipate stress energy applied to the system.

Next, the rheological responses of the EDC crosslinked CRC hydrogels with angular frequency were determined at $T = 295$ K, as shown in Figure 5.8. As the concentration of the CRC hydrogels in Figure 5.8 is increased, the values of the moduli are increased, as expected from the data given in Figure 5.7. The moduli do show slight angular frequency dependencies, with the storage modulus increasing and the loss modulus decreasing at higher angular frequencies. This is due to physical associations that have not yet been chemically crosslinked, as discussed in section 5.3.1.

The relative behavior of all three concentrations is also very similar, save shifted to higher modulus for larger concentrations. The 5% CRC sample seems to be much more dependent upon angular frequency as its storage and loss modulus are much closer in magnitude at low frequencies. This further reinforces the idea that the angular frequency dependence of the modulus

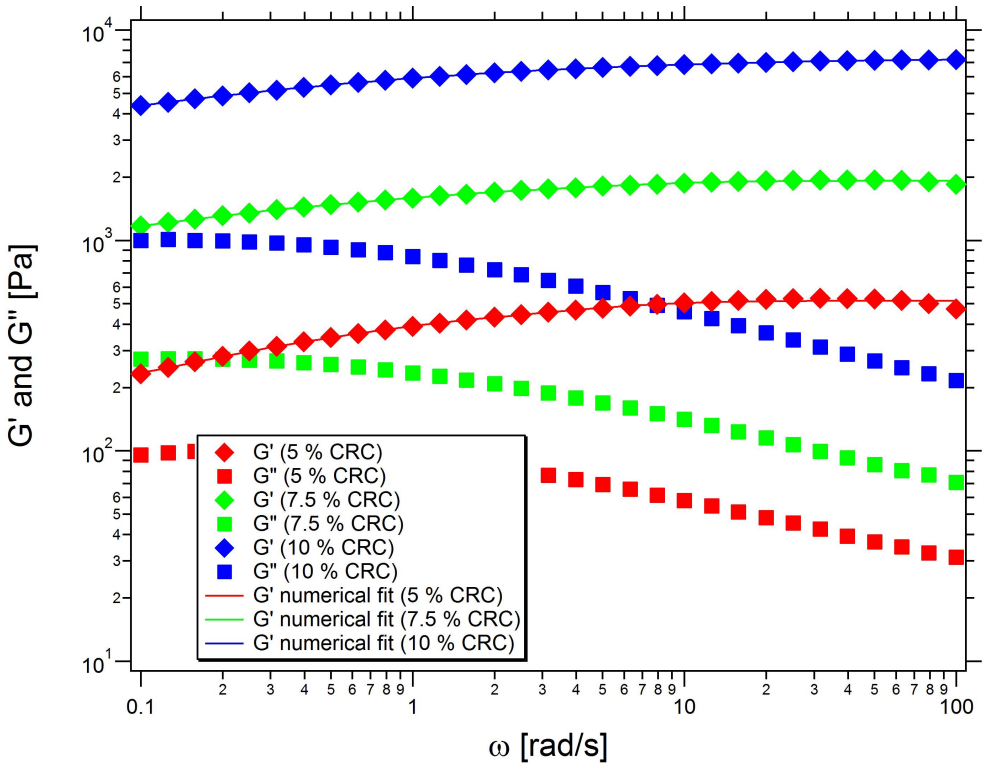

Figure 5.8: G' (◆) and G'' (■) vs. ω for CRC hydrogels at various concentrations and 50 mg/mL EDC.

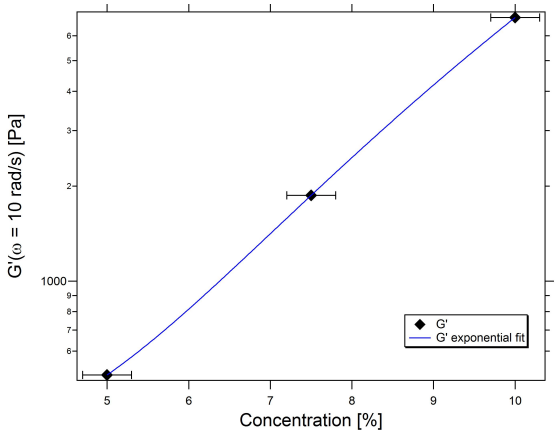

Figure 5.9: G' (◆) vs. concentration at $\omega = 10$ rad/s and T = 295 K. An exponential fit has been made of the concentration dependence.

depends on physical associations that EDC has not chemically crosslinked because at this dilute concentration the CRC protein molecules are less likely to contact one another. This decrease in contact due to lower proximity also decreases the chance that an EDC molecule will enable a chemical crosslink to occur, resulting in a slight increase in non-chemically crosslinked physical associations.

Due to the complex nature of the system (i.e. both physical and chemical crosslinks), the dependence of the moduli on concentration can be expected to be different from the linear, theoretical predictions for both chemical and physical gel systems. This can be demonstrated via a plot of the storage modulus at $\omega = 10$ rad/s vs. concentration, as in Figure 5.9. The dependence of the storage modulus on concentration was modeled with an exponential fit for the storage modulus. Here, the modulus is plotted as a function of concentration via the relation

$$\begin{aligned} G' &= G'_o + G_\infty \kappa' \\ &= G'_o + AkT\mathrm{e}^{\alpha c}\kappa' \end{aligned} \tag{5.3}$$

where G'_o is a constant modulus term, κ' is the stretched exponential compo-

nent defined in section 5.3.1, A and α are constants with respect to concentration, and c is the percent (w/w) concentration of the CRC hydrogel. The $AkT\mathrm{e}^{\alpha c}$ term is derived from $G_\infty = \nu kT$, where ν are the number of elastically effective chains. The value of ν therefore demonstrates an exponential dependence on concentration.

This concentration dependence is different than that predicted by the theory of section 3.1.3 for chemical gels, but there are examples of this behavior in the literature. Yarovoy, *et al* studied a poly(methyl methacrylate) (or PMMA) system that gels in an ionic solvent due to the stereochemistry of its components (86). This system displayed an exponential dependence for the moduli on polymer concentration, much like the EDC crosslinked CRC system.

The crosslinking of the CRC system is quite different from that of the PMMA system in that there exist both physical associations via the hydrophobic interactions of unreacted leucine zippers and chemical crosslinks between the lysines and glutamic acids. As stated before, the PMMA system forms a gel through its stereochemistry, specifically between the isotactic and syndiotactic versions of the polymer. Isotactic polymers are those with individual monomer unit's side chains geometrically aligned along the primary chain, while syndiotactic versions have their individual monomer units aligned such that any side branches are not aligned. This allows the PMMA molecules to lock together via Van der Waals forces (86). Thus, the crosslinking between the systems are quite different, necessitating investigation of other possibilities for this behavior.

One other way of modelling the moduli is via a power law, as demonstrated in Figure 5.10 with a constant frequency of $\omega = 10$ rad/s. A numerical fit was made to the data using a power law equation of the form

$$\begin{aligned} G' &= G'_o + G_\infty \kappa' \\ &= G'_o + AkTc^\alpha \kappa' \end{aligned} \tag{5.4}$$

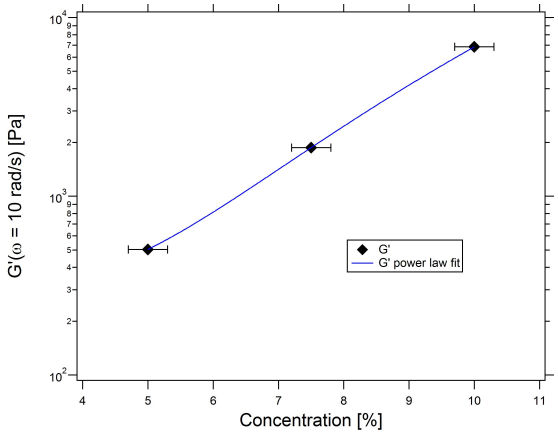

Figure 5.10: G' (◆) vs. concentration at $\omega = 10$ rad/s and T = 295 K. A power law fit has been made of the concentration dependence.

where G'_o is a constant modulus, κ' is the stretched exponential term defined in section 5.3.1, A and α are constants with respect to concentration, and c is the percent (w/w) concentration of the CRC hydrogel. Numerical estimates of α are given by 5 ± 1. A power law dependence has been found for different telechelic systems by Tsitsilianis, *et al*, with different exponents for different systems (87). Variations in the power law exponents were explained by how much larger they were from unity. As explained previously, $G_\infty = \nu kT$ which predicts a linear dependence upon concentration. Therefore, the farther the component is from unity, the fewer the strands that contributed to forming bridges between trimeric junctions.

It can also be argued that the number of elastically effective chains, ν, is related to the power law dependences on concentration, c^α and c^β. Skrzeszewska, *et al* have demonstrated that the shear modulus for triblock telechelic systems demonstrate a dependence based on the relation

$$G_o \approx \frac{Fc(2p-1)^3 RT}{p^2} \tag{5.5}$$

where F is a front factor, c is the concentration, RT is the thermal energy per

mole, and p is the probability that a certain end group will form a trimeric junction (88). The prefactor F is equal to 1 if the affine network theory is adhered to, while a value of 1/3 is used when dealing with trifunctional nodes (88). Concentration dependencies are slightly more complicated than this equation suggests at first glance.

The probability that a certain end group will be a part of a trimeric junction specifically, p, is inherently dependent upon the concentration of protein. At lower concentrations, it is statistically less likely that an end group will encounter another end group. It is therefore less likely to be involved in a junction, giving it a lower probability. In addition, this also encourages the formation of dimeric junctions which don't add to the network as they essentially create longer strands. As the concentration increases, the likelihood of an end group contributing to network strength will also increase, causing a related increase in probability.

It is difficult to determine which of the aforementioned relations between the storage modulus and concentration is the true relationship. This arises mostly due to a lack of modulus data: in this study, only half a decade of information is presented. To determine conclusively which of the two relations can be ascribed to EDC crosslinked CRC systems, it is necessary to extend the range of the data to more than one decade, allowing more information about the overall behavior of the gels to be considered.

5.3.5 Conclusion

Chemically crosslinking CRC protein molecules creates chemical gels with rheological behavior indicating a mix of physically crosslinked components that follow a stretched exponential model with $\beta = 0.5$ and chemically crosslinked components. Decreasing the concentration of EDC causes the gels to take longer to fully crosslink. An EDC concentration of 50 mg/mL is sufficient to crosslink CRC molecules fairly quickly. Increasing the protein concentration causes a slight increase in the speed at which the networks

crosslink, and increases the magnitude of both storage and loss moduli. The behavior of these gels is nearly independent of angular frequency, with slight variations in modulus strength due to physical associations that have not been chemically crosslinked. This frequency dependence is more pronounced for lower concentrations of CRC.

Chapter 6

Biomimetic Gluten Proteins

6.1 The System

W6 is a wheat gluten derived protein composed of 6 repetitions of a specific amino acid sequence (W1). The W1 sequence is based on the A and N mutated gluten sequences studied by Wellner, *et al* with the exception that the glycines present in a normal gluten molecule are replaced by glutamic acids to enhance solubility (30). The W1 sequence makes use of this enhanced solubility as it is composed of half an A block and half an N block, the latter of which is not very soluble. The resulting amino acid sequence is given in Figure 6.1.

Other than its increased solubility, W6 cannot physically self-assemble into a gel form as it lacks the necessary electrostatic, hydrophobic, and hydrogen bonding mechanisms for physical gelation. However, due to the presence of six tyrosines (the Y in Figure 6.1), W6 can undergo chemical crosslinking via an addition polymerization reaction through the use of horseradish peroxidase (HRP) and H_2O_2. HRP reacts with hydrogen peroxide to create free radicals. These free radicals react with tyrosine residues to create an intermediate free radical that can react with other tyrosines to form what are called dityrosines (89, 90). The formation of dityrosines as a means of bond-

MAPGQGQCEYDPTSLQEPGQGQPEYDPTSLQEPGQGQPEYD
PTSLQEPGQGQPEYDPTSLQEPGQGQPEYDPTSLQEPGQGQP
EYDPTSLQEPGQGQPEYDPTSLQEPGQGQPEYDPTSLQEPGQ
GQPEYDPTSLQEPGQGQPEYDPTSLQEPGQGQPEYDPTSLQE
PGQGQPEYDPTSLQEPGQGQPEYDPTSLQCPGQGQP

Figure 6.1: The W6 amino acid sequence. W6 is composed of six repetitions of the W1 insert, highlighted in red here.

ing and strengthening elastomeric proteins is a known natural phenomenon in resilin (91, 92) and elastin (93). The process itself requires the presence of hydrogen peroxide (H_2O_2) as an oxidizing agent to react with two tyrosines to produce the dityrosine, as in Figure 6.2 (89, 90). The rheological characteristics of W6 gels would then behave as a chemically cross-linked gel, obeying the mechanics of kinetic gelation described in section 3.1.3.

Methods of crosslinking elastomeric proteins are varied, though they always result in covalent bonding between molecules. Gamma radiation has been used to crosslink elastin aggregates to form nanoparticles which can be used as drug delivery systems (94, 95). Advantages to this crosslinked system include the lack of potentially toxic crosslinking chemicals, the sterilization of the material by the gamma rays, and the creation of a biodegradable drug delivery system (94).

This reaction involves the conversion of hydrogen peroxide to a free radical intermediate (89). It is this free radical that reacts with a tyrosine to form a tyrosine radical, which in turn reacts with another tyrosine to form the dityrosine. Such reactions are known as *addition polymerization* reactions, and are further discussed in section 3.1.3.

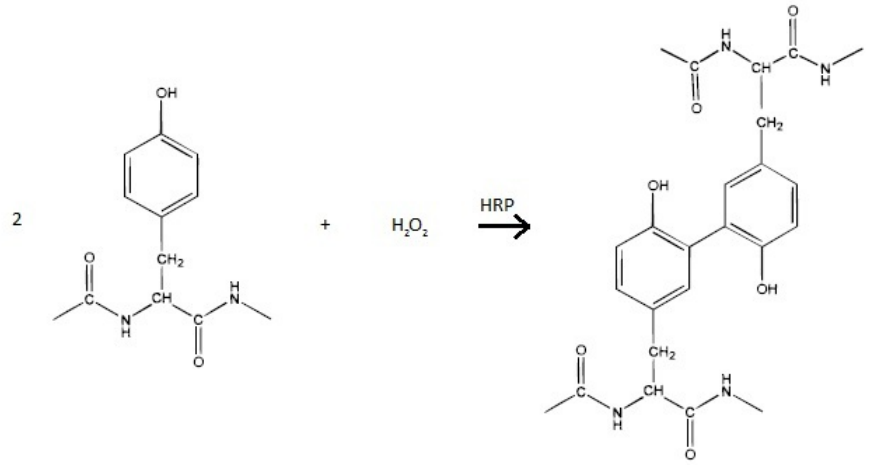

Figure 6.2: HRP catalyzed reaction of two tyrosines with a hydrogen peroxide to produce a dityrosine

6.2 Methodology

W6 was expressed, purified, freeze-dried and donated by Dr. Scott Dick. Samples were weighed into 1.5 mL tubes, and dissolved in 150 mM sodium pyrophosphate (pH 10.2) buffer. The concentration was verified by using 990 μL sodium pyrophosphate to dilute 10 μL of sample, mixing well, and then measuring the Abs_{280} with sodium pyrophosphate as a blank as per previous instructions. HRP solutions were prepared by weighing dry HRP into a tube, and adding enough 25 mM borate buffer solution for a final concentration of 50 mg/mL HRP. Hydrogen peroxide (H_2O_2) solution was prepared by diluting pure solution to 100 mM with DI water.

The volumes of W6, HRP, H_2O_2 and DI water solutions needed for a desired concentration were calculated. The W6, HRP and DI water were then mixed together using a micropipette. For cases of higher concentrations of W6 (40 mg/mL, or above), the reaction occurred too quickly at room temperature to remove the sample from the tube, so all samples were kept

on ice for these concentrations. Once the H_2O_2 was added, the sample was quickly mixed and pipetted onto a 25 mm diameter mould. This mould was placed into a heater set to 37°C for a period of 1 hour before the sample was transferred to the rheometer.

6.3 Results and Discussion

All gels in this section were characterized by measuring the moduli, G' and G'', versus angular frequency, ω, on the Anton Paar MCR 301 rheometer. A shorthand description of W6 gels is also used in the following section to describe the relative concentrations of the three major components. If a W6 gel possesses A mg/mL W6, B mg/mL HRP, and C mM H_2O_2, then such a gel will be denoted as an A-B-C W6 hydrogel.

As in Chapters 4 and 5, only one sample was tested in order to obtain each data set as it was very time consuming to obtain significant amounts of W6 to perform each test. Again, this results in no standard deviation, n-values, or p-values for each data set.

A plot of G' and G'' vs. ω for two different samples of 20 mg/mL W6, 1 mg/mL HRP, and 10 mM H_2O_2 at $T = 298$ K is given in Figure 6.3. As with CRC gels, there were large sample-to-sample variations in moduli measured for nominally equivalent samples, presumably due to the strong sensitivity of rheological parameters on uncertainties in protein and crosslinker concentrations as well as the loading procedure. Another possible culprit for the large uncertainties could perhaps be the presence of an impurity. Each sample in Figure 6.3 was obtained from a different batch of protein, and in each purification of W6 there exists a small amount of impurity that absorbs 280 nm light. When a sample with more impurity (in this case, the first sample) has its concentration measured using 280 nm absorption, its calculated concentration will read higher than it should. It is very possible that this occurred here, where the first sample had a higher level of impurity making

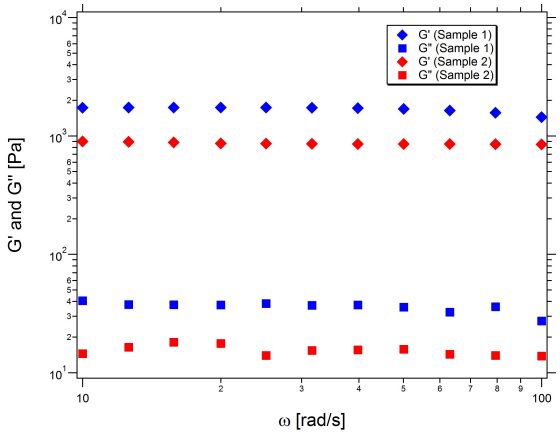

Figure 6.3: G' (◆) and G'' (■) vs. ω for two 20-1-10 W6 hydrogels at $T = 298$ K.

its measured W6 concentration higher than it actually was.

6.3.1 Thermal Dependence

To determine the behavior of W6 gels with temperature, a sample with concentrations of 20 mg/mL W6, 1 mg/mL HRP and 10 mM H_2O_2 were tested on the rheometer at three temperatures: 298 K, 310 K, and 318 K. The data are presented in Figure 6.4.

From these data, it is clear that neither the storage nor loss moduli depend appreciably on the angular frequency, ω, indicating nearly ideal elastic behavior. The presence of dropped channels (values of G'' that drop to 0) for the $T = 318$ K sample may be a result of the crosslinking process used for W6. The free radical peroxide crosslinking of W6 molecules together seems to create a gas as a byproduct. This reaction continues even during testing on the rheometer as there is no means of completely stopping it short of changing the chemistry of the gel. The resultant bubbles could cause slippage to occur. In addition, at higher temperatures the hydrogel system tends to contract, as per the theory presented in section 3.1.3. This contraction squeezes solvent out of the gel, placing it between the sample and the top

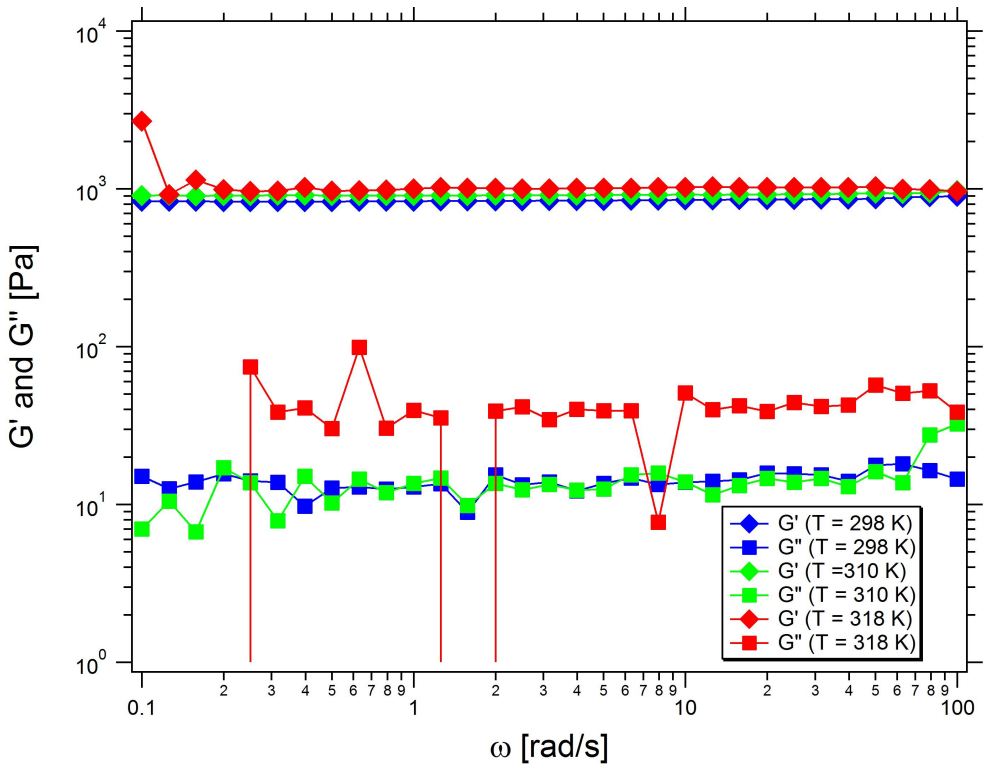

Figure 6.4: G' (◆) and G'' (■) for a 20-1-10 W6 hydrogel at various temperatures.

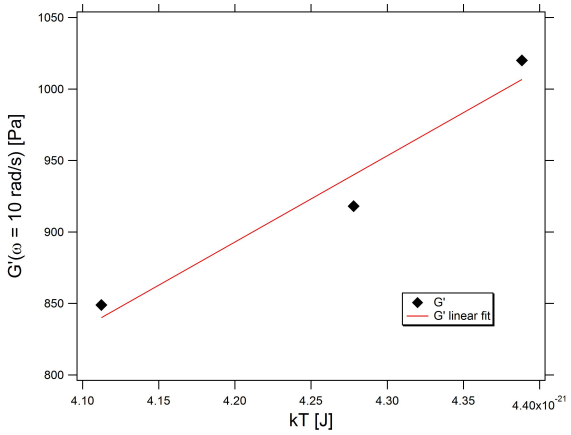

Figure 6.5: G' (◆) versus kT for a 10 mg/mL W6, 1 mg/mL HRP, 10 mM H_2O_2 sample. The red line represents a linear fit made to the data.

rheometer plate. The solvent can then increase the chances of slip occuring for the sample, causing G'' to be measured as 0.

As also can be seen, G' increases as T increases. To estimate the dependence of the storage modulus on temperature, values of G' were plotted versus kT. Assuming a linear relation with temperature, the results were then fit to a linear numerical model, as shown in Figure 6.5. From Figure 6.5, the relation between the storage modulus and temperature could be modelled by $G' \propto kT$, as expected from equation 3.23 presented in section 3.1.3. Assuming a linear relationship, the exact value of the proportionality constant between the two was determined by the fit to be $(6 \pm 1) \times 10^{23}$ Pa/J. This constant should be equal to the density of the elastically effective protein molecules. Assuming the storage modulus dependence on kT is linear and noting its independence of ω indicate that W6 gels could behave as chemically crosslinked gels when an oscillating stress is applied. If the relation is truly linear, then the thermal conditions vary with temperature exactly as predicted from the theory of rubber elasticity.

The variation between the data and the linear fit may be due to slipping occurring between the rheometer tool and the gel. This slippage would cause

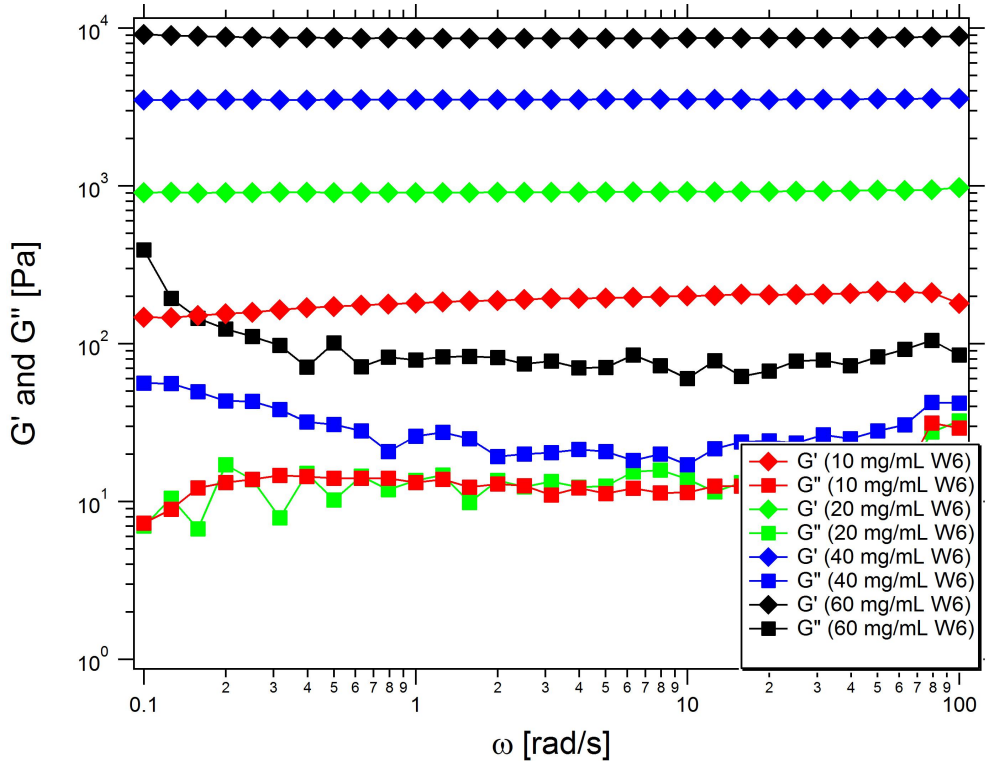

Figure 6.6: G' (◆) and G'' (■) vs. ω for varying concentrations of W6. Data were taken at $T = 310$ K, and a strain of 0.25%

the measured stress to be lower than it should for a specific strain, resulting in a lower storage modulus.

6.3.2 Protein Concentration Dependence

Samples with varying W6 concentrations were tested on the rheometer with constant concentrations of HRP and H_2O_2 to determine the effects of concentration on the gels. The data are presented in Figure 6.6.

It is clear that as the concentration of W6 increases, so do the values of G' and G''. To determine exactly the relation between the concentration and moduli, logG' and logG'' were plotted as functions of *log* concentration (log c) at $\omega = 10$ rad/s, $T = 310$ K, and $\gamma = 0.25\%$. A linear fit was calculated

for G' using Igor software, with the results presented in Figure 6.7.

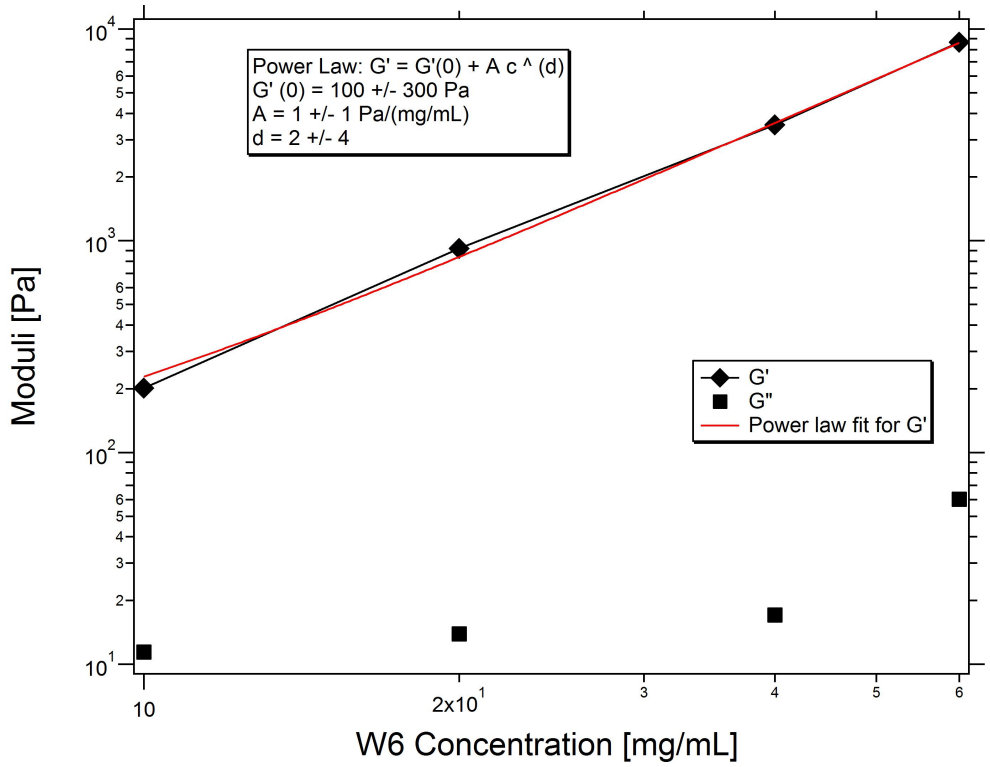

Figure 6.7: log G' (◆) and log G'' (■) vs. log c. A power law fit has been calculated for the data, with the results displayed.

From the linear fit, we can see that the data for G' follows a power series law,

$$G' = G_o + Ac^{\delta} \tag{6.1}$$

where $G_o = 100 \pm 300$ Pa, $A = 1 \pm 1$ Pa/(mg/mL), and $\delta = 2 \pm 4$, as determined by a power series fit. Of these three calculated values, only that of G_o is an inherent property of W6 while the other two are consequences of the way the polymer solution forms a gel network. This is a consequence of the osmotic pressure created once the elastic network and the solvent which permeates it reach an equilibrium in which the elastic energy of contraction is exactly balanced by the swelling brought about by the solvent. The value

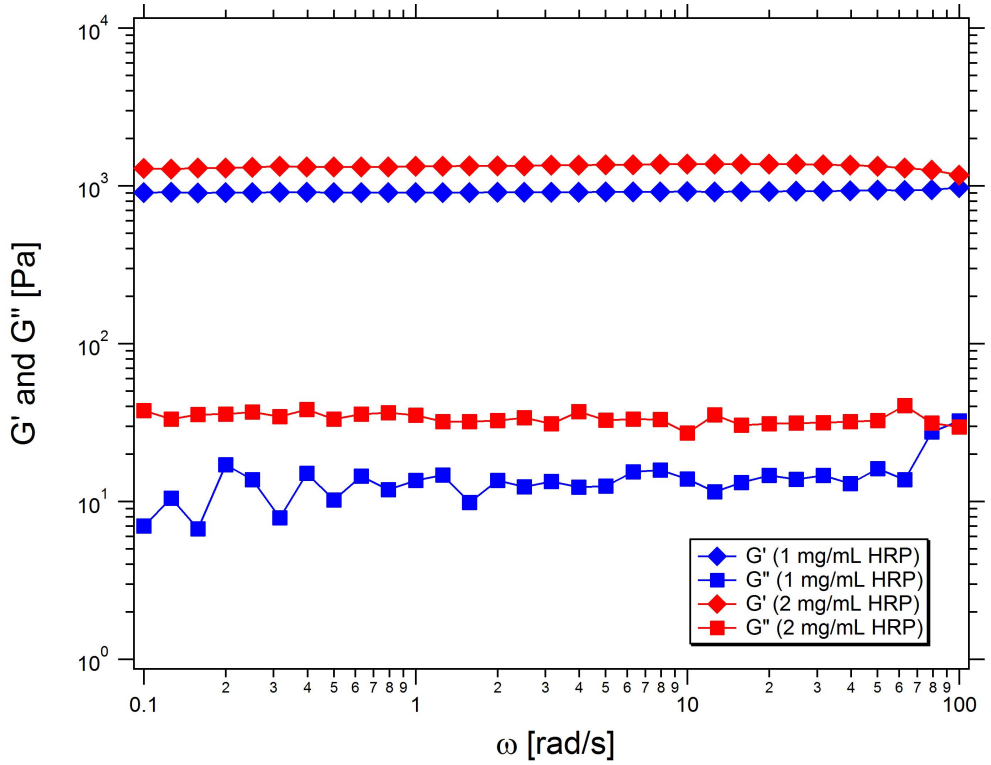

Figure 6.8: G' (◆) and G'' (■) vs. ω for 20 mg/mL W6 samples with 10 mM H_2O_2. Data were taken at $T = 310$ K, 0.25% strain

of δ calculated by the software above is very close to the value of $9/4 = 2.25$ predicted by theory in section 3.1.3. This predictability based on rubber elasticity theory further reinforces the idea that W6 gels are well-behaved chemically crosslinked hydrogels.

6.3.3 HRP Concentration Dependence

To determine whether the concentration of HRP would have an effect on modulus behavior, two 20 mg/mL W6 samples were prepared with 10 mM H_2O_2. The results are shown in Figure 6.8. From the graph, it can be seen that the additional HRP has little effect on G'. The variation between the storage moduli of the two samples is likely explained by differences in purity

of the two samples, as explained previously. The difference in the storage moduli is then not derived from differences in HRP concentration, indicating that the sample with 1 mg/mL HRP is fully crosslinked. This shows that for 20 mg/mL W6, above a HRP concentration of 1 mg/mL, the system has enough enzyme to fully crosslink. The addition of more crosslinker above this point will therefore not affect the gel in any manner.

6.3.4 Scaling Dependence

To see what range of moduli could be obtained, various samples of W6 hydrogels were tested. All these samples had the concentrations of each component proportional to each other by the ratio 10:1:5 (W6 [mg/mL]:HRP [mg/mL]:H_2O_2 [mM]). The data are presented in Figure 6.9.

As can be seen, the range of both moduli stretches over a few orders of magnitude. The loss modulus lies in a range from 10^0 Pa $< G'' < 10^5$ Pa, while the storage modulus is within 10^2 Pa $< G'' < 10^6$ Pa. These ranges are much larger than those presented in section 6.3.2. This is due to the increased amount of H_2O_2 present in the gels, allowing more protein to be crosslinked at higher concentrations due to the increased availability of the hydrogen peroxide. This in turn is reflected in much larger moduli. The moduli data between 10 mg/mL W6 and 40 mg/mL W6 seem to follow a trend, as expressed in Figure 6.10. The moduli data again follow a power law with an exponent equal to approximately $2.25 = 9/4$, as expected from the theory of rubber elasticity, as presented in section 3.1.3. The biggest difference between these data sets and those where the HRP and H_2O_2 concentrations are held constant is the strength of the modulus for the gel with 60 mg/mL W6, 6 mg/mL HRP, 30 mM H_2O_2. This sample has much higher moduli than expected. This could be due to HRP and H_2O_2 present in such high concentrations along with very high W6 concentrations that individual W6 molecules are crosslinked with themselves. This would create extra crosslinks, reducing the distance between crosslinks of protein.

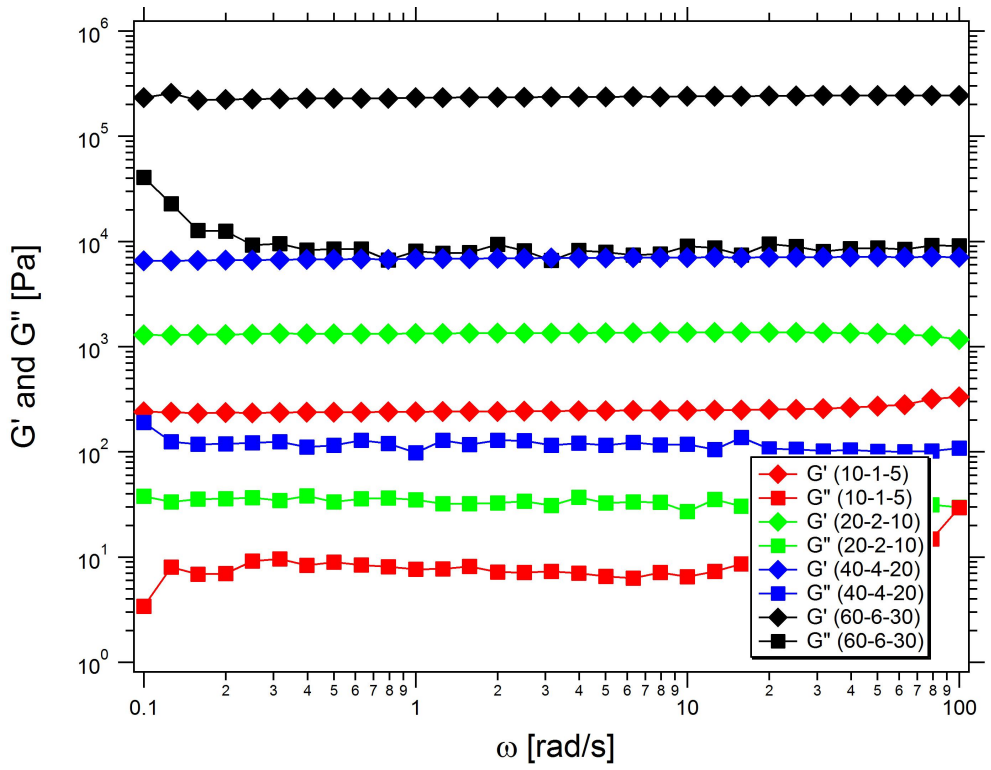

Figure 6.9: G' (◆) and G'' (■) vs. ω for various W6 samples. Data are taken at $T = 310$ K with a strain of 0.25%

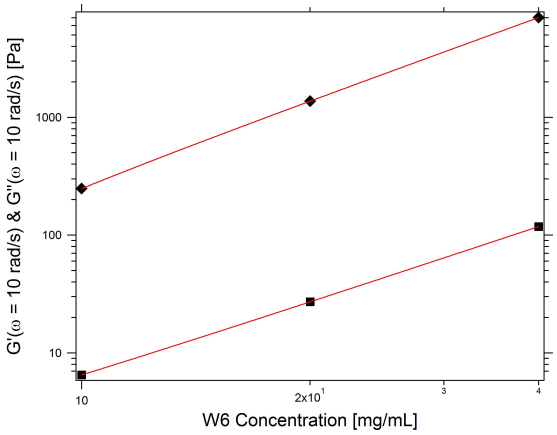

Figure 6.10: Log G' (◆) and log G'' (■) vs. log c for W6 gels with HRP and H_2O_2 concentrations increasing relative to the protein concentrations. Numerical fits are expressed by the red lines.

6.3.5 Conclusion

W6 gels behave as chemically crosslinked gels swollen in solvent. Their thermal dependence indicates increases in their moduli with temperature due to increased elasticity of the protein chains. Moduli demonstrate a dependence on concentration according to a power law with $c^{9/4}$ when the concentration of W6 is increased while keeping that of HRP and H_2O_2 are held constant. Changing the concentration of HRP in the samples does not affect either the storage or loss moduli above a concentration of 10 mg/mL. In addition, scaling the concentrations of HRP and H_2O_2 with that of W6 causes the gels to possess much larger moduli than the gels whose HRP and H_2O_2 remain constant. Even with this scaling, the gels still demonstrate a modulus dependence on the concentration equal to $c^{9/4}$ for modest concentrations (with more rapid increases at high concentrations of protein and H2O2).

Chapter 7

Conclusion

The invention of novel biomaterials for use in various areas of medicine and scientific research is on the rise. Protein hydrogels, one particular type of novel biomaterial, has previously been shown to be of use as cellular scaffolds. The protein CRC has already been proven to work as a cellular scaffold, while the newly created W6 protein may yet prove the same. As the physical properties of the hydrogel networks composing these cellular scaffolds is of particular importance, the rheological properties of CRC and W6 hydrogels were determined by rheometric techniques.

The telechelic properties of CRC were demonstrated to have an effect on the rheological properties of CRC hydrogels. Storage modulus and loss modulus data were measured by varying the angular frequency to determine that the CRC networks behave as weakly, physically crosslinked systems that follow stretched exponential modulus behavior with a value of β very close to 0.5. As temperature was increased, the moduli behavior was shifted towards higher frequency. This was elaborated upon by collapsing the data for a 10.4% CRC hydrogel at various temperatures within the range 285 - 305 K onto a single master curve using their relaxation times. This curve showed very little variation between the various data ranges plotted on it. From this, the relaxation times were found to depend on the energy of association

through an Arrhenius dependence, and that this energy was equal to $(1.76 \pm 0.02)X10^{-19}$ J. CRC hydrogel samples at concentrations of 5.3%, 7.5%, and 10.4% were also tested by measuring modulus data vs. angular frequency at a temperature of 285 K. As concentration was increased, the relaxation frequency decreased and the strengths of the moduli increased. These data were also collapsed onto a single master curve where it was shown that despite differences in concentration; the gel behavior was overall the same. CRC proteins with modular integrin binding domains were then allowed to form a network and tested rheometrically. The data were compared with that of a regular CRC network at a similar concentration and pH and found to be nearly identical. A number of samples with differing pH values and similar concentrations were then tested on the rheometer, demonstrating that at pH values of 6.5, 7.5 and 8.5 the rheological behavior of the protein networks remained the same.

CRC networks were then chemically crosslinked with EDC. The resultant gel networks were tested on the rheometer where it was shown the data agree with a model where the moduli could be expressed as a combination of components from the physically crosslinked CRC network and that of a chemically crosslinked network. The physical associations of the network continued to demonstrate stretched exponential behavior with $\beta = 0.5$. The storage modulus was also shown to be much stronger than that of the purely physically crosslinked hydrogel. 5% CRC gels with 5 mg/mL, 10 mg/mL, and 50 mg/mL EDC were also tested on the rheometer with modulus data measured as a function of time. It was shown that higher concentrations of EDC resulted in a plateau in the moduli much quicker than those with lower concentrations of EDC, though the moduli of all the gels with time seemed to converge towards the same values. A time of ~10 hours was chosen for these data to ensure that most crosslinking for the materials was complete. The storage and loss moduli of these gels were then tested with varying angular frequency, where it was shown that the samples with lower EDC

concentrations displayed stronger dependencies on angular frequency than that with the higher EDC concentration. As temperature was increased for a 5% CRC gel crosslinked with 50 mg/mL EDC, the moduli were shown to decrease, indicating that physical associations play a stronger role in the crosslinked network than covalent interactions. Samples with 5%, 7.5%, and 10% CRC and 50 mg/mL EDC were also tested at a temperature of 295 K. Their moduli were determined first as functions of time, where it was demonstrated that the modulus behavior for all three samples was the same, with crosslinking occurring only slightly quicker for higher concentrations of CRC. The same samples then had their moduli tested as functions of angular frequency to determine that there were two possible explanations for storage modulus behavior: one as an exponential dependence via the relation $G' \propto e^{\alpha c}$, the other via the relation $G' \propto c^5$.

The rheological properties of chemically crosslinked W6 hydrogels were then determined by testing various samples on the rheometer. A 20 mg/mL W6, 1 mg/mL HRP, 10 mM H_2O_2 sample was shown to have no modulus dependence on the angular frequency. As the temperature was increased for this hydrogel, the moduli demonstrated an increase in strength. Linear fits made to the moduli showed a dependence on the temperature for this gel to be linear, exactly as expected from theory, with a proportionality constant of $(6 \pm 1) \times 10^{23}$ Pa/J. Next, 10 mg/mL, 20 mg/mL, 40 mg/mL, and 60 mg/mL W6 samples with constant HRP and H_2O_2 concentrations were tested and plots of their moduli vs. angular frequency at a temperature of 310 K were made. The storage modulus was shown to increase with increasing concentration via the relation $G' \propto c^{9/4}$, exactly as expected from theory for a chemically crosslinked gel. Next, 20 mg/mL W6, 10 mM H_2O_2 samples with HRP concentrations of 1 mg/mL and 2 mg/mL were compared by plotting their moduli vs. angular frequency data on a plot at 310 K. It was shown that the gels displayed no dependence on the HRP concentration as expected since HRP is a catalyst and therefore will only affect the rate of reaction.

Finally, W6 samples were tested where HRP concentrations and H_2O_2 concentrations were scaled linearly with W6 concentrations. These gels displayed much higher moduli than the gels where the HRP and H_2O_2 concentrations were held constant, and again showed the moduli depended on the concentration by a factor of 9/4 for W6 concentrations less than 60 mg/mL. At this concentration, however, it was postulated that entanglements may begin to make a contribution to the storage and loss moduli strength due to high W6 density within the gel. This caused the moduli to no longer display the theoretical concentration dependence of 9/4 for the moduli.

Despite this progress in characterizing these protein hydrogels, there still remains much work to be done. Full thermal spectra of CRC hydrogels remain to be completed, allowing the full range of the hydrogel behavior to be explored. In addition, the behavior of the CRC hydrogels above a concentration of 10% remains experimentally undetermined. Another unclear aspect of these hydrogels is what effect the salt concentration has on the hydrogel's rheological properties.

For EDC crosslinked CRC hydrogels, similar work to that required for CRC hydrogels remains in that the full thermal, rheological behavior and the effects of different salt concentrations remains unknown. It is also necessary to determine whether the moduli vary concentration via an exponential relation or power law dependence as this should allow someone to predict what the modulus data will be for a certain concentration. This can be done by accumulating a larger range of modulus data at higher and lower concentrations than presented here in order to expand the range of data to over one decade. In addition to these problems, it remains to be seen at what concentration of EDC these crosslinked CRC hydrogels begin to behave as predicted by the theory of rubber elasticity, or whether this type of behavior is even possible.

Despite their theoretical simplicity in comparison to CRC hydrogels, W6 hydrogels still have much more work to be done. Their behavior with varying

H_2O_2 concentrations is still largely unknown, as is the effect of different pH levels. There is also the question as to how exactly entanglements above a W6 concentration of 60 mg/mL play a role in rheological behavior. Integrin binding domains, such as RGDS, are also theoretically possible in the W6 sequence, making experimental, rheological behavior of such protein hydrogels an open question.

Biomaterials will continue to play an important role in research and medicine in the years to come. The results displayed in this work demonstrate that protein hydrogels possess interesting, predictable rheological behavior. With further refinement of the purification process and more experimental data from their use as cellular scaffolds, CRC and W6 hydrogels could prove to be very useful tools for scientists looking to finely control the extracellular environment of their samples.

Bibliography

[1] Alejandro Saenz, Eric Rivera-Munoz, Witold Brostow, and Victor M. Castano. Ceramic biomaterials: an introductory overview. *Journal of Materials Education*, 21(5–6):297–306, 1999.

[2] Brian D. Lawrence, Mark Cronin-Golomb, Irene Georgakoudi, David L. Kaplan, and Fiorenzo G. Omenetto. Bioactive silk protein biomaterial systems for optical devices. *Biomacromolecules*, 9(4):1214–1220, 2008.

[3] Teruo Miyata, Toshio Taira, and Yasuharu Noishiki. Collagen engineering for biomaterial use. *Clinical Materials*, 9(3–4):139–148, 1992.

[4] Joel Rosenbloom, William R. Abrams, and Robert Mecham. Extracellular matrix 4: The elastic fiber. *The FASEB Journal*, 7(13):1208–1218, 1993.

[5] Torkel Weis-Fogh. Molecular interpretation of the elasticity of resilin, a rubber-like protein. *Journal of Molecular Biology*, 3(5):648–667, 1961.

[6] N. M. Edwards, S. J. Mulvaney, M. G. Scanlon, and J. E. Dexter. Role of gluten and its components in determining durum semolina dough viscoelastic properties. *Cereal Chemistry*, 80(6):755–763, 2003.

[7] Niraikulam Ayyadurai, So-Yeon Kim, and Sun-Gu Lee. Biological synthesis of alkyne-terminated telechelic recombinant protein. *Macromolecular Research*, 17(6):424–429, 2009.

[8] Tom Annable, Richard Buscall, Rammile Ettelaie, and Diane Whittlestone. The rheology of solutions of associating polymers: Comparison of experimental behavior with transient network theory. *Journal of Rheology*, 37(4):695–726, 1993.

[9] Ronald G. Larson. *The Structure and Rheology of Complex Fluids*. Oxford University Press, New York, 1999.

[10] L. A. Hough and H. D. Ou-Yang. Viscoelasticity of aqueous telechelic poly(ethylene oxide) solutions: Relaxation and structure. *Physical Review E*, 73(3), 2006.

[11] Stephen E. Fischer, Lixin Mi, Hai-Quan Mao, and James L. Harden. Biofunctional coatings via tageted covalent cross-linking of associating triblock proteins. *Biomacromolecules*, 10(9):2408–2417, 2009.

[12] Stephen E. Fischer, Xingyu Liu, Hai-Quan Mao, and James L. Harden. Controlling cell adhesion to surfaces via associating bioactive triblock proteins. *Biomaterials*, 28(22):3325–3337, 2007.

[13] Krishanu Saha, Albert J. Keung, Elizabeth F. Irwin, Yang Li, Lauren Little, David V. Schaffer, and Kevin E. Healy. Substrate modulus directs neural stem cell behavior. *Biophysical Journal*, 95(9):4426–4438, 2008.

[14] Nicholas D. Evans, Caterina Minelli, Eileen Gentleman, Vanessa LaPointe, Sameer N. Patankar, Maria Kallivretaki, Xinyong Chen, Clive J. Roberts, and Molly M. Stevens. Substrate stiffness affects early differentiation events in embryonic stem cells. *European Cells and Materials*, 18:1–14, 2009.

[15] Kefeng Ren, Thomas Crouzier, Christian Roy, and Catherine Picart. Polyelectrolyte multilayer films of controlled stiffness modulate myoblast cell differentiation. *Advanced Functional Materials*, 18(9):1378–1389, 2008.

[16] Adam J. Engler, Shamik Sen, H. Lee Sweeney, and Dennis E. Discher. Matrix elasticity directs stem cell lineage specification. *Cell*, 126(4):677–689, 2006.

[17] Y. Shona Pek, Andrew C. A. Wan, and Jackie Y. Ying. The effect of matrix stiffness on mesenchymal stem cell differentiation in a 3d thixotropic gel. *Biomaterials*, 31(3):385–391, 2009.

[18] R. McBeath, D. M. Pirone, C. M. Nelson, J. Bhadriraju, and C. S. Chen. Cell shape, cytoskeletal tension, and rhoa regulate stem cell lineage commitment. *Developmental Cell*, 6(4):483–495, 2004.

[19] Paul J. Flory. Molecular size distribution in three dimensional polymers. *Journal of the American Chemical Society*, 63(11):3083–3100, 1941.

[20] Walter H. Stockmayer. Theory of molecular size distribution and gel formation in branched-chain polymers. *The Journal of Chemical Physics*, 11(2):45–55, 1943.

[21] J. P. Munch, S. Candau, J. Herz, and G. Hild. Inelastic light scattering by gel modes in semi-dilute polymer solutions and permanent networks at equilibrium swollen state. *Journal de Physique*, 38(8):971–976, 1977.

[22] Michael Rubinstein and Ralph H. Colby. *Polymer Physics*. Oxford University Press, 2009.

[23] Alexi V. Finkelstein and Oleg Ptitsyn. *Protein Physics*. Academic Press, 2002.

[24] Hubert Bradford Vickery and Carl L.A. Schmidt. The history of the discovery of the amino acids. *Chemical Reviews*, 9(2):169–318, 1931.

[25] Gerald Karp. *Cell and Molecular Biology*. John Wiley & Sons, Inc., third edition, 2002.

[26] F. Sanger. The arrangement of amino acids in proteins. *Advances in Protein Chemistry*, 7:1–67, 1952.

[27] Linus Pauling, Robert B. Corey, and H.R. Branson. The structure of proteins: Two hydrogen-bonded helical configurations of the polypeptide chain. *Proceedings of the National Academy of Science in Washington*, 37(4):205–211, 1951.

[28] Linus Pauling and Robert B. Corey. The pleated sheet, a new layer configuration of polypeptide chains. *Proceedings of the National Academy of Sciences of the United States of America*, 37(5):251–256, 1951.

[29] F. H. C. Crick. The packing of α-helices: Simple coiled-coils. *Acta Crystallographica*, 6(8–9):689–697, 1953.

[30] Nikolaus Wellner, Justin T. Marsh, Andrew W. J. Savage, Nigel G. Halford, Peter R. Shewry, E. N. Clare Mills, and Peter S. Belton. Comparison of repetitive sequences derived from high molecular weight subunits of wheat glutenin, and elastomeric plant protein. *Biomacromolecules*, 7(4):1096–1103, 2006.

[31] Ashley H. Carter. *Classical and Statistical Thermodynamics*. Prentice-Hall, Inc., 2001.

[32] J. Wojcik, K.-H. Altmann, and H. A. Scheraga. Helix-coil stability constants for the naturally occurring amino acids in water. xxiv. half-cystine parameters from random poly (hydroxybutylglutamine-co-s-methylthiol-cysteine). *Biopolymers*, 30(1–2):121–134, 1990.

[33] Peter Y. Chou and Gerald D. Fasman. Conformational parameters for amino acids in helical, β-sheet, and random coil regions calculated from proteins. *Biochemistry*, 13(2):211–222, 1974.

[34] K.-H. Altmann, J. Wojcik, M. Vasquez, and H. A. Scheraga. Helix-coil stability constants for the naturally occurring amino acids in water.

xxiii. proline parameters from random poly (hydroxybutylglutamine-co-1-proline). *Biopolymers*, 30(1–2):107–120, 1990.

[35] R. Krystek Jr., Stanley, Robert E. Bruccoleri, and Jiri Novotny. Stabilities of leucine zipper dimers estimated by an empirical free energy method. *International Journal of Peptide and Protein Research*, 38(3):229–236, 1991.

[36] Dmitry Krylov, Joe Barchi, and Charles Vinson. Inter-helical interactions in the leucine zipper coiled coil dimer: ph and salt dependence of coupling energy between charged amino acids. *Journal of Molecular Biology*, 279(4):959–972, 1998.

[37] Paul J. Flory. Thermodynamic relations for high elastic materials. *Transactions of the Faraday Society*, 57:829–838, 1961.

[38] Christopher M. Elvin, Andrew G. Carr, Mickey G. Huson, Jane M. Maxwell, Roger D. Pearson, Tony Vuocolo, Nancy E. Liyou, Darren C. C. Wong, David J. Merritt, and Nicholas E. Dixon. Synthesis and properties of crosslinked recombinant pro-resilin. *Nature*, (437):999–1002, 2005.

[39] Torkel Weis-Fogh. A rubber-like protein in insect cuticle. *The Journal of Experimental Biology*, 37:889–907, 1961.

[40] Stanislav N. Gorb. Serial elastic elements in the damselfly wing: Mobile vein joints contain resilin. *Naturwissenschaften*, 86(11):552–555, 1999.

[41] Miriam Rothschild and J. Schlein. The jumping mechanism of xenopsylla cheopis i. exoskeletal structures and musculature. *Philosophical Transactions of the Royal Society of London. Series B, Biological Sciences*, 271(914):457–490, 1975.

[42] Malcolm Burrows, Stephen R. Shaw, and Gregory P. Sutton. Resilin and chitinous cuticle form a composite structure for energy storage in jumping by froghopper insects. *BMC Biology*, 6(41), 2008.

[43] P. R. Shewry, N. G. Halford, P. S. Belton, and A. S. Tatham. The structure and properties of wheat gluten: an elastic protein from wheat grain. *Philosophical Transactions of the Royal Society*, 357(1418):133–142, 2002.

[44] Paul J. Flory. The configuration of real polymer chains. *The Journal of Chemical Physics*, 17(3):303–310, 1949.

[45] Montgomery T. Shaw and William J. MacKnight. *Introduction to Polymer Viscoelasticity*. John Wiley and Sons, Inc., third edition, 2005.

[46] Allan H. Clark and Simon B. Ross-Murphy. Structural and mechanical properties of biopolymer gels. *Advances in Polymer Science*, 83:57–192, 1987.

[47] Masao Doi and S. F. Edwards. Dynamics of concentrated polymer systems. part 1. - brownian motion in the equilibrium state. *Journal of the Chemical Society*, 74:1789–1801, 1978.

[48] F. Tanaka and S. F. Edwards. Viscoelastic properties of physically cross-linked networks. transient network theory. *Macromolecules*, 25(5):1516–1523, 1992.

[49] Sauveur Candau, Jacques Bastide, and Michel Delsanti. Structural, elastic, and dynamic properties of swollen polymer networks. *Advances in Polymer Science*, 44:27–71, 1982.

[50] R. F. Fedors. Osmotic effects in water adsorption of polymers. *Polymer*, 21(2):207–212, 1980.

[51] F. Tanaka and S. F. Edwards. Viscoelastic properties of physically crosslinked networks part 1. non-linear stationary viscoelasticity. *Journal of Non-Newtonian Fluid Mechanics*, 43(2–3):247–271, 1992.

[52] F. Tanaka and S. F. Edwards. Viscoelastic properties of physically crosslinked networks: Part 2. dynamic mechanical moduli. *Journal of Non-Newtonian Fluid Mechanics*, 43(2–3):273–288, 1992.

[53] Ludwik Leibler, Michael Rubinstein, and Ralph H. Colby. Dynamics of reversible networks. *Macromolecules*, 24(16):4701–4707, 1991.

[54] C. A. Uraneck, H. L. Hsieh, and O. G. Buck. Telechelic polymers. *Journal of Polymer Science*, 46(148):535–539, 1960.

[55] Mehmet A. Tesdelen, Muhammet U. Kahveci, and Yusuf Yagci. Telechelic polymers by living and controlled/living polymerization methods. *Progress in Polymer Science*, 36(4):455–567, 2010.

[56] Christopher W. Macosko. *Rheology - Principles, Measurements and Applications*. John Wiley & Sons, 1994.

[57] A. C. Pipkin. *Lectures on Viscoelastic Theory*. Springer-Verlag New York Inc., New York, second edition, 1986.

[58] Jiri Horsky, Jana Mikesova, Otakar Quadrat, and Jaromir Snuparek. The effect of (2-hydroxypropyl)-β-cyclodextrin on rheology of hydrophobically end-capped poly(ethylene glycol) aqueous solutions. *Journal of Rheology*, 48(1):23–38, 2004.

[59] Fabrice Lafleche, Taco Nicolai, Dominique Durand, Yves Gnanou, and Daniel Taton. Association of adhesive spheres formed by hydrophobically end-capped peo. 2. influence of the alkyl end-group length and the chain backbone architecture. *Macromolecules*, 36(4):1341–1348, 2003.

[60] S. Bhargava and S. L. Cooper. Effect of water on viscosity and shear-thickening behavior of telechelic ionomers in nonpolar solvents. *Macromolecules*, 31(2):508–514, 1998.

[61] Nathalie Cathebras, Andre Collet, Michel Viguier, and Jean-Francois Berret. Synthesis and linear viscoelasticity of fluorinated hydrophobically modified ethoxylated urethanes (f-heur). *Macromolecules*, 31(4):1305–1311, 1998.

[62] Jean-Francois Berret, Damien Calvet, and Michel Collet. Fluorocarbon associative polymers. *Current Opinion in Colloid & Interface Science*, 8(3):296–306, 2003.

[63] Constantinos Tsitsilianis and Ilias Iliopoulos. Viscoelastic properties of physical gels formed by associative telechelic polyelectrolytes in aqueous media. *Macromolecules*, 35(9):3662–3667, 2002.

[64] Frederic Bossard, Thierry Aubry, Georgios Gotzamanis, and Constantinos Tsitsilianis. ph-tunable rheological properties of a telechelic cationic polyelectrolyte reversible hydrogel. *Soft Matter*, 2(6):510–516, 2006.

[65] Melvin Mooney. A shearing disk plastometer for unvulcanized rubber. *Industrial and Engineering Chemistry*, 6(2):147–151, 1934.

[66] Alexander Ya Malkin and Avraam I. Isayev. *Rheology - Concepts, Methods, & Applications*. ChemTec Publishing, Toronto-Scarborough, 2006.

[67] Donald J. Plazek. Magnetic bearing torsional creep apparatus. *Journal of Polymer Science*, 6(3):621–638, 1968.

[68] G. Benmouffok-Benbelkacem, F. Caton, C. Baravian, and S. Skali-Lami. Non-linear viscoelasticity and temporal behavior of typical yield stress fluids: Carbopol, xanthan and ketchup. *Rheologica Acta*, 49(3):305–314, 2010.

[69] Don W. Cleveland, Stuart G. Fischer, Marc W. Kirschner, and Ulrich K. Laemmli. Peptide mapping by limited proteolysis in sodium dodecyl sulfate and analysis by gel electrophoresis. *The Journal of Biological Chemistry*, 252(3):1102–1106, 1977.

[70] Esmat S. Hemdan and Jerker Porath. Development of immobilized metal affinity chromatography : Ii. interaction of amino acids with immobilized nickel iminodiacetate. *Journal of Chromatography A*, 323(2):255–264, 1985.

[71] Tai-Tung Yip, Yasuo Nakagawa, and Jerker Porath. Evaluation of the interaction of peptides with cu(ii), ni(ii), and zn(ii) by high-performance immobilized metal ion affinity chromatography. *Analytical Biochemistry*, 183(1):159–171, 1989.

[72] Frances H. Arnold. Metal-affinity separations: A new dimension in protein processing. *Nature Biotechnology*, 9:151–156, 1991.

[73] B. Monjon and J. Solms. Group separation of peptides by ligand-exchange chromatography with a sephadex containing n-(2-pyridylmethyl)glycine. *Analytical Biochemistry*, 160(1):88–97, 1987.

[74] B. Monjon and J. Solms. The theory and practice of freeze-drying. *Annals of the New York Academy of Sciences*, 85:641–681, 1960.

[75] Christa M. Stoscheck. [6] quantitation of protein. *Methods in Enzymology*, 182:50–68, 1990.

[76] Rammohan V. Maikala. Modified beer's law - historical perspectives and relevance in near-infrared monitoring of optical properties of human tissue. *International Journal of Industrial Ergonomics*, 40(2):125–134, 2009.

[77] Werner Brügel. *An Introduction to Infrared Spectroscopy. Translated from the German Original by A.R. Katritzky and A.J.D Katritzky.* Wiley & Sons, Inc., New York, 1962.

[78] Harold Edelhoch. Spectroscopic determination of tryptophan and tyrosine in proteins. *Biochemistry*, 6(7):1948–1954, 1967.

[79] Stanley C. Gill and Peter H. von Hippel. Calculation of protein extinction coefficients from amino acid sequence data. *Analytical Biochemistry*, 182(2):319–326, 1989.

[80] G. Holzwarth and P. Doty. The ultraviolet circular dichroism of polypeptides. *Journal of the American Chemical Society*, 87(2):218–228, 1965.

[81] Robert Townend, T. F. Kumosinski, Serge N. Timasheff, Gerald D. Fasman, and Betty Davidson. The circular dichroism of the β structure of poly-l-lysinenext term. *Biochemical and Biophysical Research Communications*, 23(2):163–169, 1966.

[82] Sharon M. Kelly, Thomas J. Jess, and Nicholas C. Price. How to study proteins by circular dichroism. *Biochimica et Biophysica Acta (BBA) - Proteins & Proteomics*, 1751(2):119–139, 2005.

[83] Priscilla E. Greenwood and Mikhail S. Nikulin. *A Guide to Chi-Squared Testing.* John Wiley and Sons, 1996.

[84] Naoki Nakajima and Yoshito Ikada. Mechanism of amide formation by carbodiimide for bioconjugation in aqueous media. *Bioconjugate Chemistry*, 6(1):123–130, 1995.

[85] L.H.H. Olde Damink, P.J. Dijkstra, M.J.A. van Luyn, P.B. van Wachem, P. Nieuwenhuis, and J. Feijen. Cross-linking of dermal sheep collagen using a water-soluble carbodiimide. *Biomaterials*, 17(8):765–773, 1996.

[86] Y. K. Yarovoy, H. P. Wang, and S. L. Wunder. Dynamic mechanical spectroscopy and conductivity studies of gel electrolytes based on stereocomplexed poly(methyl methacrylate). *Solid State Ionics*, 118(3–4):301–310, 1999.

[87] Nikoletta Stavrouli, Thierry Aubry, and Constantinos Tsitsilianis. Rheological properties of aba telechelic polyelectrolyte and aba polyampholyte reversible hydrogels: A comparative study. *Polymer*, 5(3):1249–1256, 2008.

[88] Paulina J. Skrzeszewska, Fritz A. de Wolf, Marc W. T. Werten, Antoine P. H. A. Moers, Martien A. Cohen Stuart, and Jasper van der Gucht. Physical gels of telechelic triblock copolymers with precisely defined junction multiplicity. *Soft Matter*, 5(6):510–516, 2009.

[89] Arthur J. Gross and Irwin W. Sizer. The oxidation of tyramine, tyrosine, and related compounds by peroxidase. *The Journal of Biological Chemistry*, 234:1611–1614, 1959.

[90] Thierry Michon, Michel Chenu, Nicolas Kellershon, Michel Desmadril, and Jacques Guéguen. Horseradish peroxidase oxidation of tyrosine-containing peptides and their subsequent polymerization: a kinetic study. *Biochemistry*, 36(28):8504–8513, 1997.

[91] Svend O. Andersen. Characterization of a new type of cross-linkage in resilinm a rubber-like protein. *Biochimica et Biophysica Acta*, 69:249–262, 1963.

[92] Svend O. Andersen. The cross-links in resilin identified as dityrosine and trityrosine. *Biochimica et Biophysica Acta*, 93(1):213–215, 1964.

[93] Frank LaBella, Frederick Keeley, Stanley Vivian, and Donald Thornhill. Evidence for dityrosine in elastin. *Biochemical and Biophysical Research Communications*, 26(6):748–753, 1967.

[94] Mari Fujimoto, Kouji Okamoto, and Masakazu Furuta. Preparation of alpha-elastin nanoparticles by gamma irradiation. *Radiation Physics and Chemistry*, 78(12):1046–1048, 2009.

[95] Mari Fujimoto, Mayuko Takeda, Kouji Okamoto, and Masakazu Furuta. Effect of gamma irradiation dose on the fabrication of α-elastin nanoparticles by gamma-ray crosslinking. *Radiation Physics and Chemistry*, 80(2):142–144, 2010.

Appendix A

Protocols

A.1 Bioreactor Protocol

CRC and CRC-RGDS were cloned into Escherichia coli (E. coli) strain pQE30/SG13009 obtained from Qiagen, and stab cultures of media containing these samples were placed into a -80^{o}C freezer for storage by Dr. Stephen E. Fischer. Samples were extracted from these stab cultures and were streaked onto lysogeny broth (LB) plates containing ampicillin and kanamycin antibiotics using sterile technique. In addition, this particular E. coli strain possesses plasmids (bacterial DNA) that encode for particular enzymes (β-lactamase and Neomycin phosphotransferase II) that break down ampicillin and kanomycin, respectively, making these antibiotics harmless to bacteria encoding these enzymes. Cultures were then grown overnight in a $T = 37^{o}$C oven.

One individual colony was chosen and placed using sterile technique into a 5 mL autoclaved, LB solution with 100 g/mL ampicillin, 25 μ g/mL kanamycin. This seed culture was placed in a 37^{o}C shaker to grow for 8 hours. The seed culture was then inoculated using sterile technique into a 500 mL autoclaved, LB solution mixed with 100 μg/mL ampicillin, 25 μg/mL kanamycin and left to grow overnight in a 37^{o}C shaker.

While the seed cultures were being prepared, a New Brunswick Scientific Bioflo 110 bioreactor was also being prepared. About 4.6 L of deionized water was mixed with 200 g of yeast extract inside the 14.0 L glass chamber of the bioreactor. The system was then sealed and autoclaved to sterilize the contents. After waiting for it to cool, it was hooked up to the control unit. A number of solutions were also prepared and sterilized using either an autoclave or filter sterilization. These were then mixed together to make ~1200 L of feed solution (500 g/L glucose, 200 g/L yeast extract, 15 g/L $MgSO_4 \bullet 7H_2O$, 25 mg/L kanamycin, 100 mg/L ampicillin). A 20X concentrated media salts solution was also prepared, as per the protocol mentioned in appendix B.1.1

The feed solution and concentrated ammonium hydroxide were then fed through the control unit's peristaltic pumps and attached to lines leading into the glass chamber of the bioreactor. The pH of the culture in the bioreactor is monitored and controlled by the control unit by measuring the actual pH to the desired pH. When there is a variation of approximately 0.05 pH units, the peristaltic pumps push through a small amount of base or acid to attain the desired pH. The culture itself is acidic in nature, requiring the base in order to obtain the desired pH of 7. As the culture grows and begins to produce protein, the pH becomes basic and the control unit will pump solution attached to the acid input into the glass chamber. The basic pH of the culture is also an indication that the bacteria require sustenance in the form of feed solution, and so this solution is hooked up to the bioreactor's acid input.

Determination of the relative concentration of bacteria in the sample was performed using sterile technique to extract a sample. This sample was then diluted with LB media, and the $Abs_{280\ nm}$ measured with LB media used as a blank. Typical values were between 2.00 and 3.00 OD units. The culture was inoculated into the bioreactor media with ~55 mL of 918 mg/mL glucose, . The temperature of the bioreactor's glass chamber is controlled

at 37^oC, while the pH is set to 7.0. The bacterial culture is then monitored until an optical density (OD) of ~20. At this point, a 1 mL sample was collected and centrifuged. The supernatant liquid was disposed of, and the pellet stored as a pre-induction sample. 5 mL of 1 M of filter-sterilized isopropyl-β-D-thio-galactoside is added to the culture to induce the E. coli to produce protein. The resulting solution is left for 4 hours, and collected in centrifuge bottles. At this point, the OD of the culture is measured and a post-induction sample is collected exactly as outlined for the pre-induction sample. The bottles containing the culture are then centrifuged at 8000g for 15 minutes. Supernatant liquid is then disposed of, and the cell pellets are collected and frozen in a -20^oC freezer.

Appendix B

Solutions

B.1 Bioreactor Solutions

B.1.1 20X Concentrated Media Salts Solution

20X concentrated media salts solutions added directly into the bioreactor, as mentioned in section 4.2.1, were prepared as follows. About 10 g of $(NH_4)_2HPO_4$, 33.75 g of KH_2PO_4, 4.25 g of citric acid, and 3.5 g of $MgSO_4 \bullet 7H_2O$ were stirred in with ~25 mL of trace metals solution. The total volume was brought to 250 mL with DI H_2O, and the resulting solution was heated and stirred until fully dissolved. It was then filter-sterilized. Ingredients for the trace metals solution are given in Table B.1.

B.2 Protein Purification Solutions

B.2.1 Urea Buffer Solutions

Urea is known to denature proteins in aqueous solution, making it a perfect candidate to use as an ingredient in specific kinds of solutions in protein labwork. By denaturing poteins imbedded in the cell membrane, it can be used

Ingredient	Concentration
$FeCL_3 \bullet 6H_2O$	26.98 g/L
$ZnCl_2$	2.74 g/L
$CaCl_2$	1.0 g/L
$Na_2MoO_4 \bullet 2H_2O$	2.0 g/L
$CuSO_4 \bullet 5H_2O$	1.9 g/L
H_3BO_3	0.5 g/L
Concentrated HCl	100 mL/L

Table B.1: Concentrations for the ingredients of the trace metals solution.

to lyse cells, as mentioned in section 4.2.2. For this work specifically, the native conformations of CRC and CRC-RGDS allow hydrogels to self-assemble in aqueous solution, a condition undesirable when using column purification as the gels will form directly on the column, making it problematic to remove. As such, urea buffers are well suited for use with CRC and CRC-RGDS.

In this work, the standard urea buffer used consisted of 8 M urea, 100 mM sodium phosphate (monobasic), and 7.6 mM tris base. The high urea concentration ensures that proteins remain in the denatured state, while the tris base and sodium phosphate ensure that the pH of the solutions is controlled. By adding small amounts of acids or bases to such a solution, no significant change will happen to the pH due to the presence of counterions in the form of sodium phosphate and tris. This allows these solutions to maintain pH at a reasonable level, avoiding very high or very low pH values that might harm biological materials, such as the proteins.

Three main kinds of urea buffer solutions were used in this work: Buffer B, Buffer C, and the elution buffer. All three used the same composition of urea, sodium phosphate (monobasic), and tris base mentioned above. The main difference between Buffer B and Buffer C is in their pH values, with Buffer B using a pH of 8, and Buffer C using a pH of 7. Proteins have been found to bind to IMAC resin much more easily at a pH value of around 8, and less so arond pH values or 7 or lower (71). Thus, Buffer B is a suitable

choice as a binding buffer, existing at a pH amenable to protein binding, while Buffer C will was out more weakly bound protein, leaving those more strongly bound (such as CRC and CRC-RGDS) which contain a His-tag. The elution buffer used possesses the same pH of Buffer B, but has the addition of 250 mM imidazole to competitively bind to the IMAC resin. As imidazole is smaller than either CRC or CRC-RGDS, it has a higher capacity for binding than the His-tags present on the CRC molecules, allowing it to take the place of any protein bound to the IMAC resin.